# ENHANCING THE NEURONAL DIFFERENTIATION OF MOUSE EMBRYONIC STEM CELLS USING BIOMATERIALS

by

Jeremy M. Holzwarth

A dissertation submitted in partial fulfillment
of the requirements for the degree of
Doctor of Philosophy
(Biomedical Engineering)
in The University of Michigan
2015

Doctoral Committee:

      Professor Peter X. Ma, Chair
      Professor Sue O'Shea
      Assistant Professor Brian A. Pierchala
      Professor Jan P. Stegemann

## DEDICATION

I would like to dedicate this work to my family for supporting me all along the way. You never wavered with your belief in me and that made all the difference.

## ACKNOWLEDGEMENTS

## PREFACE

This dissertation is original and independent work performed by the author, Jeremy M. Holzwarth.

**TABLE OF CONTENTS**

# LIST OF TABLES

# LIST OF FIGURES

**ABSTRACT**

Nervous system injuries remain significant clinical issues that affect hundreds of thousands of individuals each year. Spinal cord injuries are especially difficult since the wound healing process results in a glial scar, inhibiting regeneration. Current strategies for dealing with spinal cord injuries focus on stabilization and rehabilitation with minimal likelihood of any significant functional regeneration. The outlook for peripheral injuries is not quite as dire as peripheral nerve has the capacity to regenerate. However, if the defect is beyond a critical size of around 1cm, that ability is compromised. The gold standard for treating large defects is an autologous nerve graft, but there are significant drawbacks. Clearly there is room for improvement.

In this study, conducting composite electrospun nanofibrous substrates were fabricated to investigate if topography and electrical stimulation could control embryonic stem cell (ESC) differentiation. First, it was determined that poly (l-lactic acid) (PLLA) nanofibers of at least 900nm promoted neuronal differentiation and neurite outgrowth. ESCs interacted with these fibers through integrin $\alpha6\beta1$ and induced differentiation via early ERK activation. Fiber size did not have a significant effect on p38 activity. Next, PLLA was doped with polypyrrole (PPy) to improve its electrical properties. Nerve conduits fabricated with PPy/PDLLA were successful at promoting the regeneration of a rat sciatic nerve defect on par with an autologous graft. The sciatic function indices (SFI), nerve conduction velocities, triceps surae weights, and nerve fiber

morphologies were all comparable between the PPy/PDLLA conduits and autografts, and both significantly better than the PDLLA conduits. Finally, PPY/PLLA was electrospun into random and aligned nanofibers. ESCs seeded on these aligned nanofibers were stimulated with 100mV for 2hrs, which induced a higher percentage of neurite-bearing cells, from around 13% to around 23%, and longer neurites, from around 80μm to around 130μm. Thus, it is clear that conducting aligned fibers combined with electrical stimulation improves ESC neurite growth. Determining the links between nanofiber-stimulated differentiation and neurogenesis allow for a better understanding of the application of ESCs in neural tissue engineering. These results provide guidance to neural tissue engineering scaffold design and insight into how ESCs interact with different topographies.

# CHAPTER 1

## Introduction

## Background and Motivation

Nerve injuries in both the peripheral nervous system (PNS) and central nervous system (CNS) are extremely difficult clinical issues that affect a large population. Around 270,000 people in the US have a spinal cord injury (SCI), including 12,000 new cases each year [1]. SCI costs those individuals as much as $5M over their lifetime [2], and that does not even include indirect costs such as lost wages and productivity. The majority of SCIs arise from a traumatic injury, usually from an auto crash or an accidental fall [3].

Currently, there is no clinical treatment that has successfully regenerated an SCI. While the majority of tissues in the body have the capacity to regenerate, the wound healing process in the spinal cord after an injury prevents full recovery. When the spinal cord is injured, the damage disrupts the integrity of nerve fibers in the white matter and their cell bodies in the grey matter. While this primary injury is devastating, secondary degeneration results in inflammation, bleeding, and scarring [4-6]. Macrophages and reactive astrocytes are recruited to the wound site to clean up the debris, but the astrocytes become hypertrophic and form a glial scar. The formation of a glial scar prevents the surrounding nerve from regenerating across the wound site, resulting in a permanent state of dysfunction.

Treatment regimens now are broken down into two stages. In the early stage, the focus is on preventing any further injury through immobilization and surgery. Some medications exist, such as methylprednisolone, but their benefit is very mild. Thus, significant work is being done on new pharmacologic candidates to administer post-injury [7, 8]. After the initial trauma, later stage treatments focus on rehabilitation, including physical therapy, occupational therapy, and quality of life adaptations. There are also medications to alleviate some long term SCI effects such as pain, muscle spasticity, bladder control, and bowel control. With no options available to fully regenerate an SCI, tissue engineering provides some promise.

While an SCI might be more difficult to treat, a PNS injury is more common and also challenging. Between the US and Europe, approximately 100,000 peripheral nerve repair procedures are performed every year [9]. These injuries can arise from trauma, cancer, or congenital defects [10, 11].

Compared to SCI, there are more methods available to treat a peripheral nerve injury. Normally, short gaps can be reconnected surgically with microsutures [12] or various nerve guidance channels [13-15]. However, if the defect is longer than 10mm, it becomes much more challenging to treat. For the longer, critically-sized nerve defects, the current gold standard is an autologous nerve graft (often the sural nerve [16], a sensory nerve located along the calf), though there are severe drawbacks including donor side morbidity, multiple surgical sites, and possible size mismatch.

Clinically, there is a need for a new approach to treating nerve injuries. Nerve tissue engineering provides a promising approach by attempting to create a synthetic implant.

# Nerve Tissue Engineering Overview

Tissue engineering as a whole is a burgeoning field, bringing together myriad research areas including polymer chemistry, materials science, cell and molecular biology, and clinical medicine. At the base lie three components: a scaffold, cells, and soluble factors. Each plays a pivotal role in the healing and regeneration process, and each can be tailored to the specific application.

*Peripheral nerve scaffolds*

For the scaffold, the main role is to provide a structurally relevant 3D environment that defines the shape of the tissue and allows the cells to adhere. For peripheral nerve, that most commonly means a nerve guidance conduit [17]. The use of biological conduits dates back to the 19th century when an artery was explored [18], but it did not translate to the clinic until the early 1900s when vein grafts were employed [19-21]. Veins are still used today for defects ranging from 2-70mm but success has been varied [22-25]. Denatured muscle tissue has also been explored, albeit less so than veins, because the basal lamina contains collagen IV and laminin, two extracellular matrix proteins known for promoting nerve growth [26, 27]. Muscle tissue has had some success [28, 29], though it does not control the regenerating nerve fibers very well. Combining it with a nerve guidance channel, however, is a more viable option [30, 31]. Though they are still being researched [32], the use of both vein and muscle has some drawbacks limiting their use. Structurally, veins are not strong so they have the propensity to collapse if the distance bridged is too great. Denatured muscle tissue has the ability to promote regeneration, but lacks the ability to control growth so nerve fibers can potentially grow out of the graft. In addition, since both are biologically sourced, they require an additional surgical site for an autologous

graft, or carry the risks of immune rejection and disease transmission as an allograft. For those reasons, synthetic grafts have been employed.

A wide variety of materials have been used as nerve conduits, both bioabsorbable and non-bioabsorbable. Biodegradable substrates are preferred to prevent the need for a second surgery. If not removed, non-degradable conduits run the risk of suppressing full regeneration through a chronic foreign body response [33, 34]. When silicone was first used [35], patients reported irritation after only 2 years, and that trend continued [33, 36]. Other non-biodegradable conduits that have seen use in the clinic include polytetrafluoroethylene (PTFE) [37], polyethylene, polyvinyl, and rubber [38]. Biodegradable conduits are a much more attractive option and more research has been done on such materials. In the clinic, poly (glycolic acid) (PGA) [39, 40] has been explored with some success. In the research labs, a wider variety of polymers and materials are being studied including poly (lactic acid) (PLA) [41-45], peptide amphiphiles [46], poly (lactic-co-glycolic) acid (PLGA) [43, 46-48], polycaprolactone (PCL) [49-51], polypyrrole (PPy) [52], carbon nanotubes [53], silk [54, 55], collagen [51, 56-58], and chitosan [55, 59, 60], among others [61].

In addition to the variety of materials, there are several different architectural archetypes employed, including solid-walled conduits and nanofibrous conduits. Solid-walled conduits are the simplest to fabricate, but do not mimic the natural fibrous extracellular matrix that cells adhere to in the body. Nanofibers do a much better job and mimicking natural cellular environments and have been shown to have a positive effect on adhesion and differentiation [62-64]. Having favorable cellular interactions is one of the most desirable traits in designing a scaffold so nanofibrous architecture is vital. Currently, electrospinning and self-assembly are the

two dominant techniques used to create nanofibers for nerve tissue engineering [65], though thermally-induced phase separation (TIPS) has also been employed [66].

*Spinal cord scaffolds*

Spinal cord tissue engineering has not been explored as much as peripheral nerve tissue engineering, but some scaffolds have been investigated [67] in an attempt to provide a bridge across the wound site, preventing the formation of the glial scar and allowing regenerating axons to cross the gap.

Natural polymers collagen [68, 69] and alginate have been used to treat spinal cord injuries with very limited success. The use of collagen is controversial since as a component of the glial scar, it could inhibit nerve growth [70], though as long as the collagen tube is aligned with the spinal cord, axons were able to grow through it [71]. Alginate also has mixed results. On one hand, it inhibited dorsal root ganglia neuron growth [72], while on the other hand, it was used to make an anisotropic hydrogel and successfully increased the growth of regenerating axons [73]. Other naturally-derived materials, including fibrin [74], Matrigel [75], fibronectin [76, 77], and agarose [78], most of which were applied in gel form, have also been studied with extremely limited success. Synthetic gels have been developed, including poly [N-2-(hydroxypropyl) methacrylamide] (PHPMA, NeuroGel™) [79] and poly (2-hydroxyethyl methacrylate-co-methyl methacrylate) (PHEMA-MMA) [80], both of which have similar mechanical properties to the spinal cord [81-83]. NeuroGel was able to promote some level of functional recovery [84], while PHEMA-MMA channels promoted neuronal regeneration without functional recovery [80]. While promising, both of these polymers are non-biodegradable, limiting the amount of regeneration that can occur. Synthetic biodegradable

options include PLGA [85] and poly (l-lactic acid) PLLA [86-88], and while both can promote axonal regeneration, neither has been able to achieve functional recovery.

Development of spinal cord scaffolds has been slow compared to peripheral nerve scaffolds, but work is gradually accelerating as more advances are made.

*Cell source*

The scaffold is just one component of the tissue engineering picture. Incorporating cells can greatly increase the performance of many strategies by jump-starting the tissue regeneration process. Finding an appropriate cell source, however, has been a struggle for nerve tissue engineering. Options include adult cells and stem cells, and both have their advantages and disadvantages.

The use of adult cells can be challenging for both spinal cord and peripheral nerve since they can be difficult to harvest and grow in clinically relevant numbers. Schwann cells have been used for both applications with more success in peripheral nerve [44, 48, 49, 52, 89]. They have the ability to remyelinate regenerating axons [90, 91], produce extracellular matrix proteins [92, 93], and secrete trophic factors [94, 95]. However, they must be isolated from healthy nerve, commonly the sciatic nerve in animal models. In addition, there are several issues with their use in treating SCI, such as their inability to properly guide regeneration and their poor results when compared with olfactory ensheathing cells (OECs) [96]. OECs are similar to Schwann cells in that they are a type of glial cell. They are derived from the olfactory bulb or nasal mucosa and have been primarily used to treat SCIs with good success even in humans [97, 98], but have also been applied to peripheral nerve [32]. Other cell sources for the CNS include macrophages [99, 100] and dendritic cells [101-103] to promote recovery.

Stem cells are an alternative to adult cells and can be expanded to a greater cell number *in vitro*. Stem cells come in a variety of flavors, from late stage neural stem cells (NSCs) to pluripotent embryonic stem cells (ESCs). NSCs are attractive since they are easier to differentiate than more pluripotent cells, though they suffer from similar drawbacks to adult cells. They need to be isolated from either developing spinal cord [104], cerebral cortex [105], and brain [106], or adult spinal cord [107], cerebral cortex [108], and subventricular zone of the lateral ventricle [109, 110], making them very difficult to harvest in a clinically relevant way. Mesenchymal stem cells and hematopoietic stem cells are much more accessible, easily isolated from bone marrow, but more difficult to differentiate into neural and glial cells. However, that has not deterred their use in both spinal cord [111-115] and peripheral nerve [47, 116]. ESCs are an attractive choice for tissue engineering as a whole since they can proliferate indefinitely and can differentiate into any cell type in the body [117]. Their pluripotency, however, also makes controlling their fate relatively difficult. Commonly, ESCs are used to derive NSCs *in vitro*, and then applied to nerve tissue engineering [118]. Separate from their scientific validity, ESCs incite moral and ethical concerns. For that reason, induced pluripotent stem cells (iPSCs) provide a promising alternative [119-121]. They are derived from adult somatic cells, commonly fibroblasts, and reprogrammed with genes, either Oct3/4, Sox2, c-Myc, and KLF4 [122, 123], or Oct3/4, Sox2, Nanog, and Lin28 [124]. Other cell sources explored include adipose-derived stem cells [57, 125-127] and amniotic fluid-derived stem cells [128].

It is clear that pluripotent stem cells, with their wide variety of applications, have the most promise for use in tissue engineering. Controlling their differentiation is a critical step to prevent the formation of teratomas *in vivo*. If allowed to spontaneously differentiate *in vitro*, only a low level of neuronal differentiation takes place [129, 130], thus, methods were developed to

increase neuronal commitment. The two most successful methods are retinoic acid (RA) induction and lineage selection [131]. RA, a derivative of vitamin A, was able to greatly increase the neuronal differentiate rate when applied in high concentrations at early stages of development [129, 132-134]. Growth factor-mediated lineage selection of neuronal cells starts with the formation of all three germ layers, removes growth factors to selectively differentiate neuroectodermal cells, and then uses inductive factors such as epidermal growth factor (EGF) [135], fibroblast growth factor-8 (FGF8), and sonic hedgehog (Shh) [136] to maintain neural precursor cells before finally inducing terminal differentiation.

*Summary*

Soluble factors for neuronal differentiation have been well established, but for tissue engineering, there is a desire to involve the scaffold in an active role in controlling cell behavior. The interactions between nanofibers and NSCs, MSCs, and other cells have been explored, but little has been done on exploring the interaction between nanofibers and pluripotent stem cells. Current strategies for neural tissue engineering are scattered with many researchers trying myriad materials and cells with high variable results. A better understanding of the interaction between ESCs and a nanofibrous substrate will help focus neural tissue engineering efforts and guide research moving forward.

**Thesis Outline**

With the current landscape of nerve tissue engineering as scattered as it is, this work delves into the interactions between ESCs and nanofibers in order to inform the design of tissue engineering scaffolds.

Chapter 2 describes the effect of fiber size on the neuronal differentiation of mouse D3 ESCs. An array of electrospun PLLA fibers along with TIPS fibers were fabricated with fiber diameters ranging from 129nm up to 1,889nm. Mouse D3 ESCs were seeded on each nanofibrous matrix in three different medium conditions and their neuronal differentiation and neurite growth was assayed. This chapter encompasses a manuscript to be published.

Chapter 3 discusses the inclusion of PPy at various weight percentages with PDLLA to create conducting composite polymers. Electrical stimulation was used to stimulate rat pheochromocytoma 12 (PC12) cells to determine the ability of PPy/PDLLA to support neurite growth. A conducting nerve conduit was then fabricated to test the ability of PPy/PDLLA to regenerate a rat sciatic nerve defect *in vivo*. This chapter has been published as a manuscript in Biomaterials.

Chapter 4 details the fabrication of an array of PPy/PLLA nanofibers with electrospinning. D3 ESCs were seeded on the nanofibers and stimulated with a potential to examine the effect of electrical stimulation on the neuronal differentiation and neurite growth of ESCs. In addition, aligned fibers were fabricated to exact greater control over the direction and orientation of neurite growth. This chapter also encompasses a manuscript to be published.

Chapter 5 summarizes the results of this thesis as a whole and outlines the significance and impact on the field.

Chapter 6 addresses the different directions that this project could be taken in with future work.

# CHAPTER 2

## Effect of fiber size on the neuronal differentiation of mouse embryonic stem cells

## Abstract

Nanofibers have a significant effect on gene expression, differentiation, and cell morphology. However, the interaction between mouse embryonic stem cells (ESCs) and a nanofibrous substrate with respect to neuronal differentiation has not been fully explored. In this study, we began by comparing ESC behavior on poly (l-lactic acid) (PLLA) films to phase separated and electrospun nanofibers. Surprisingly, ESCs grown on phase separated matrices maintained some level of pluripotency despite being induced to differentiate with defined neural medium, while ESCs grown on electrospun fibers differentiated under the same conditions. We explored this further by electrospinning nanofibers with controlled fiber sizes from 129nm to 1889nm. ESCs cultured on the small fibers did not undergo neuronal differentiation while differentiation and neurite growth increased as fiber size increased. In addition, extracellular signal-regulated kinase (ERK) activity increased on the larger fiber sizes. These findings indicate that a specific size range of nanofibers, around 1-2μm, promote neuronal differentiation of ESCs via ERK signaling.

**Introduction**

Embryonic stem cells (ESCs) are capable of indefinite proliferation and have the ability to differentiate into all three germ layers and subsequent lineages [137]. Their pluripotency makes them a desirable model for studying early development and differentiation. In addition, there are many applications in tissue engineering, a field that bridges regenerative medicine, engineering, and materials science. Neural tissue engineering seeks to combine a scaffold with cells and soluble factors to treat central or peripheral nervous system defects, significant clinical issues with limited treatment options, especially for spinal cord injuries. While ESC pluripotency makes their use attractive for use in this field, it also provides a challenge to control their fate. The primary means used to differentiate them into neurons is by using soluble factors. Retinoic acid (RA), a derivative of vitamin A and important morphogen during neural development, is arguably the most common [131, 134], but other growth factors such as brain-derived neurotrophic factor (BDNF), glial cell line-derived neurotrophic factor (GDNF), and insulin-like growth factor (IGF) have been used [138, 139]. However, it is desirable to employ the substrate in an active role to exact another layer of control over stem cell fate.

Nanofibers mimic the natural extracellular matrix (ECM) and have the ability to control cell behavior, including adhesion, proliferation, and differentiation. An extensive amount of work has been done to show that nanofibers promote differentiation and neurite growth in more mature cell lines. Neural stem cells (NSCs) were cultured on laminin-coated polyethersulfone (PES) fibers with average fiber diameters of 283, 749, and 1452nm [140]. NSC proliferation decreased and neuronal differentiation increased as fiber size increased. On the other hand, mouse cerebellum C17.2 stem cells showed little difference in neurite growth across poly(l-lactic acid) (PLLA) fibers ranging from 307nm to 1150nm [62]. Only when the fibers were aligned did

size have an effect, and longer neurites were found on the smaller fibers. When it comes to the effect of nanofibers on ESC differentiation, very little has been done [141-143].

Even less has been done to elucidate the mechanism by which nanofibers control stem cell fate. Nanofibers have been shown to selectively adsorb proteins and this could affect how cells adhere [144]. In fact, osteoblasts were seeded on nanofibrous and solid scaffolds, with and without 3,4-dehydroproline, an inhibitor of collagen fibril formation [145]. On the nanofibers, osteoblasts expressed integrin subunit α2, part of integrin α2β1 that binds collagen, in presence and absence of 3,4-dehydroproline. On the solid surface, osteoblasts only expressed α2 without 3,4-dehydroproline, showing that nanofibers can interact with cells similar to the way they interact with collagen through integrins. In this study, the integrin responsible for the interaction between ESCs and nanofibers in the context of neuronal differentiation is investigated. In addition, the connection between the extracellular interaction with the ECM and intracellular signaling was explored. Understanding the mechanism by which intracellular signals travel and which pathways are employed has always been a significant challenge when studying development or tissue engineering. The mitogen-activated protein kinase (MAPK) pathway is especially interesting for its role during neural development regulating proliferation, differentiation, and apoptosis. Out of the three major cascades, extracellular signal-regulated kinase (ERK), c-Jun N-terminal kinase (JNK), and p38, ERK has been shown to play a significant role in neural development. ERK is activated by an upstream kinase, MEK, via phosphorylation of threonine and tyrosine residues and then translocates to the nucleus where it phosphorylates transcription factors and cytoskeletal proteins [146]. The activation of one such transcription factor, signal transducer and activators of transcription protein 3 (STAT3), has been shown to be vital in developing NeuN-positive neurons [147]. However, this interaction is

12

complicated as other reports have shown that ERK negatively regulates STAT3 [148]. In PC12 cells, multiple studies have implicated ERK activity as a requirement for neuronal differentiation [149, 150]. However, little is known about how the nanofibrous architecture of the ECM could affect MAPK signaling in ESCs.

In this study, an array of fibers was fabricated from 129nm in diameter to 1889nm. Mouse D3 ESCs were cultured on these nanofibers and their neural differentiation was assayed. Our data showed that larger fibers, greater than approximately 900nm, promoted neuronal differentiation and neurite growth. In addition, we discovered that early ERK activation was required for fiber size-mediated neuronal differentiation, and this was due at least in part to the laminin-binding integrin α6β1.

## Materials and Methods

*Materials*

PLLA was purchased from Boehringer Ingelheim (Ingelheim, Germany). All other chemicals were analytical grade reagents.

*Fabrication and characterization of PLLA matrices*

For thermally-induced phase separated (TIPS) films, PLLA was dissolved in tetrahydrofuran (THF) at 60°C to make a 10% w/v PLLA solution. The nanofibrous PLLA matrix (thickness ~40μm) was fabricated by first casting 0.4ml of the PLLA solution on a glass support plate that had been pre-heated to 45°C for 10min, and then sealing the polymer solution on the glass support plate by covering it with another pre-heated glass plate. The polymer

solution was phase separated at -20°C for 2hrs and then immersed into a mixture of ice and water for 24hrs to exchange the tetrahydrofuran. The matrix was washed with distilled water at room temperature for 24hrs, changing the water every 8hrs. After washing, the matrix was freeze-dried and then cut to size.

For electrospun fibers, a PLLA solution was prepared by dissolving either 6%, 8%, 15%, or 20% w/v PLLA in hexafluoroisopropanol (HFIP). Fibers were electrospun using a horizontal electrospinning setup. A high-voltage power supply (Gamma High-voltage Research, Ormond Beach, FL, USA) provided a 15kV potential between the needed and the grounded collector. A syringe pump housed a 10ml syringe attached to a 22 gauge flat point needle and was placed 12cm away from the collector. PLLA solution was dispensed at 1.5ml/hr.

Matrices were gold coated (Desk-II, Denton Vacuum, Moorestown, NJ, USA) and observed using a Philips XL30 FEG scanning electron microscope. Images of fibers were analyzed with ImageJ (National Institutes of Health, Bethesda, MD, USA) to determine the average fiber diameters. At least 100 fibers for each matrix were measured.

*Matrix preparation*

The PLLA matrices were placed on a glass coverslip backing and placed in 6-well plates. The matrices were sterilized under UV light for 30min, wet briefly with ethanol, and then washed 3 times with phosphate-buffered saline (PBS). A polydimethylsiloxane (PDMS, Sylgard 184®, Dow Corning, Midland, MI, USA) donut was used to secure the matrices in the bottom of the wells. Prior to seeding, the matrices were incubated in either non-directional (ND) media (DMEM supplemented with 2% FBS, $10^{-4}$M β-mercaptoethanol, 0.224mg/ml L-glutamine and 1.33µg/ml HEPES), neural permissive (NP) media (80% F-12/20% Neurobasal media with N2

and B27 supplements and 10mM sodium pyruvate) or neural media (80% F-12/20% Neurobasal media with N2 and B27 supplements, 10mM sodium pyruvate and 1µM retinoic acid) for 1hr.

*D3 culture and seeding*

D3 mouse embryonic stem cells [151] were cultured on 0.1% gelatin-coated tissue culture flasks in complete ESC media (DMEM supplemented with 10% FBS, $10^{-4}$M β-mercaptoethanol, 0.224µg/ml L-glutamine, 1.33µg/ml HEPES, and 1,000 units/ ml human recombinant LIF). Cells were passaged every 2 days and stored in a humid 37°C incubator with 5% $CO_2$. 50,000 cells were seeded on each matrix in the appropriate media and it was changed daily for the duration of the experiments.

*PCR*

Samples were first homogenized with a Tissue-Tearor (BioSpec Products, Bartlesville, OK, USA) and then total RNA was isolated using an RNeasy Mini Kit (Qiagen, Valencia, CA, USA) according to the manufacturer's protocol. The cDNA was reverse-transcribed using TaqMan reverse transcription reagents (Life Technologies, Carlsbad, CA, USA). Real-time PCR was performed using TaqMan Universal PCR Master Mix (Life Technologies) for each of the following: βIII-tubulin, Nestin, Ripk2, Oct3/4, and Gfap. Expression levels were normalized using glyceraldehyde-3-phosphate dehydrogenase (GAPDH).

*Immunofluorescence and image analysis*

Samples were washed 3 times in PBS, fixed in 4% paraformaldehyde, washed an additional 3 times in PBS, and permeabilized with 0.2% Triton X-100. After 2 more PBS washes, samples were blocked with 1% bovine serum albumin (BSA) in PBS for 1hr. Samples

were then incubated in primary antibodies for βIII-tubulin (TUJ1, Covance, Princeton, NJ, USA) at 1:500, followed by an appropriate secondary antibody. 4',6-diamidino-2-phenylindole (DAPI, Vectashield®, Vector Laboratories, Burlingame, CA, USA) was used to stain the nucleus. Images were acquired using a Nikon Eclipse C1 confocal microscope (Nikon, Tokyo, Japan). Cell counts were made using ImageJ using at least 1,000 cells from 3 replicate samples. Median neurite lengths were also measured with ImageJ using a population of at least 400 cells.

*Integrin blocking*

Cells were seeded as described in neural media and allowed to adhere for 24hrs. Antibodies were then added to the culture medium at 10μg/ml to block specific integrin subunits as follows: β1 (CD29, BioLegend, San Diego, CA, USA), α1 (CD49a, BioLegend), α3 (CD49c, R&D Systems, Minneapolis, MN, USA), α5 (CD49e, BioLegend), α6 (CD49f, BioLegend), and α11 (R&D Systems). Neural medium was changed daily for a total of 7 days of culture before immunofluorescence was performed.

*Western blots*

Protein was collected from samples using an EpiQuik Whole Cell Extraction Kit (Epigentek, Farmingdale, NY, USA) according to the manufacturer's protocol. 20μg of sample protein was mixed with an equal volume of 2X Laemmli buffer and heated to 95°C for 5min. The samples were then loaded into a polyacrylamide gel for electrophoresis. The protein was transferred to polyvinylidene fluoride (PVDF) membranes, blocked in 3% BSA in tris-buffered saline (TBS) with 0.05% Tween 20 (TBST), and incubated overnight at 4°C in primary antibody. Antibodies for active extracellular signal regulated kinase 1/2 at 1:2,000 (p-ERK1/2, Cell Signaling Technology, Danvers, MA, USA), total ERK1/2 at 1:1,000 (CST), active p38 at

1:1,000 (CST), and heat shock protein 60 at 1:200 (HSP60, Santa Cruz Biotechnology, Dallas, TX, USA) were used. Blots were then incubated in a secondary antibody conjugated to horseradish peroxidase (HRP) at 1:10,000 and treated with an enhanced chemiluminescent (ECL) substrate.

*Statistical analysis*

For all experiments, values are reported as a mean ± standard deviation (SD). Experiments were repeated at least 2 times to validate results. Two-way analysis of variance was used to determine the statistical significance of differences between data sets. For the neurite analysis, median lengths were calculated since the distribution was not normal. Statistical differences between medians were determined with a Mann-Whitney U test. A value of $p<0.05$ was considered to be statistically significant.

## Results

*Nanofiber morphology*

Nanofibrous matrices fabricated using TIPS had an average fiber diameter of 135±65nm and initial electrospun fibers had an average fiber diameter of 529±141nm (**Figure 2.1**A, B). Mouse D3 ESCs were seeded on both nanofibrous matrices and cultured in non-directional medium for 7 days. Cells on the electrospun fibers expressed βIII-tubulin, a late market of neuronal differentiation and also developed some neurite growth. In contrast, cells seeded on the TIPS fibers exhibited very minimal βIII-tubulin (**Figure 2.1**C, D). Clearly the cells behaved

differently on the two sets of nanofibers and we sought to determine if this could be explained by

the difference in fiber size.
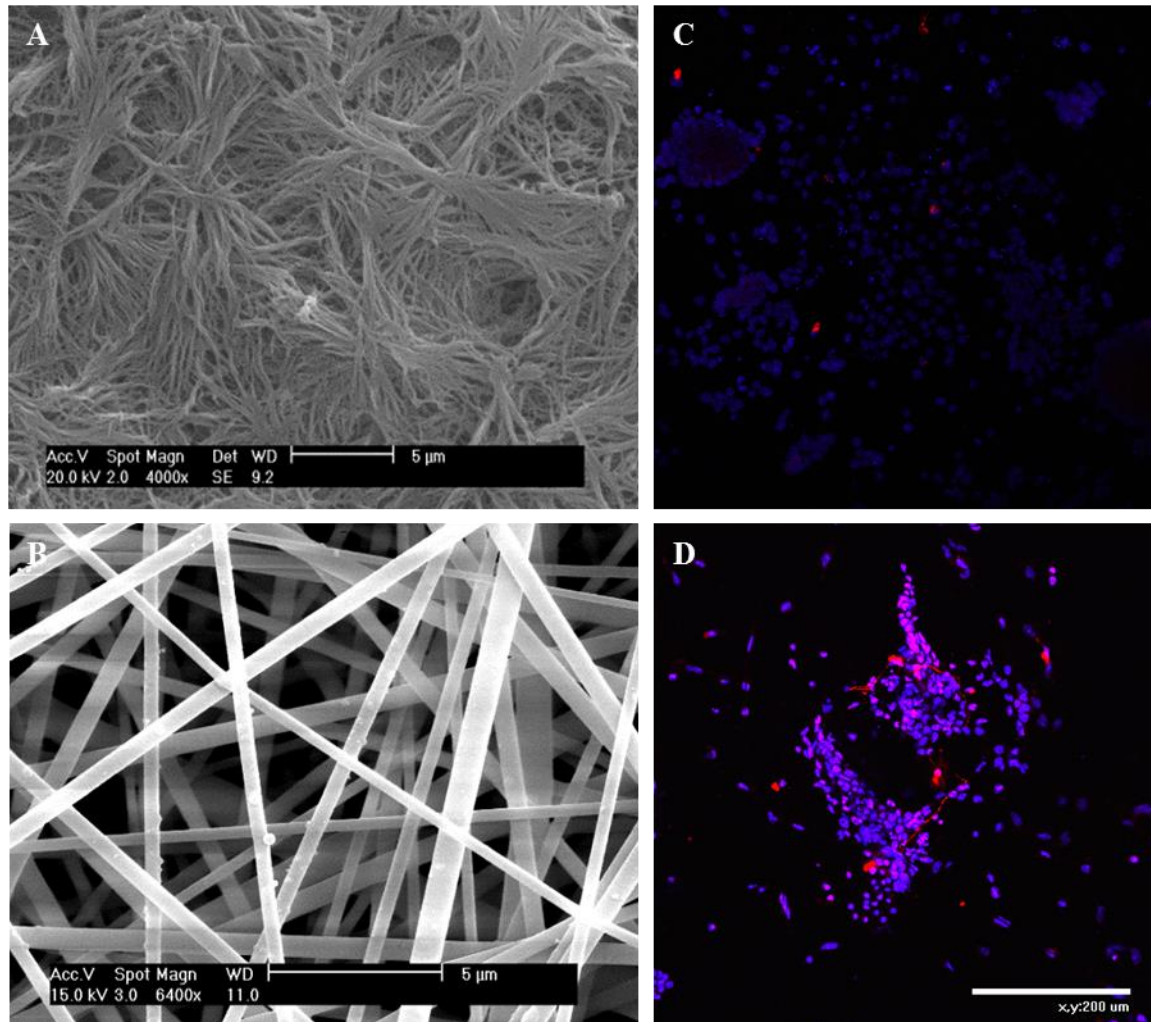


**Figure 2.1. TIPS and electrospun nanofiber morphology and ESC neuronal differentiation. A) and B) shown scanning electron micrographs of TIPS (A) and electrospun (B) nanofibers. TIPS nanofibers come in a mat of fibrous bundles while electrospun fibers are long and continuous. Immunofluorescence images (C, D) labeling with DAPI for nucleii (blue) and βIII-tubulin (red) revealed minimal βIII-tubulin on the TIPS fibers (C), while some ESCs on the electrospun fibers (D) were βIII-tubulin positive and even grew neurites. Immunofluorescence scale bar 200μm.**

Electrospinning was used to create an array of PLLA fibers with varying fiber size. The concentration of PLLA in HFIP displayed great control over modulating the fiber diameter. **Table 2.1** summarizes the nanofibrous matrices fabricated with their respective PLLA solution and resultant fiber size. **Figure 2.2** shows scanning electron micrographs of the array of nanofibers. Electrospun fibers were arranged in a pseudo-two dimensional (2D) fibrous mat in a random orientation while TIPS fibers were partly arranged in bundles in a more 2D fashion. From here on out, the nanofibers will be denoted by their size and fabrication method, with ES denoting electrospinning: TIPS, 129ES, 529ES, 901ES, and 1889ES. It should be noted that electrospinning was attempted with solutions containing less than 6% or more than 20% PLLA, however, the low concentrations yielded a large amount of beading and the high concentration solutions became overly viscous without any significant increase in fiber size.

**Table 2.1. Summary of nanofibrous matrices and fiber size.**

| Processing Method (w/v) | PLLA Solution (w/v) | Fiber Size (nm) |
|---|---|---|
| Thermally-Induced Phase Separation | 10% in THF | 135±65 |
| Electrospinning | 6% in HFIP | 129±27 |
| Electrospinning | 8% in HFIP | 529±141 |
| Electrospinning | 15% in HFIP | 901±214 |
| Electrospinning | 20% in HFIP | 1889±216 |
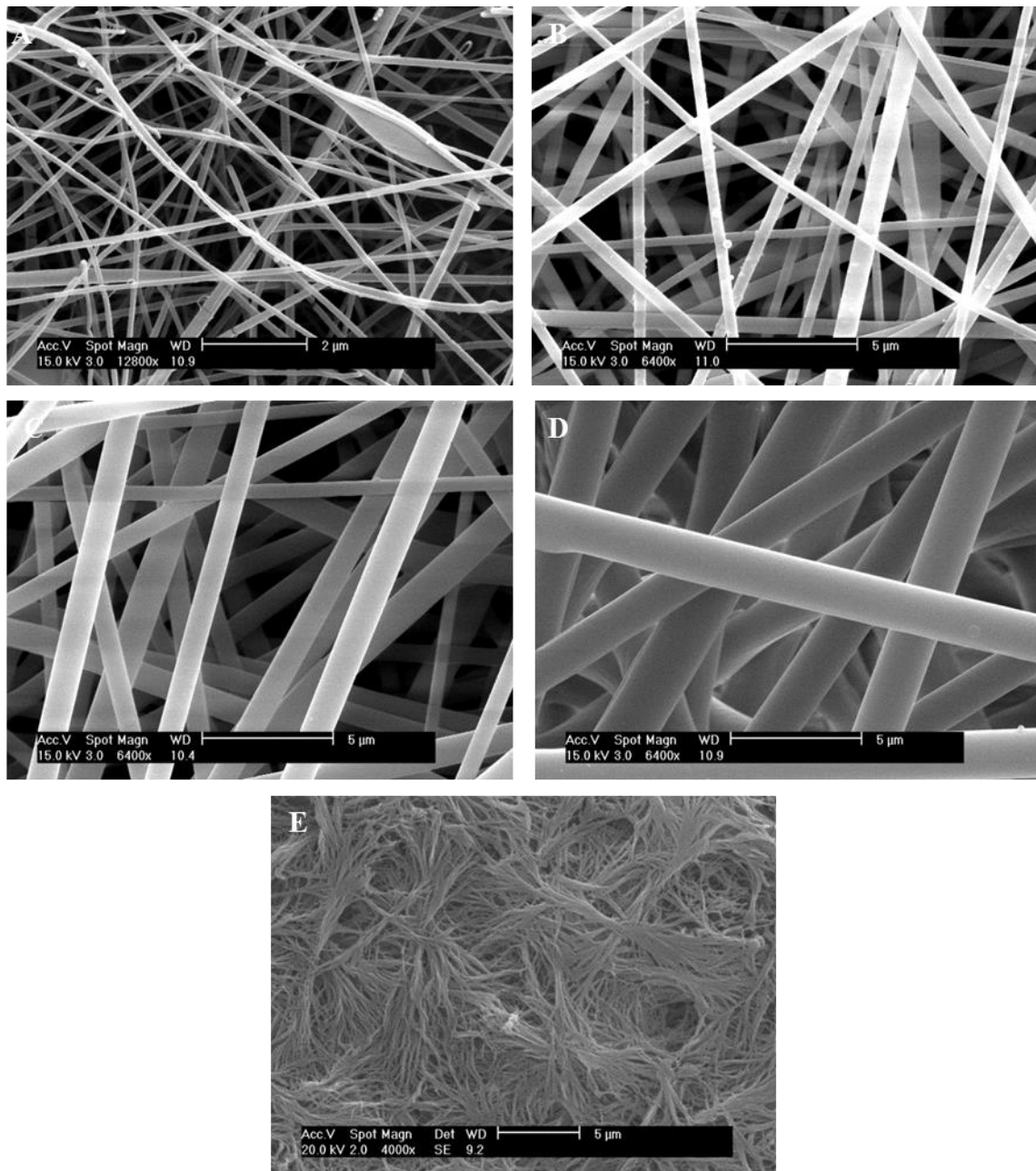
**Figure 2.2. Scanning electron micrographs of nanofibrous matrices. Nanofibers fabricated from electrospinning (A-D) and TIPS (E) exhibited differing morphologies. TIPS nanofibers (E) formed a mat of fibrous bundles. 129ES (A), 529ES (B), 901ES (C), and 1889ES (D) nanofibers were long and continuous with larger pores in between the fibers.**

*Synergistic effects of media conditions and fiber size*

ESCs were seeded on the electrospun and TIPS fibers in 3 different media conditions: non-directional (ND), neural permissive (NP), and neural. ND medium is growth medium without LIF and with a reduced amount of FBS, 2% instead of 10%, to minimize cell aggregation. NP medium is 80/20 induction medium, and neural medium is NP medium with the addition of retinoic acid (RA). After 7 days in culture, the cells were fixed and labeled with TUJ1, the antibody for βIII-tubulin, a marker for mature neuronal differentiation (**Figure 2.3**). Across the 3 media conditions, there was minimal βIII-tubulin expression on the TIPS and 129ES fibers. There was also little expression on any of the fiber sizes in the ND medium. However, in both the NP and neural media, there was a clear increase in βIII-tubulin expression as fiber size increased. From the TIPS and 129ES fibers to the 529ES fibers, there are cells that have grown small neurites. Then from the 529ES fibers to the 901ES and 1889ES fibers, more cells were βIII-tubulin positive and there were more and longer neurites.
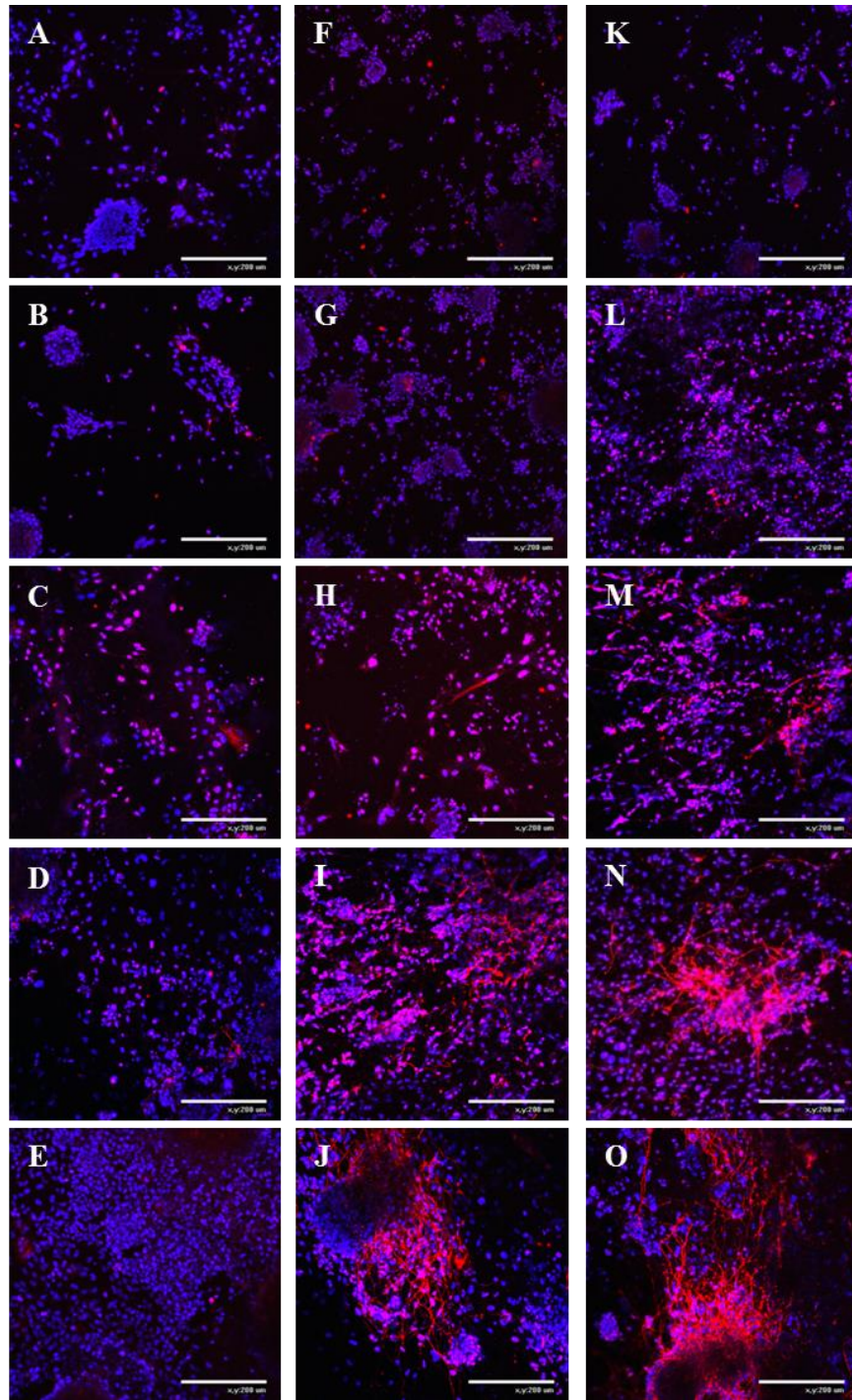
**Figure 2.3. Immunofluorescence of neurite outgrowth in different media conditions and on different fiber sizes. ESCs cultured on the array of fibers were labeled with DAPI for nucleii (blue) and βIII-tubulin (red). ESCs cultured in ND medium (A-E) exhibited little βIII-tubulin expression and neurite growth compared to cells in NP (F-J) or neural medium (K-O). On the smaller fiber sizes, TIPS (A, F, K) and 129ES (B, G, L), there was also little neurite growth. As fiber size increased to 529ES (C, H, M), there was an increase in neurite growth in NP and neural media. More noticeable, on the larger fibers, 901ES (D, I, N) and 1889ES (E, J, O), there was significant neurite growth in NP and neural media. The combination of medium conditions with an increase in fiber size resulted in a large increase in neurite growth. Scale bar 200μm.**

22

To get a better idea of the neural differentiation the ESCs undergo on the fiber sizes, we assayed the gene expression of pluripotency marker Oct3/4, early neuronal marker Nestin, mature neuronal marker βIII-tubulin, oligodendrocyte precursor marker Olig2, and astrocyte marker Gfap (**Figure 2.4**). Statistical significance was determined by comparing samples against 129ES fibers in the corresponding medium condition. For Oct3/4 (**Figure 2.4**A), there was a clear decrease in expression as fiber size increased, and this was more noticeable in the NP and neural media. Surprisingly, despite the neural medium, the smallest fibers were able to maintain some level of Oct3/4 expression, indicating some cells remained pluripotent.

Looking at Nestin (**Figure 2.4**B) and βIII-tubulin (**Figure 2.4**C), the larger fibers seemed to promote neuronal differentiation. Nestin expression was highest on the larger fibers in NP medium, while expression dropped on the larger fibers in neural medium. On the other hand, βIII-tubulin expression was highest on the 901ES and 1889ES fibers in neural medium. Thus, it seems that neural medium produces more maturely differentiated cells on the larger fibers, while NP medium, without RA, lags behind. In the ND medium, while the fiber size dependent effect was still significant for Nestin, it was negligible for βIII-tubulin. In essence, this gave evidence of a synergistic effect between the large fiber sizes and medium conditions to promote neuronal differentiation of D3 ESCs.

We also looked at two other neural markers for oligodendrocyte precursors and astrocytes. Similar to βIII-tubulin, there was minimal trend in the ND medium for Olig2 (**Figure 2.4**D) and Gfap (**Figure 2.4**E). However, Olig2 expression remained high on the TIPS and 129ES fibers in NP and neural media compared to 529ES, 901ES, and 1889ES fibers, where expression was negligible. The trend for Gfap was minimal, though there was a decrease in expression on the 901ES and1889ES fibers in NP and neural media conditions.
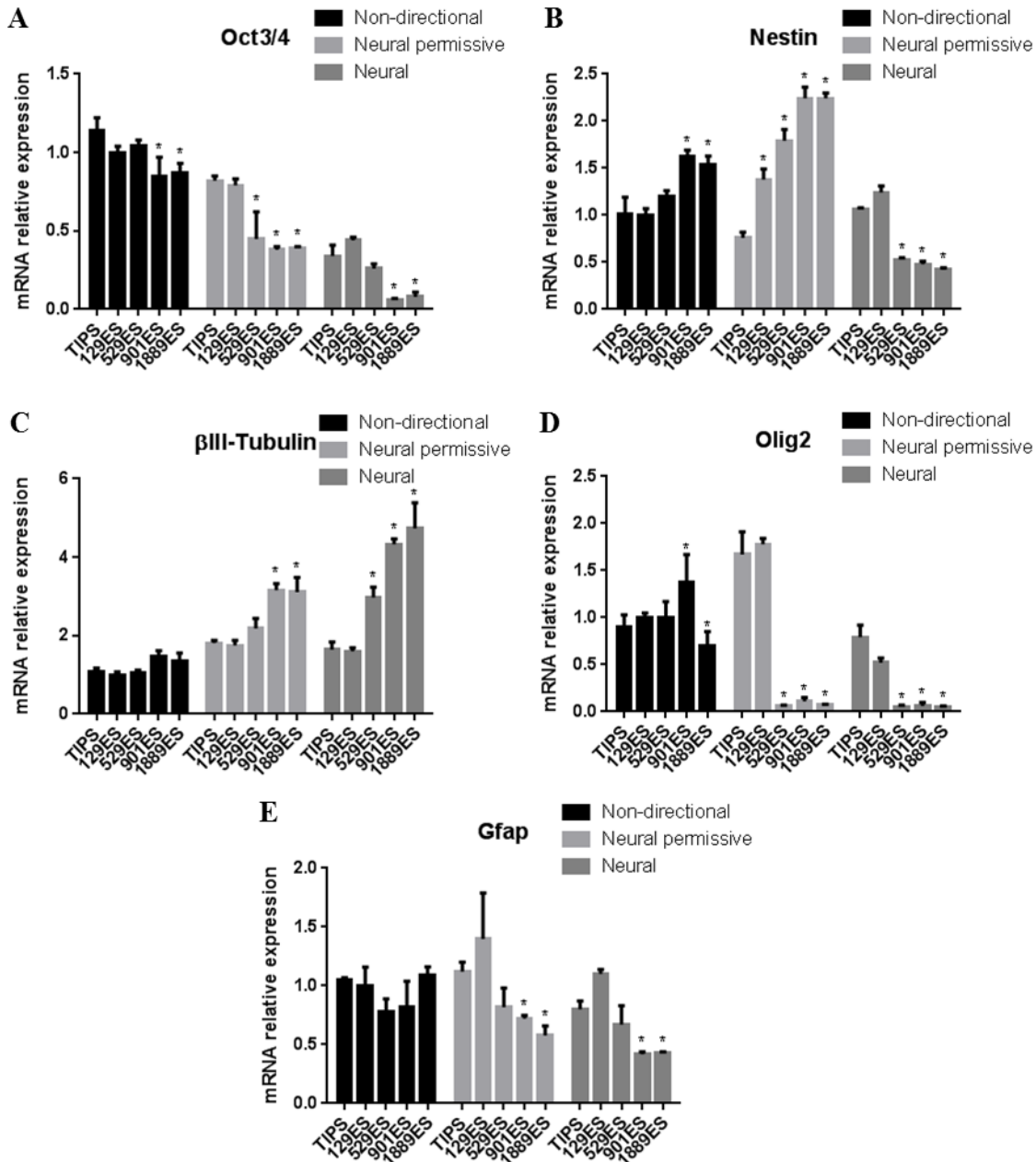
**Figure 2.4. Gene expression of ESCs in different media conditions and on different fiber sizes. Real-time PCR was used to assay the gene expression of pluripotency marker Oct3/4 (A), early neuronal marker Nestin (B), mature neuronal marker βIII-tubulin (C), oligodendrocyte precursor marker Olig2 (D), and astrocyte marker Gfap (E). Oct3/4 expression decreased as fiber size increased in the NP and neural media. Nestin expression was highest in NP medium and large fibers while βIII-tubulin expression was highest in neural medium on large fibers. Large fibers promoted neuronal differentiation with more precursors in NP medium and more mature cells in neural medium. Olig2 expression was knocked down significantly as fiber size increased in NP and neural medium. Gfap expression also decreased with increasing fiber size, indicating smaller fibers could be better for glial differentiation. Statistical significance is denoted by comparison to the129ES group in the respective medium. (\*p<0.05)**

*Integrin mediated interactions with fibers*

To elucidate the interaction between the ESCs and the nanofibers, we investigated if there were specific integrins that were responsible for the fiber size mediated effect on neuronal differentiation. The cells were allowed to adhere for 24h before antibodies against specific subunits were introduced to the neural media. We investigated subunits α1 (binds collagens including I, II, IV, V, VI, XIII [152, 153]), α3 (binds laminin [154, 155]), α5 (binds fibronectin [156]), α6 (binds laminin [154, 155]), α11 (binds collagen I, IV [157, 158]), and β1. Compared to the control where IgG was used, blocking α1, α3, α5, and α11 did not affect the fiber size dependent expression of βIII-tubulin (**Figure 2.5**A, B, C, E). However, when α6 or β1 was blocked, expression of βIII-tubulin on the larger fiber sizes was knocked down (**Figure 2.5**D, F). Thus, integrin α6β1, a major laminin receptor, was required for fiber size mediated neuronal differentiation. **Figure 2.6** corroborates this result by showing the lack of neurite growth in the presence of α6 (**Figure 2.6**F – J) or β1 (**Figure 2.6**K – O) blocking antibodies.
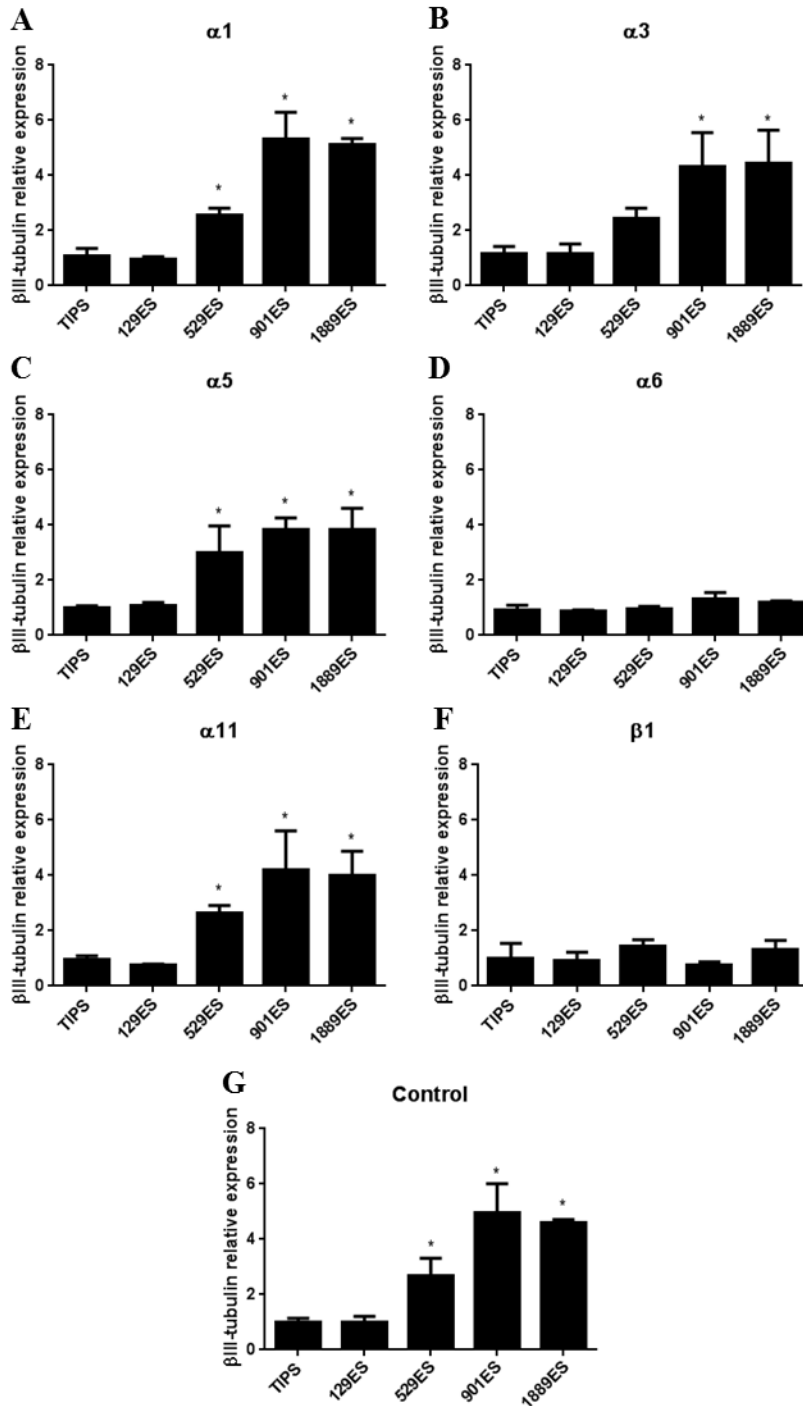
**Figure 2.5. Integrin-mediated interaction between ESCs and nanofibers. An array of integrin blocking antibodies were used to determine how the ESCs are interacting with the nanofibrous matrix with regards to neuronal differentiation. There was no difference in βIII-tubulin expression when α1 (A), α3 (B), α5 (C), α11 (D), or IgG (G) was used. However, α6 (D) and β1 (F) blocking was able to eliminate the fiber size-mediated effect on βIII-tubulin expression. Statistical significance was determined by comparison to 129ES. (\*p<0.05)**
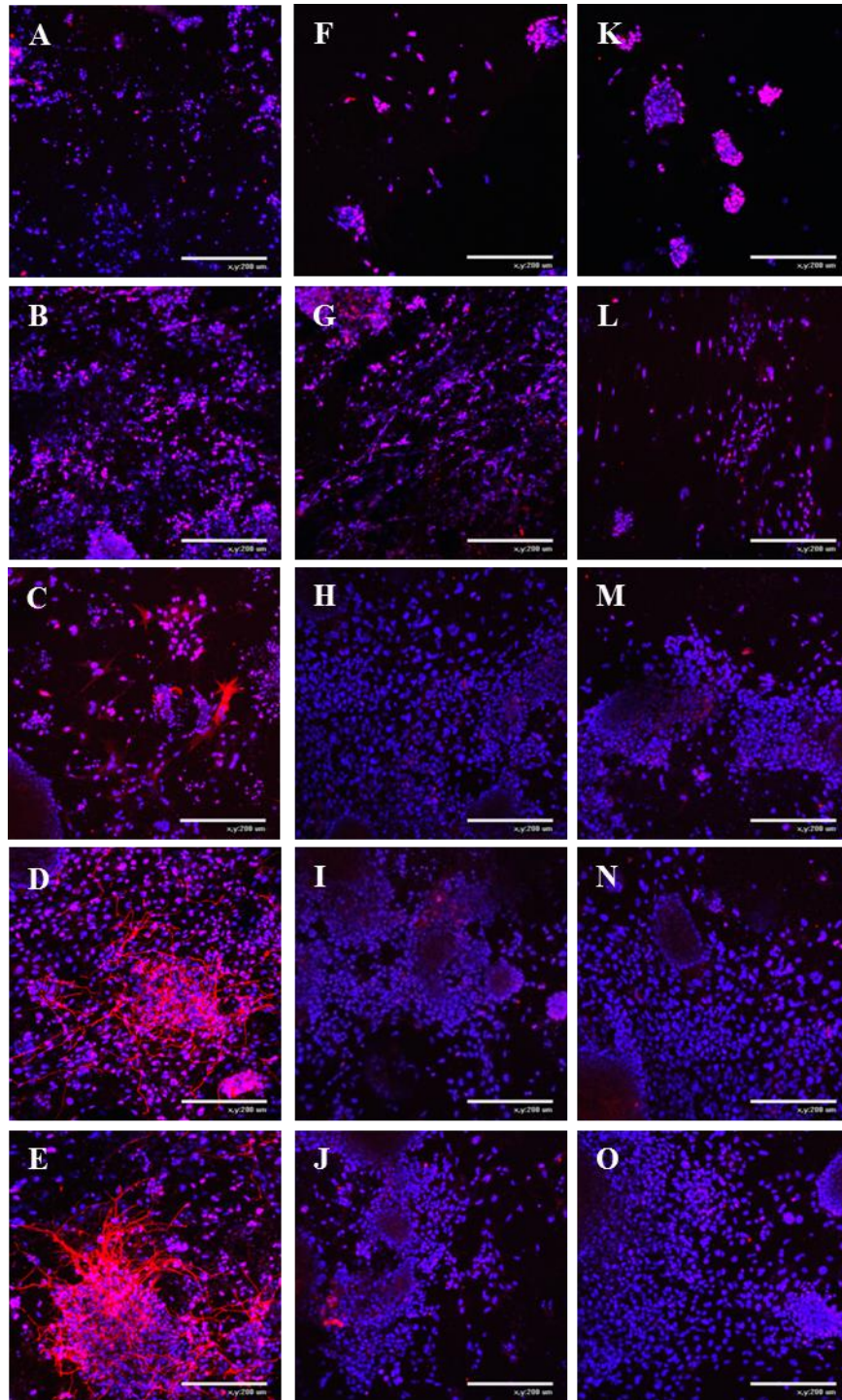
**Figure 2.6. Neurite growth in the presence of integrin blocking. Immunofluorescence of ESCs cultured on the array of fibers were labeled with DAPI for nucleii (blue) and βIII-tubulin (red). Compared to IgG (A-E), antibodies blocking α6 (F-J) and β1 (K-O) completely knocked out the ability of ESCs to form neurites on the nanofibrous matrices. A, F, K) TIPS. B, G, L) 129ES. C, H, M) 529ES. D, I, N) 901ES. E, J, O) 1889ES. Scale bar 200μm.**

After implicating integrin α6β1 for its extracellular role, we attempted to connect it to an intracellular pathway. Understanding the signaling pathway responsible for regulating stem cell fate is crucial if pluripotent cells are to be used clinically. One of the major signaling cascades is the MAPK pathway, and it has been shown to play a role in numerous cell processes, including proliferation, differentiation, cell division, apoptosis, and others. To determine if one of the MAPK cascades plays a role in fiber size mediated neuronal differentiation, we investigated the activity of ERK and p38. RA has been shown to activate ERK [147] so we used both NP and neural media to determine if the nanofibers alone were sufficient in activating ERK.

**Figure 2.7** shows the phosphorylation of p38 and ERK in the two medium conditions across the 4 electrospun fibers. In both the NP and neural media, p-p38 levels were statistically similar across the nanofibers. However, p-ERK drastically increased from the 529ES to the 901ES nanofibers. Activation was similar on the two largest fiber sizes. This trend was similar in both the NP and neural media. The addition of RA in the neural medium increased p-ERK levels across the board, maintaining the sharp jump in ERK activation from 529ES to 901ES nanofibers. With the trend present in both NP and neural media, the large nanofibers were able to increase ERK activation with the presence of RA.
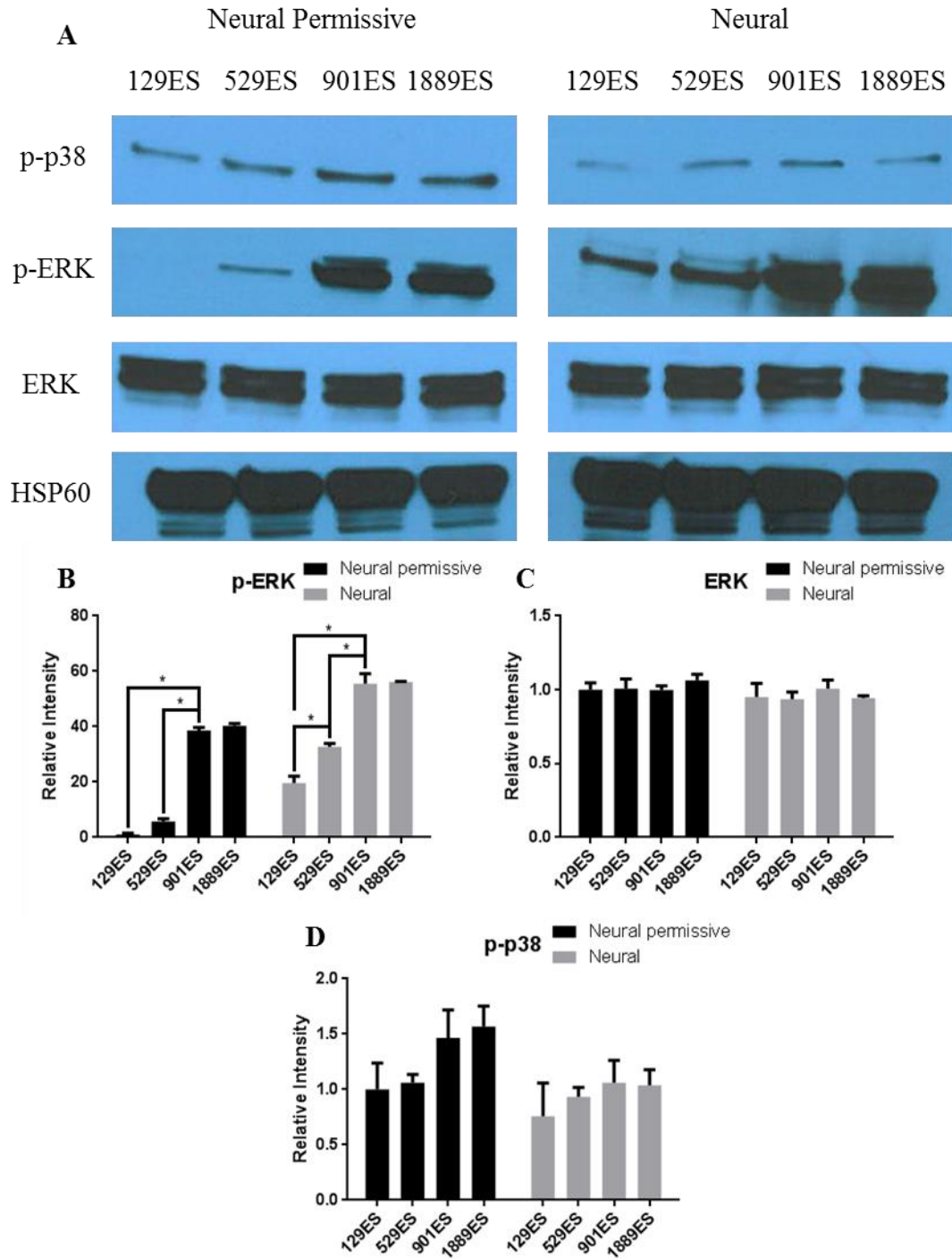
**Figure 2.7. MAPK signaling on electrospun nanofibers. Western blots for p-p38, p-ERK, total ERK, and loading control HSP60 were performed (A). While p-p38 remained relatively constant across the medium conditions and fiber sizes (D), ERK activity was significantly higher on the 901ES and 1889ES fibers (B). This trend was present both in the presence (neural) and absence (NP) of RA. (\*p<0.05)**

To further demonstrate this, timeline of ERK activation was investigated in order to see at what point ERK participates (**Figure 2.8**). D3 ESCs were seeded on 901ES fibers in neural medium in the presence and absence of 10μM U0126, an inhibitor of ERK phosphorylation. The inhibitor was used to determine if ERK was responsible for the neuronal differentiation. Prior to seeding, there was minimal p-ERK in the undifferentiated ESCs. After the first day, there was a significant increase in ERK activation. A similar level was noted on day 2, while p-ERK decreased slightly thereafter, though maintained a higher level compared to day 0. This shows that ERK is activated early with the highest levels on the first two days post-seeding, and maintains activity throughout at least the first week of differentiation. Connecting this to neurite growth, the presence of U0126 inhibited the neurite formation throughout the 5 days of culture (**Figure 2.9**)

**A**

| Day | 0 | 1 | | 2 | | 3 | | 5 | |
|---|---|---|---|---|---|---|---|---|---|
| U0126 | - | + | - | + | - | + | - | + | - |

p-ERK

ERK

**B**
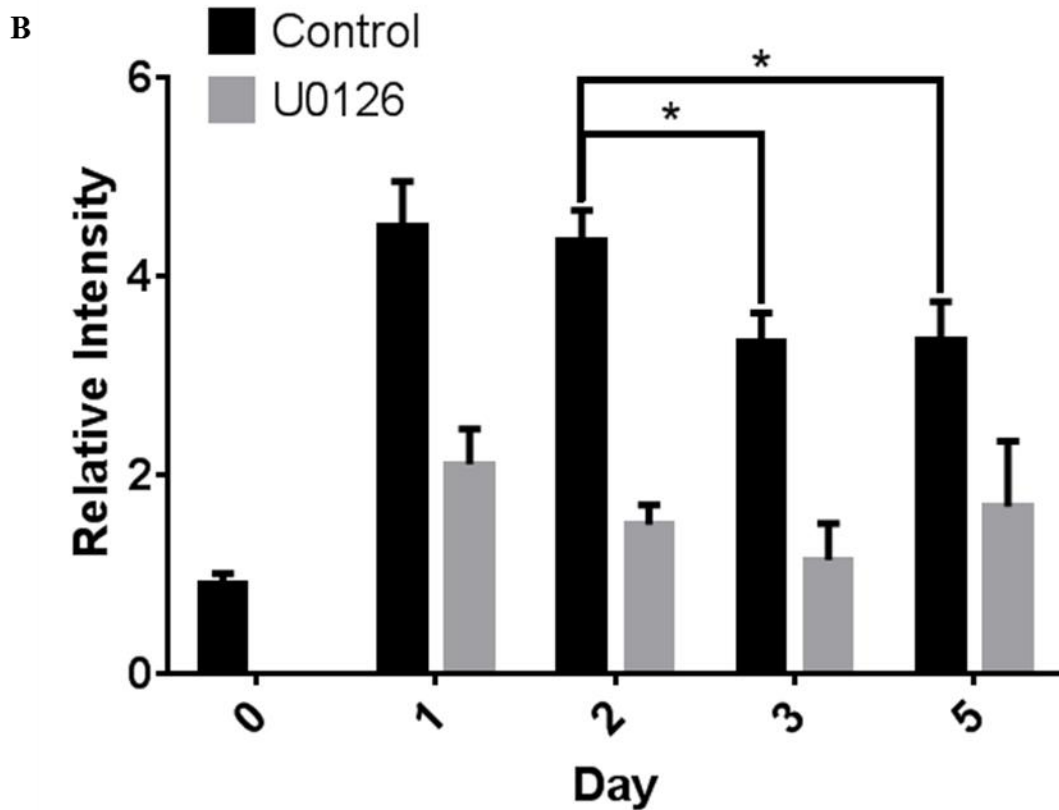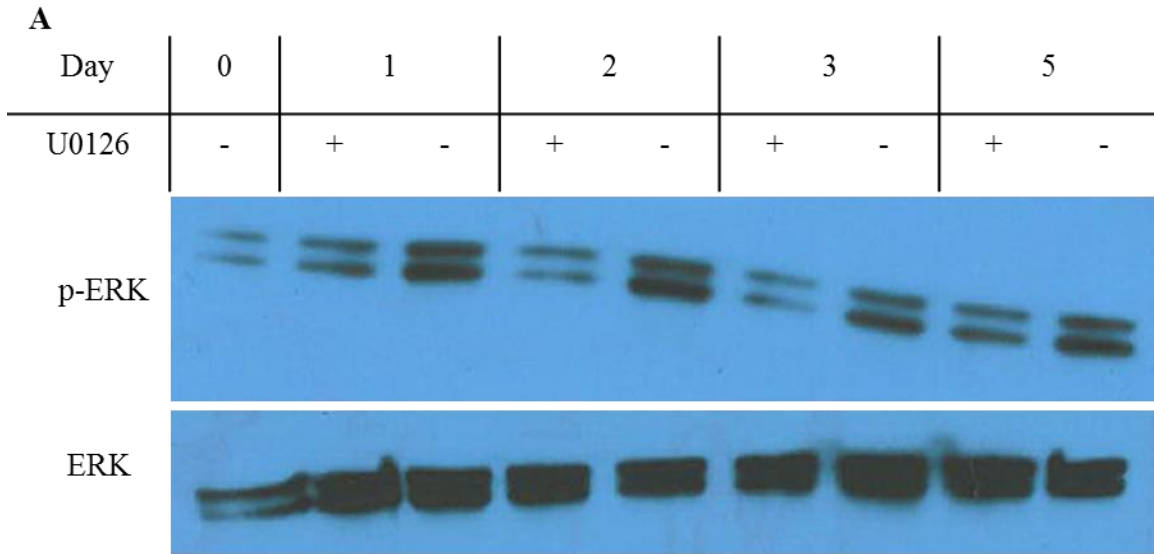
**Figure 2.8. Time-dependent activation of ERK. ESCs were seeded on 901ES nanofibers in neural medium. Day 0 indicates ESCs prior to seeding. Western blots of p-ERK and total ERK in the presence of absence of U0126 showed that ERK is active early and remains active, though p-ERK drops from day 2 to day 3 (A). U0126 was able to inhibit ERK activity to levels near day 0 (B). (*p<0.05)**

31
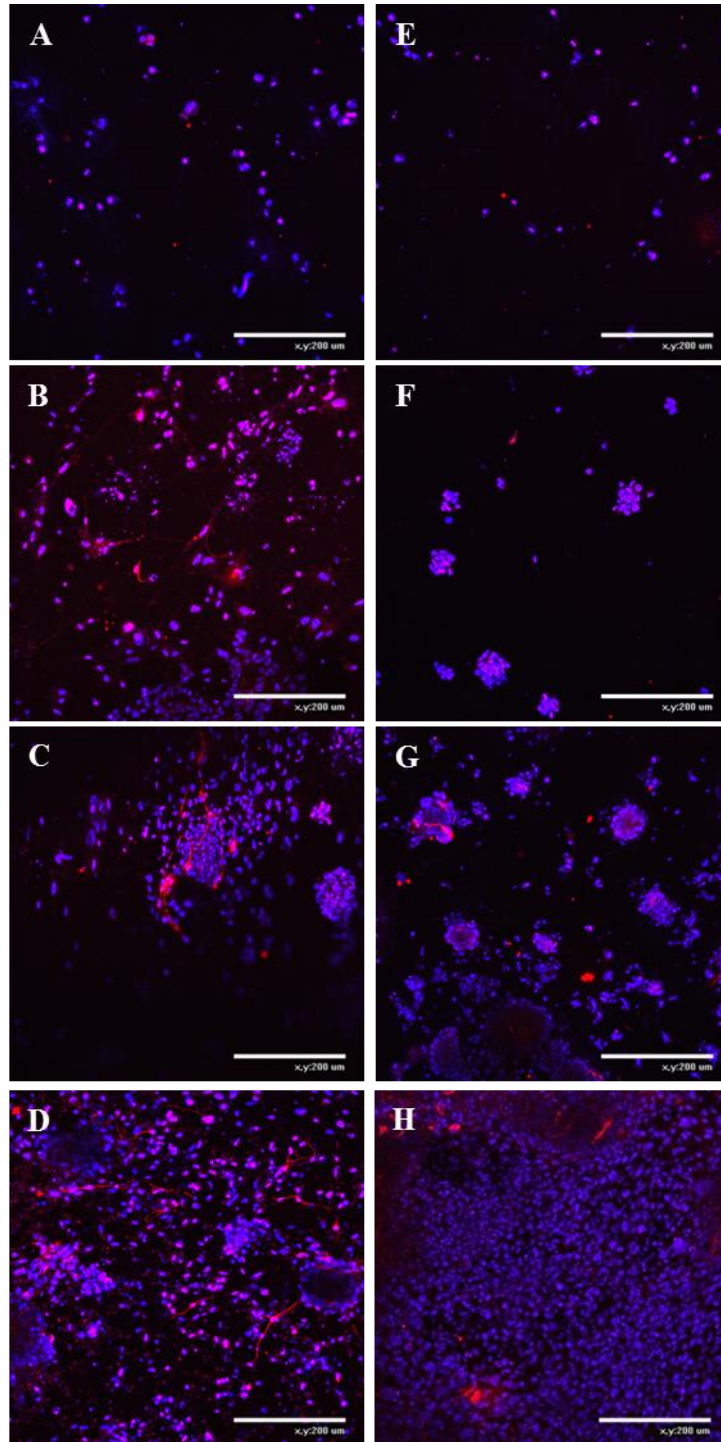
**Figure 2.9. Time dependent neurite growth with ERK inhibition. Immunofluorescence of ESCs cultured on 901ES nanofibers in neural medium were labeled with DAPI for nucleii (blue) and βIII-tubulin (red). Without U0126 (A-D), a significant amount of neurites grew by day 5. In the presence of U0126 (E-H), very few neurites formed, indicating ERK activity is required for neurite growth. A, E) Day 1. B, F) Day 2. C, G) Day 3. D, H) Day 5. Scale bar 200μm.**

**Discussion**

The extracellular environment plays an important role in maintaining pluripotency and inducing differentiation [159, 160]. During neurogenesis, alterations in both composition and structure of the ECM play a role in proliferation, cell migration, and differentiation [161-163]. For tissue engineering, which seeks to create an artificial ECM, understanding the interaction between stem cells and their ECM is critical scaffold design, especially when using pluripotent stem cells.

Nanofibrous architecture has been shown to have a significant effect on the attachment, proliferation, differentiation, and migration of numerous cell types [164]. Previous studies have been done on progenitor cells to show that fiber size can have an effect on neuronal differentiation [62, 140], however, little work has been done to study how fiber size affects ESCs. In this study, nanofibers with diameters from 129nm up to 1889nm were fabricated to investigate the behavior of mouse D3 ESCs on different fiber sizes. Larger fiber sizes greater than approximately 900nm, close to the size of focal adhesions [165], promoted neuronal differentiation in concert with neural medium containing RA. The smallest nanofibers, TIPS nanofibers around 135nm and 129ES nanofibers, inhibited differentiation and maintained a level of pluripotency.

Once the relationship between fiber size and neuronal differentiation was established, the interaction between the cells and the nanofibers was investigated. Integrin α6β1 was found to mediate the fiber size dependent neuronal differentiation of mouse D3 ESCs. Integrin α6β1 has been commonly studied for its role in liver cancer [166, 167]. In addition, α6β1 plays an early transient role in the differentiation of cardiomyocytes during development [168]. Importantly,

neural progenitor cells (NPSs) from the embryonic mammalian forebrain binds laminin through α6β1, which is vital for adhesion and migration [169]. Laminin is a key extracellular matrix protein, especially in neural development [170, 171]. This is consistent with the results in this study where α6β1 was shown to be responsible for fiber mediated neuronal differentiation.

Connecting the interaction between the cells and the nanofibers to an intracellular pathway, the activity of MAPK proteins p38 and ERK was investigated. Both p38 and ERK have been shown to have role in ESC differentiation. The activity of p38 remained relatively constant across the fiber sizes and in both NP and neural media. This is consistent with results that showed inhibition of p38 activation induced neuronal differentiation, and RA was able to inhibit p38 activity [172]. ERK activity, however, was high on the larger 901ES and 1889ES fibers. On the smaller fibers, 129ES and 529ES, p-ERK was low. The sharp jump from 529ES to 901ES nanofibers corresponded with the increased neuronal differentiation, and this occurred with and without RA. RA has been shown to increase ERK activation [147], and while our results also showed higher ERK activity with RA, the nanofibers were able to activate ERK even without RA. Finally, this nanofiber-mediated ERK activation was evident in the presence and absence of U0126, an inhibitor of the upstream kinase MEK, giving more credence to the link between ERK activation and neuronal differentiation on the large nanofibers. Other studies have linked ERK activation and neuronal differentiation in ESCs [147, 173], neural stem cells [174], and PC12 cells [149, 175], yet most used soluble factors such as RA or insulin-like growth factor to induce neuronal differentiation. The ability to induce differentiation of ESCs with nanofibers is major advancement in understanding neurodevelopment and has great implications for tissue engineering.

Electrospun nanofibers are a common scaffold material in many areas of tissue engineering, including bone [176], cartilage [176, 177], nerve [178], and many others [179, 180]. The current state of tissue engineering, specifically neural tissue engineering, is scattered, with myriad scaffold designs, materials, and cells. This works provides guidance for scaffold design, showing that nanofibers above a certain length, around 900nm, are best to induce neuronal differentiation. In addition, the implication of laminin-binding integrin α6β1 in the fiber size mediated promotion of neuronal differentiation shows that laminin could be a great choice to be incorporated in neural tissue engineering scaffolds.

In addition to the effect large nanofibers had on neuronal differentiation, the small nanofibers also seemed to have an interesting effect. Oct3/4 expression, a marker of pluripotency, remained higher than on the larger fibers, and there was also significant Olig2 expression, a marker of oligodendrocyte precursors. Nanofibers, even small ones on the order of 130nm, have been shown to induce differentiation, so the possibility of maintaining pluripotency will need to be investigated further. In addition, the potential to differentiate oligodendrocytes on nanofibers merits further study.

# CHAPTER 3

## Conducting composite PPy/PDLLA films for nerve tissue engineering

**Abstract**

The significant drawbacks and lack of success associated with current methods to treat critically sized nerve defects have led to increased interest in neural tissue engineering. Conducting polymers show great promise due to their electrical properties, and in the case of polypyrrole (PPy), its biocompatibility as well. Thus, the goal of this study is to synthesize a conducting composite nerve conduit with PPy and poly (d, l-lactic acid) (PDLLA), assess its ability to support the differentiation of rat pheochromocytoma 12 (PC12) cells *in vitro*, and determine its ability to promote nerve regeneration *in vivo*. Different amounts of PPy (5%, 10%, and 15%) are used to synthesize the conduits resulting in different conductivities (5.65, 10.40, and 15.56ms/cm, respectively). When PC12 cells are seeded on these conduits and stimulated with 100mV for 2hrs, there is a marked increase in both the percentage of neurite-bearing cells and the median neurite length as the content of PPy increased. More importantly, when the PPy/PDLLA nerve conduit was used to repair a rat sciatic nerve defect it performed similarly to the gold standard autologous graft. These promising results illustrate the potential that this PPy/PDLLA conducting composite conduit has for neural tissue engineering.

## Introduction

In the United States and Europe, approximately 100,000 peripheral nerve repair procedures are performed every year [9]. Peripheral nerve injuries can arise from trauma, cancer, or congenital defects [10, 11], and are challenging clinical issues to address. While short gaps less than 10 mm can be reconnected surgically with microsutures [12] or various nerve guidance channels [13-15], longer defects are more difficult to treat.

Despite the need, current options to regenerate critically-sized nerve defects are limited. The gold standard is the autologous nerve graft [181-183], but there are significant drawbacks including limited donor source, donor site morbidity, multiple surgical sites, and possible size mismatch. Other options include allografts and xenografts, but those run the risk of disease transmission and immune rejection. Thus, there is a significant clinical need to address critical size nerve defects.

Nerve tissue engineering is a promising approach that has shown potential to address this need with synthetic nerve conduits. There has been a significant effort dedicated to developing synthetic nerve conduits that have resulted in encouraging regeneration and some degree of functional recovery of peripheral nerve defects [35, 51, 184-186]. However, more work needs to be done to improve their efficacy compared to autologous nerve grafts.

An important aspect of synthetic nerve grafts is their ability to conduct electricity. Wilson et al. showed that electrical stimulation can significantly promote the regeneration of peripheral nerve injuries after examining a large number of animal experiments [187]. Thus, there has been a large focus on the use of conductive materials in neural tissue engineering. Researchers are hoping to develop a novel material that can meet both the conductivity demands of nerve tissue

and the requirements of tissue engineering as a whole. Ideally, this conduit should be biocompatible, biodegradable, and provide an appropriate electrical environment.

As a means to achieve this, researchers have studied electroconducting polymers, such as polypyrrole (PPy), polyaniline, and polyphosphazene. They have been investigated in recent years for a number of applications in the field of microelectronics, polymer batteries, actuators, and biomedical engineering and have been shown to have excellent electrical properties [188, 189]. For biological and medical applications, PPy has been the most widely studied [190]. Not only does it have excellent electrical properties, *in vitro* and *in vivo* studies have proven it to have favorable cell and tissue compatibility. In addition, PPy is easy to synthesize, has a readily modifiable surface, and is inexpensive, all of which are incredibly appealing for tissue engineering applications. Thus, PPy has been recognized as a promising scaffold material for nerve tissue engineering and neural prostheses [190, 191]. To demonstrate this, Schmidt et al. first electrically stimulated PC12 cells through PPy films and observed the promotion of neurite outgrowth from the cells, showing the potential use of conducting polymers for nerve tissue engineering scaffolds [192]. Subsequent studies have focused on improving the polymer scaffolds by incorporating various cues, such as neurotrophins [193], cell adhesive molecules [194, 195], and topographical features [196], emphasizing the importance of multiple signals for improved modulation of neuronal responses [197]. For example, Gomez et al. electrochemically synthesized PPy micro-channels to fabricate conductive, topographical substrates for neural interfacing, and found that PPy micro-channels facilitated axon establishment of rat embryonic hippocampal neurons [196]. These studies demonstrated that PPy is a promising candidate for nerve regeneration.

However, the majority of the work done on PPy involves *in vitro* cell evaluation. Considering its drawbacks, including its poor solubility and degradation profile, more research needs to be done *in vivo* to confirm the viability of PPy as a scaffold material.

The purpose of this study was to investigate a possible treatment for repairing damaged nerves and to overcome the current shortcomings PPy has in tissue engineering. Poly (d, l-lactic acid) (PDLLA) is widely used in peripheral nerve tissue engineering due to its good biodegradability, biocompatibility, and mechanical properties [198, 199]. In this study, a PPy/PDLLA conductive composite nerve conduit was fabricated by emulsion polymerization to take advantage of the properties of the individual polymers. The material was tested *in vitro* for its ability to support the neuronal differentiation of rat pheochromocytoma 12 (PC12) cells in response to electrical stimulation. In addition, the nerve conduits were used to bridge 10 mm defects in the sciatic nerve of Sprague-Dawley rats *in vivo*.

## Materials and Methods

*Materials*

PDLLA was purchased from Boehringer Ingelheim (Ingelheim, Germany). Pyrrole (PY) was purchased from Sigma-Aldrich (St. Louis, MO, USA). PY was vacuum-distilled at about 130°C until it became a colorless liquid, and then stored at 4°C in the dark until use. All other chemicals were analytical grade reagents.

*Preparation of PPy/PDLLA nerve conduits*

The schematic for preparing PPy/PDLLA is outlined in **Figure 3.1**. PDLLA was dissolved in $CHCl_3$ to obtain a 10% (w/v) solution. For the emulsion polymerization of PPy, PY and 0.7% (w/v) sodium dodecyl sulfate (SDS, 99%, Sigma-Aldrich) aqueous solution were added to the PDLLA/$CHCl_3$ solution under stirring for 2hrs. The weight ratio of PY to PDLLA was 5%, 10% and 15%. Then 10% (w/v) $FeCl_3$ aqueous solution ($FeCl_3$:PY=5.3) was added drop-wise into the mixture under vigorous stirring to trigger oxidative polymerization. The polymerization continued at room temperature for 5hrs to obtain a PPy/PDLLA composite emulsion. A cylindrical mandrel was inserted into the PPy/PDLLA composite emulsion for several seconds, and then it was taken into alcohol to remove the $CHCl_3$ and water. This was repeated until a 0.2±0.05mm thick film on the cylinder mandrel was obtained. After drying, the conduit was removed from the mandrel and stored in a vacuum oven before use. To fabricate the films for cell culture studies, the PPy emulsion polymerization in a PDLLA solution continued at room temperature for 5hrs, followed by precipitation with ethyl alcohol and washing in deionized water. The 0.2mm thick films were obtained by casting the precipitated PPy/PDLLA composite onto a polytetrafluoroethylene (PTFE) plate and vacuum-dried for 2 days. Then these films were washed with alcohol and deionized water for three times before being used for cell culture.
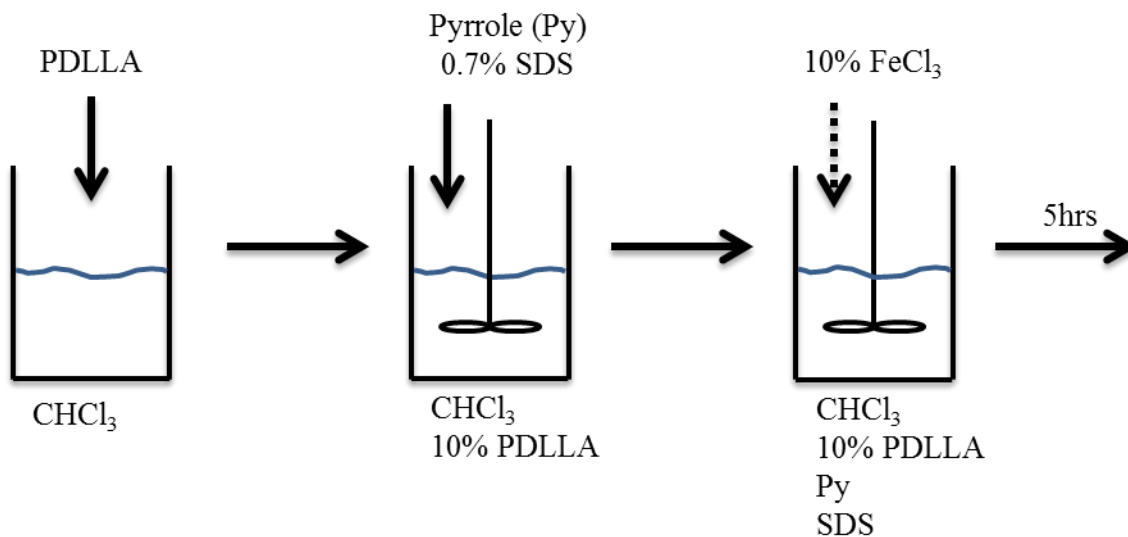
**Figure 3.1. Schematic for emulsion polymerization of PPy in PDLLA to make PPy/PDLLA.**

*PPy/PDLLA characterization*

The chemical compositions were characterized through the attenuated total reflectance Fourier transform infrared spectroscopy (ATR-FTIR) transmission spectra on a Nicolet Nexus FTIR Spectrometer (Nexus, Thermo Scientific, Waltham, MA, USA). The conductivity of the PPy/PDLLA conduits was tested by the 4-point probe method using the Hall Effect testing system (HL5500PC, Nanometrics, Milpitas, CA, USA). The nerve conduit surface elemental composition was characterized by using XPS (Escalab MK II, VG Scientific, East Sussex, UK). The morphology at the surface of the PPy/PDLLA conduit was observed using a JSM-5610LV scanning electron microscope (JEOL, Tokyo, Japan) with an accelerating voltage of 10kV. Prior to observation, the specimens were sputter-coated with gold.

*Sample preparation for in vitro evaluation*

Rectangular sections of the PDLLA and PPy/PDLLA films were cut and placed in a device similar to previously described (**Figure 3.2**) [200]. Briefly, the film was placed on a thin section of polydimethylsiloxane (PDMS, Sylgard 184®, Dow Corning, Midland, MI, USA) covering a glass slide. Two wires were placed on either side of the film and covered with a PDMS well to seal the wires from the inner chamber (1cm × 1cm × 1cm dimension). The device was clipped together on two sides and sterilized under UV light for 2hrs. The films were then incubated in a 0.1mg/ml solution of rat tail type I collagen (Sigma) for 24hrs at 4°C, washed twice with sterile tissue culture water for 5min each, and stored in phosphate buffered saline (PBS) at 4°C overnight.
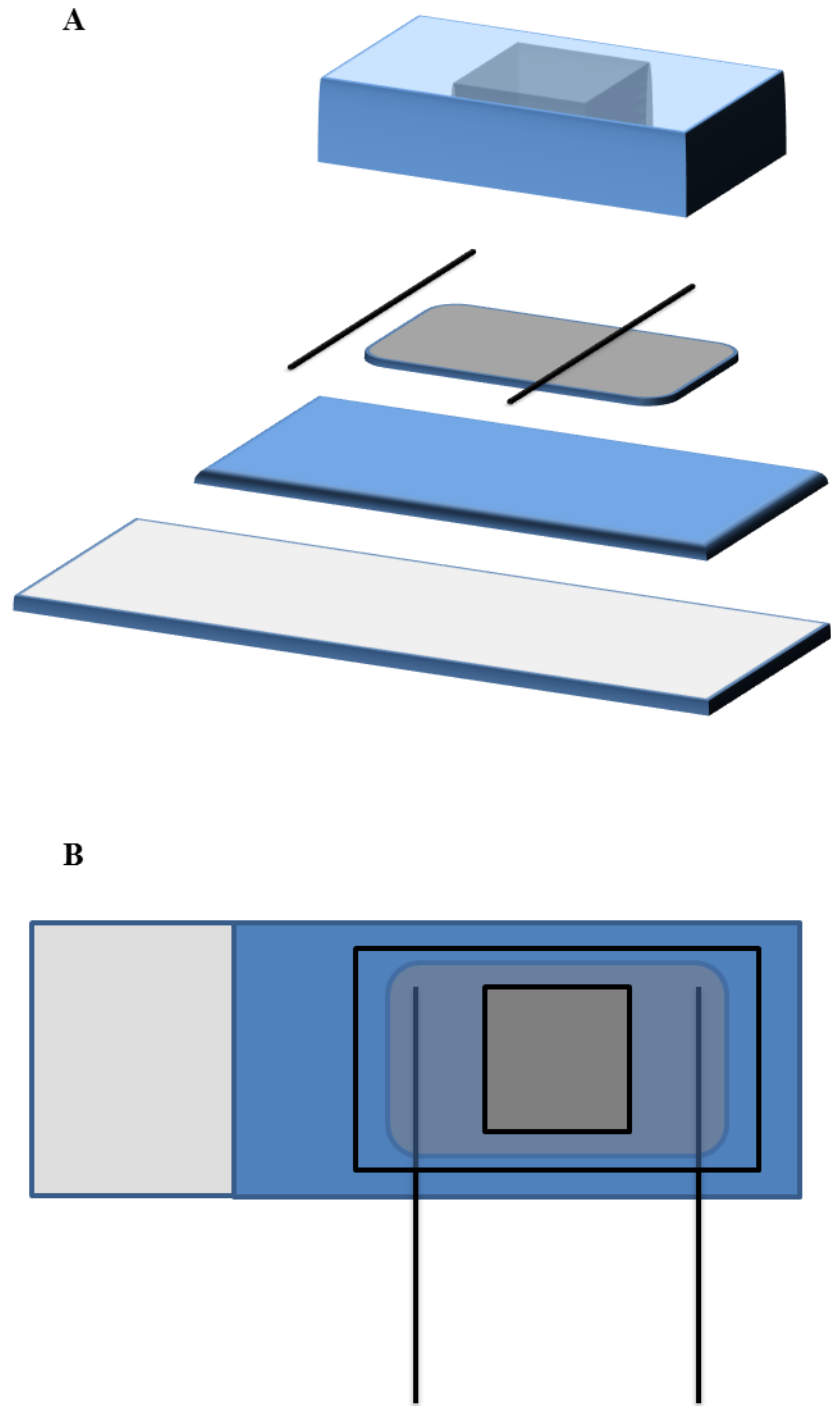
**Figure 3.2. Diagram of device used for electrical stimulation. A) Angle view. B) Top view.**

*PC12 cell culture and immunofluorescence*

PC12 cells were cultured in F-12K medium (ATCC, Manassas, VA, USA) supplemented with 15% heat-inactivated horse serum (Gibco®, Life Technologies, Carlsbad, CA, USA), 2.5% fetal bovine serum (Gibco®), and 1% Penicillin/Streptomycin solution (Gibco®) and maintained in a humid 37°C incubator with 5% $CO_2$. Three days prior to seeding, the cells were primed with 50ng/ml nerve growth factor (NGF, PeproTech, Rocky Hill, NJ, USA).

Primed cells were seeded at a density of $2 \times 10^4$ cells/cm$^2$ and allowed to adhere for 24hrs. A 100mV potential was then applied across the wires for 2hrs and the cells were cultured for an additional 24hrs. After a total of two days in culture and 24hrs post-stimulation, the cells were fixed in a 4% formaldehyde (Thermo Scientific) in PBS solution for 10min, permeabilized in a 0.1% Triton X-100 (Sigma) in PBS solution for 6min, and then blocked in 1% bovine serum albumin (Sigma) in PBS solution for 30min. The cells were labeled with Alexa Fluor® 555 phalloidin (Life Technologies), excitation at 555nm and emission at 565nm, for 20min and with 4',6-diamidino-2-phenylindole (DAPI, Vectashield®, Vector Laboratories, USA), excitation at 360nm and emission at 460nm, before being sealed under a coverslip and immediately visualized under a confocal fluorescence microscope (Nikon Eclipse C1, Tokyo, Japan). Six samples (n=6) for each film and condition were studied.

*Immunofluorescence image analysis*

Image J software (National Institutes of Health, Bethesda, MD, USA) was used to process and analyze the fluorescent images. The two parameters measured were the percentage of neurite-bearing cells and the median neurite length. The median neurite length was chosen to

account for the non-normal distribution and a cut-off of at least a 5µm neurite length was used [201]. At least 400 PC12 cells were examined for each film and condition.

*Surgical procedure*

Adult Sprague-Dawley (SD) rats were purchased from Tongji Medicinal School, Huazhong University of Technology (Wuhan, Hubei, China). All animals were housed under standard conditions, and the experimental procedures involving animals were in accordance with NIH Guidelines for the Care and Use of Laboratory Animals and under the approval of the Administration Committee of Experimental Animals, Hubei Province, China. The surgical procedure was carried out as described previously [202]. Rats weighing 200-250g were used to evaluate the nerve regeneration performance of PPy/PDLLA conduits. The animals were divided into 3 groups, each with 20 rats. 10mm defects in the sciatic nerve created by surgical removal of the nerve tissue were connected with PPy/PDLLA conduits, PDLLA conduits, or autologous nerve grafts. The surgical procedure was performed on the sciatic nerve of the right hind limb. The left limb sciatic nerve served as a pairwise control. The animals were anesthetized with 50mg/kg body weight pentobarbital sodium. The right sciatic nerve was exposed after the skin incision, and the muscles around the nerve tissues were separated using blunt dissection. Subsequently, the right sciatic nerve was severed into proximal and distal segments at the center of the right thigh. Both the proximal and the distal stumps were secured with 8-0 nylon to a depth of 1mm into the conduits, leaving a 10mm gap between the stumps. For the autograft group, after a skin incision, the sciatic nerve was exposed through a gluteal muscle-splitting incision, externally dissected to excise a 10mm nerve, and sutured back to the nerve by epineurial coaptation serving as the autograft control. The muscle layer was re-approximated with 4-0 chromic gut sutures, and the skin was closed with 2-0 silk sutures. Each rat received one

implant, which was removed at either 3 or 6 months. Walking track, electrophysiological, and histomorphometric evaluations were performed to evaluate nerve regeneration.

*Walking track analysis*

To evaluate the behavior of the rats after nerve injury and repair, walking track analysis was performed at 3 and 6 months post-operatively as described previously[203]. Briefly, the rats were allowed to walk down a wooden walking alley ($5.0 \times 8.0 \times 45cm^3$) with a darkened goal box at the end. The floor of the alley was covered with white paper. A thin film of acrylic paint was applied to the rat's plantar surface to achieve the visualization of important anatomical landmarks of the footprints. As the rats moved down the track, they left footprints on the track and recordings of footprints were made. This process was repeated a minimum of 3 times until clear footmarks were obtained. From the footprints, the following parameters were obtained: distance from the heel to the top of the third toe (print length, PL); distance between the first and the fifth toe (toe spread, TS) and distance from the second to the fourth toe (intermediary toe spread, IT). These measures were made for both the non-operated foot (measurements for this foot are designated as NPL, NTS and NIT) and the operated, experimental foot (measurements for this foot are designated as EPL, ETS and EIT). In the control animals, parameters of the right foot were compared with those from the left foot. In order to calculate the sciatic function index (SFI), these parameters were inserted into an equation used in previous studies [204-206]:

$$SFI = (-38.3 \times PLF) + (109.5 \times TSF) + (13.3 \times ITF) - 8$$

in which PLF = (EPL-NPL)/NPL; TSF = (ETS-NTS)/NTS; and ITF = (EIT-NIT)/NIT.

Interpolating identical values of PL, TS, and IT from the right and the left hind feet results in a value close to zero in normal rats. A value of -100 implies total impairment.

*Triceps surae weight analysis*

After performing the electrophysiological evaluation studies at 3 and 6 months, the animals were sacrificed and their triceps surae muscle was dissected. The moist weights of the triceps surae muscle were measured. After gently blotted with absorbent paper to remove any excess blood or serum on the surface of the retrieved tissue, the muscle was promptly weighed. To measure the target muscle reinnervation, the triceps surae muscles from the experimental and contralateral sides (un-operated) were weighed. The relative weights were presented as percentages.

$$Triceps\ surae\ weight\ \% = \frac{Triceps\ surae\ weight\ of\ the\ operated\ leg}{Triceps\ surae\ weight\ of\ the\ unoperated\ leg}$$

*Electrophysiological assessment*

Electrophysiological tests were performed on the animals three and six months after implantation. Under anesthesia, the right sciatic nerve was exposed and nerve stimulation electrodes were placed at the proximal part of the proximal joint access and recording electrodes placed in the lower leg triceps. Nerve conduction velocities (NCVs) were recorded on the lower leg triceps.

*Histological assessment*

The implanted conduits were harvested immediately after recording the NCVs. At the same time, the nerve grafts were fixed in a cold buffered 3% glutaraldehyde solution. The nerve grafts were then washed in PBS and the sciatic nerve sections were then taken from the middle regions of the regenerated nerve. After fixation, some tissues in each group were embedded in olefin, cut to 4mm thickness, and stained with hematoxylin and eosin. The other samples were

embedded in Epon 812 epoxy resin and stained with methylene blue. All nerve sections were observed under a light microscope (TE2000-U, Nikon). An image analysis system (Image-Pro Plus, Media Cybernetics, Rockville, MD, USA) was used to analyze the photographs to determine the number and areas of individual myelinated axons.

Electron microscopy was also employed to evaluate the myelin sheath regeneration. Ultra-thin sections of the regenerated nerve tissues were stained with lead citrate and uranylacetate, and then were examined under a transmission electron microscope (TEM, JEM-1200 EX, JEOL,Tokyo, Japan).

*Statistical analysis*

All numerical data are given as mean ± standard deviation. Significant differences among groups were analyzed by one-way analysis of variance (ANOVA) followed by Tukey's post hoc test using SPSS 13.0 software for Windows student version. Statistically significant differences between medians were determined with a Mann-Whitney U test. A statistically significant difference was defined as $p < 0.05$.

## Results

*Preparation and characterization of PPy/PDLLA conduits*

Pyrrole (PY) was oxidized and polymerized to PPy in a PDLLA solution using $FeCl_3$ as an oxidant and doping agent and sodium dodecyl sulfate (SDS) as an emulsifier. Then the PPy/PDLLA emulsion was used to prepare the PPy/PDLLA conduits through a repeated dip coating method with a cylindrical mandrel. Attenuated total reflectance Fourier transform

infrared spectroscopy (ATR-FTIR) was used to obtain the FTIR spectra of the PDLLA, PPy/

PDLLA, and PPy (**Figure 3.3**). In the spectrum of PPy/PDLLA, the band at $1752cm^{-1}$ is a

characteristic peak of PDLLA. The two bands at $1544cm^{-1}$ and $1040cm^{-1}$ are characteristic PPy

peaks. All the above three peaks are present in the PPy/PDLLA spectrum, verifying that the

PPy/PDLLA was successfully synthesized.
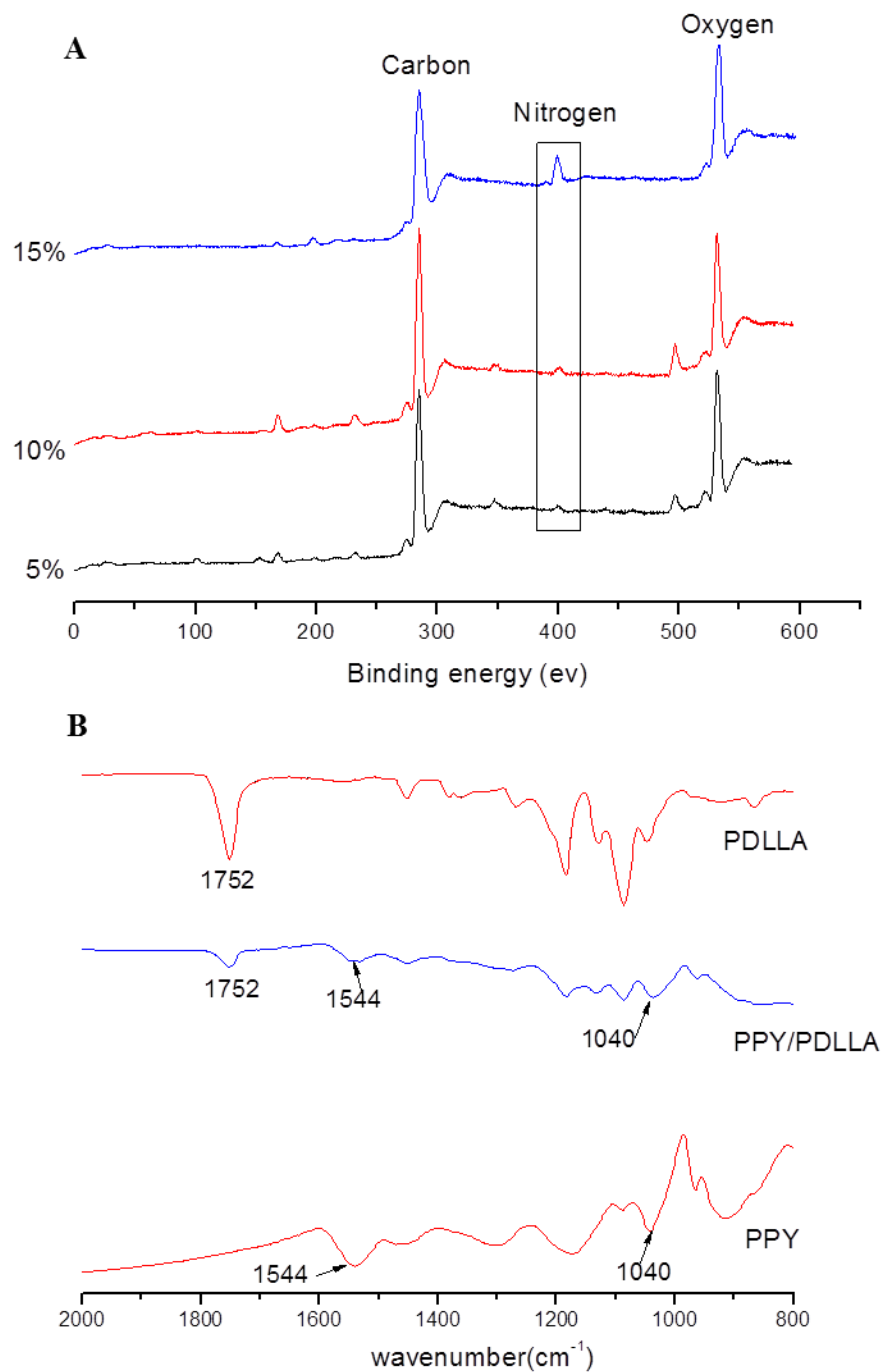
**Figure 3.3. Characterization of PPy/PDLLA synthesis. A) ATR-FTIR spectra of PDLLA, PPy/PDLLA and PPy. B) XPS of different ratio PPy/PDLLA conduits.**

PPy/PDLLA conduits with a length of 12mm, an inner diameter of 1.6mm and an outer diameter of 2.0mm were fabricated. The photographic images and scanning electron micrographs of the PPy/PDLLA films and conduits are shown in **Figure 3.4**. **Figure 3.4**A shows the PPy/PDLLA film while **Figure 3.4**B and **Figure 3.4**C show the PPy/PDLLA conduit. **Figure 3.4**D, E, and F show the surface morphology of the 5%, 10%, and 15% PPy/PDLLA conduits, respectively.
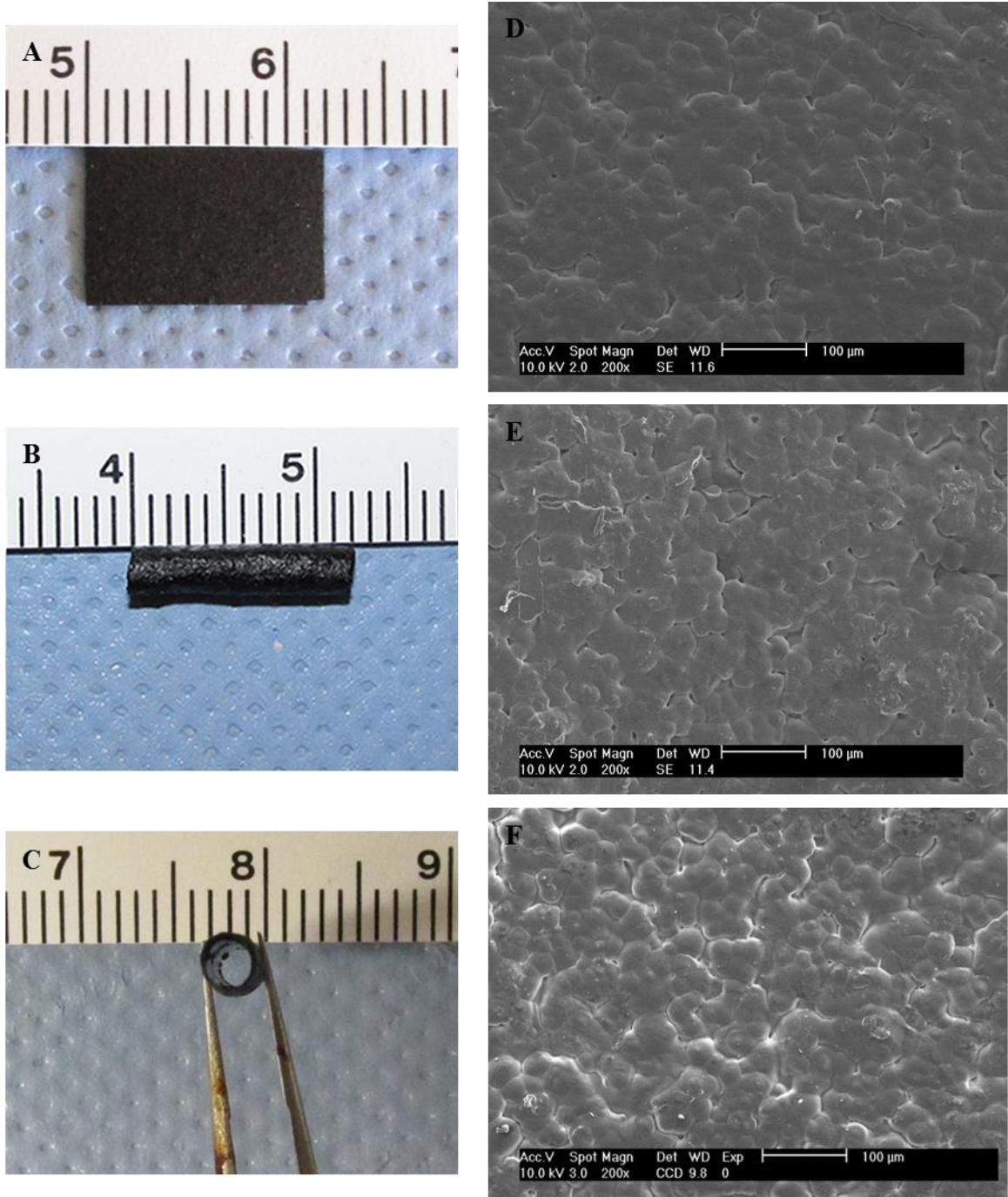
**Figure 3.4. Images and scanning electron micrographs of PPy/PDLLA films and conduits. A) Image of the PPy/PDLLA film. B) and C) Image of the PPy/PDLLA nerve conduit. D), E), and F) SEM micrographs of the surface morphology of 5%, 10%, and 15% PPy/PDLLA, respectively.**

The surface elemental compositions of the different PPy/PDLLA weight ratio conduits were analyzed using X-ray photoelectron spectroscopy (XPS) to quantify the amount of PY incorporated onto the conduit surface. All the PPy/PDLLA conduits contained C, N and O, and the content of element N was 1.74%, 1.98% and 2.51% for the 5%, 10%, and 15% PPy/PDLLA weight ratios, respectively (**Table 3.1**). The measured conductivity of a PPy/PDLLA conduit was higher as the weight ratio of PPy increased (**Table 3.1**).

**Table 3.1. Content of C, N, and O and conductivity test results for different PPy/PDLLA materials.**

| Sample | Content (%) | | | Conductivity (mS/cm) |
|---|---|---|---|---|
| | C | N | O | |
| 5% PPy/PDLLA | 74.22 | 1.74 | 24.04 | 5.65 |
| 10% PPy/PDLLA | 75.92 | 1.98 | 22.11 | 10.40 |
| 15% PPy/PDLLA | 73.97 | 2.51 | 23.53 | 15.56 |

*Cell culture evaluation*

PC12 cells were employed to study the effect that PPy/PDLLA films combined with electrical stimulation had on their behavior. In theory, this would provide an indication of how viable the PPy/PDLLA composite is for use in nerve tissue engineering. The cells were allowed to adhere to the collagen type I coated substrate for 24hrs before being stimulated with 100mV for 2hrs [192, 193]. After stimulation, the cells remained in culture for an additional 24hrs. PC12 cells were able to adhere to the array of PDLLA and PPy/PDLLA films and were viable throughout culture. There was no significant difference in the cell number throughout the experiments on any of the films (data not shown), indicating that the PPy content did not have any significant effect on adhesion or proliferation. The control cells, where no electrical

stimulation was applied, had minimal levels of differentiation across the board. Cells that were

stimulated with 100mV for 2hrs exhibited more and longer neurites, as can be seen on the actin-

labeled cells (**Figure 3.5**). On all of the control films, approximately 13% of the cells (**Figure**

**3.6**A) formed neurites with a median length around 8μm (**Figure 3.6**B). However, there was a

clear increase in both the percentage of neurite-bearing cells and the median neurite length for

the cells stimulated with 100mV for 2hrs as the PPy content increased. The percentage of

neurite-bearing cells increased from 12.5±1.3% on the PDLLA to 17.3±1.7%, 20.8±2.2%, and

22.8±2.1% on the 5%, 10%, and 15% PPy/PDLLA, respectively. The median neurite length

increased from 7.5μm on the PDLLA to 9.9μm, 11.5μm, and 12.6μm on the 5%, 10%, and 15%

PPy/PDLLA, respectively.
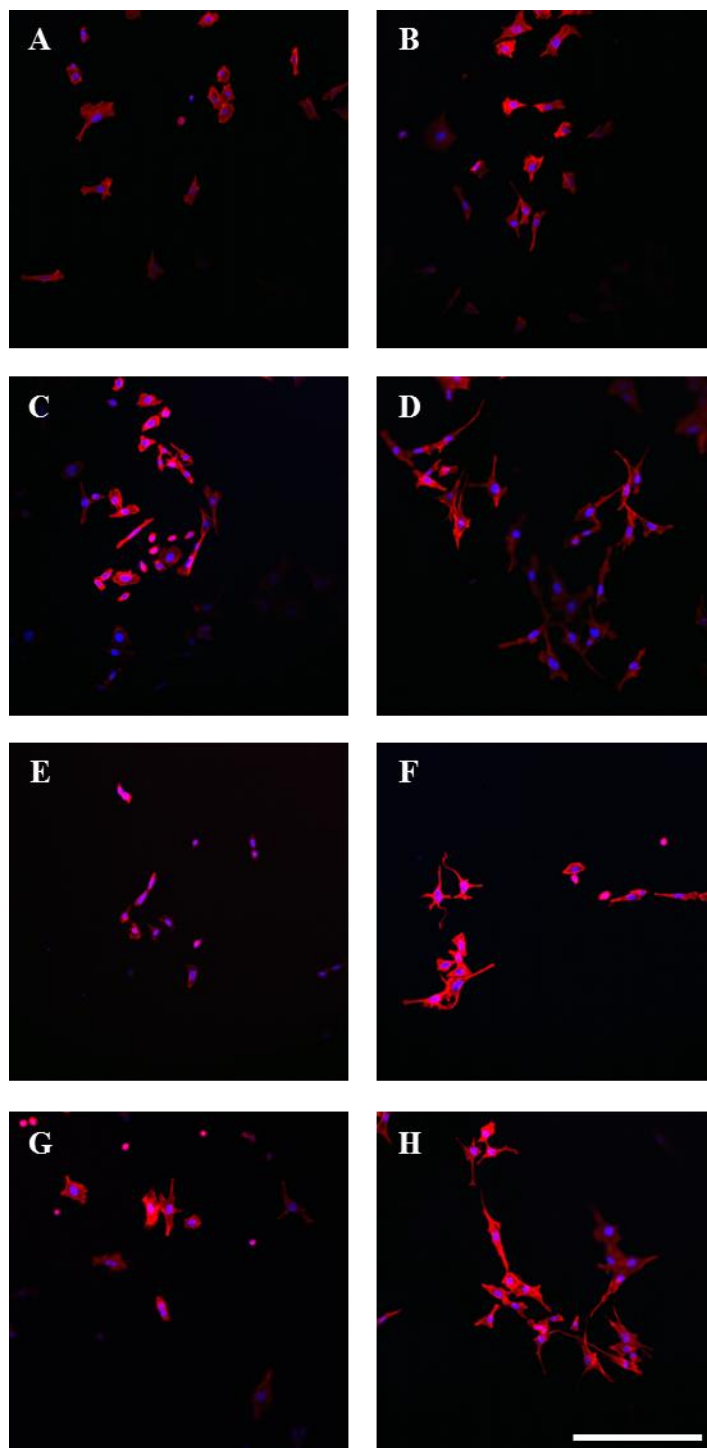
**Figure 3.5. Fluorescent images of PC12 cells on PPy/PDLLA films. Cells were labeled for actin (red) and nuclei (blue). A) and B) PDLLA. C) and D) 5% PPy/PDLLA. E) and F) 10% PPy/PDLLA. G) and H) 15% PPy/PDLLA. A), C), E), and G) Control cells. B), D), F), and H) Cells stimulated with 100mV for 2hrs. Scale bar 200μm.**
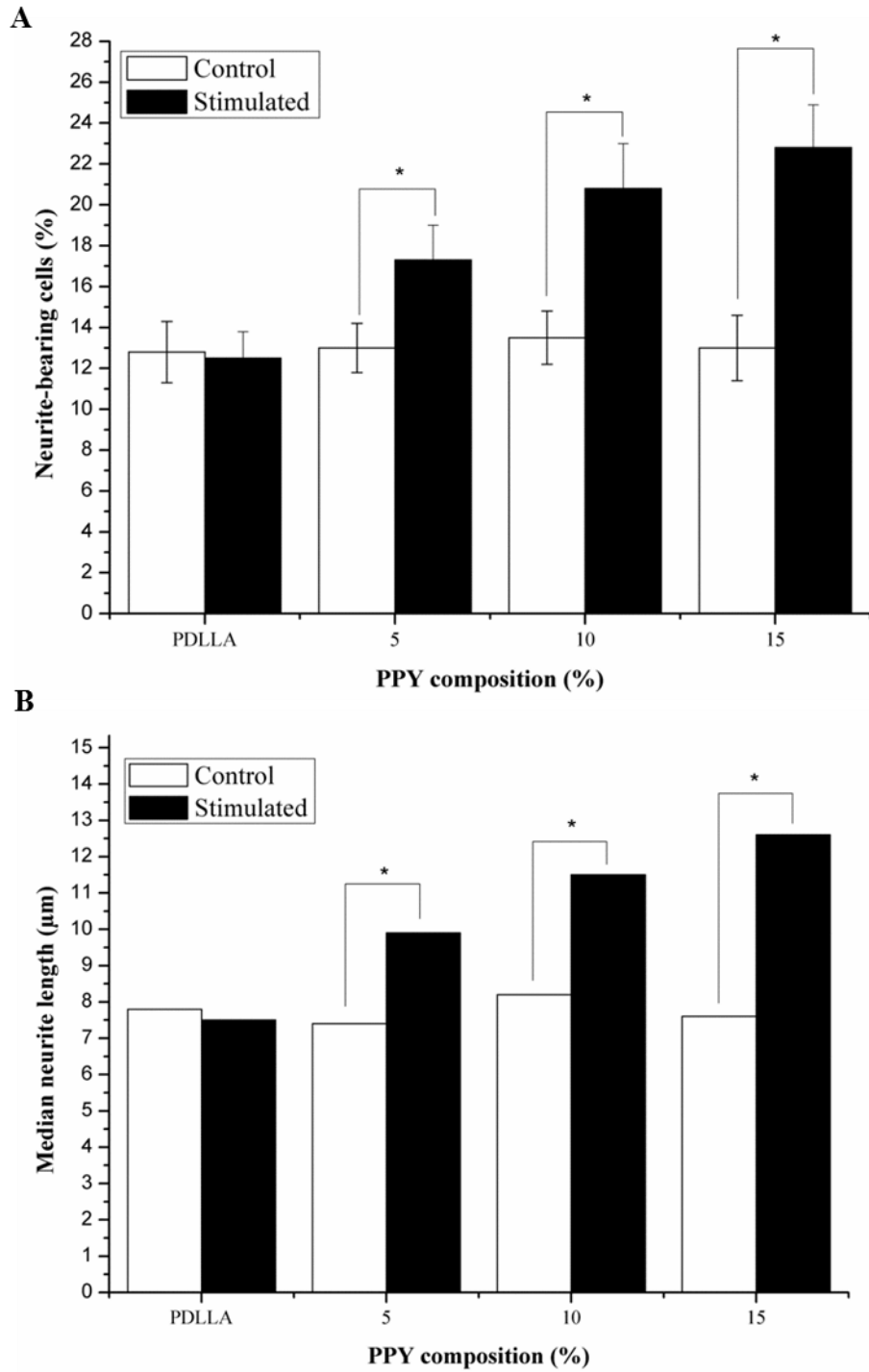
**Figure 3.6. Quantification of neurite growth on PPy/PDLLA films. A) Percentage of neurite-bearing PC12 cells on PPy/PDLLA composite films with varying PPy composition (n=4, *p<0.05). B) Median neurite length on PPy/PDLLA composite films with varying PPy composition.**

*Animal study*

A 10mm defect in the sciatic nerve of adult Sprague-Dawley (SD) rats was used as a model for *in vivo* nerve regeneration. The defects were repaired with 5% PPy/PDLLA conduits, PDLLA conduits, and the gold standard autografts. Samples were harvested after 3 and 6 months. The 5% PPy/PDLLA conduit was chosen to minimize the amount of PPy since it degrades very slowly.

*General observations post-operation*

The animals in this study tolerated the anesthetic and operative procedures, and showed no sign of infection at any time. The animals showed none of the complications typically associated with the operation, and all wounds healed without any issues. Moreover, no signs of discomfort were observed throughout the 6 month evaluation period.

**Figure 3.7** shows the PPy/PDLLA conduit immediately after implantation, 3 months post-surgery, and 6 months post-surgery. Significant levels of degradation can be seen over time, with the conduit becoming thin and crisp after 3 months, but it still maintained lumen and wall integrity. The degradation was even more severe at 6 months, but significant regeneration had occurred, indicating that the conduit had met the demand.
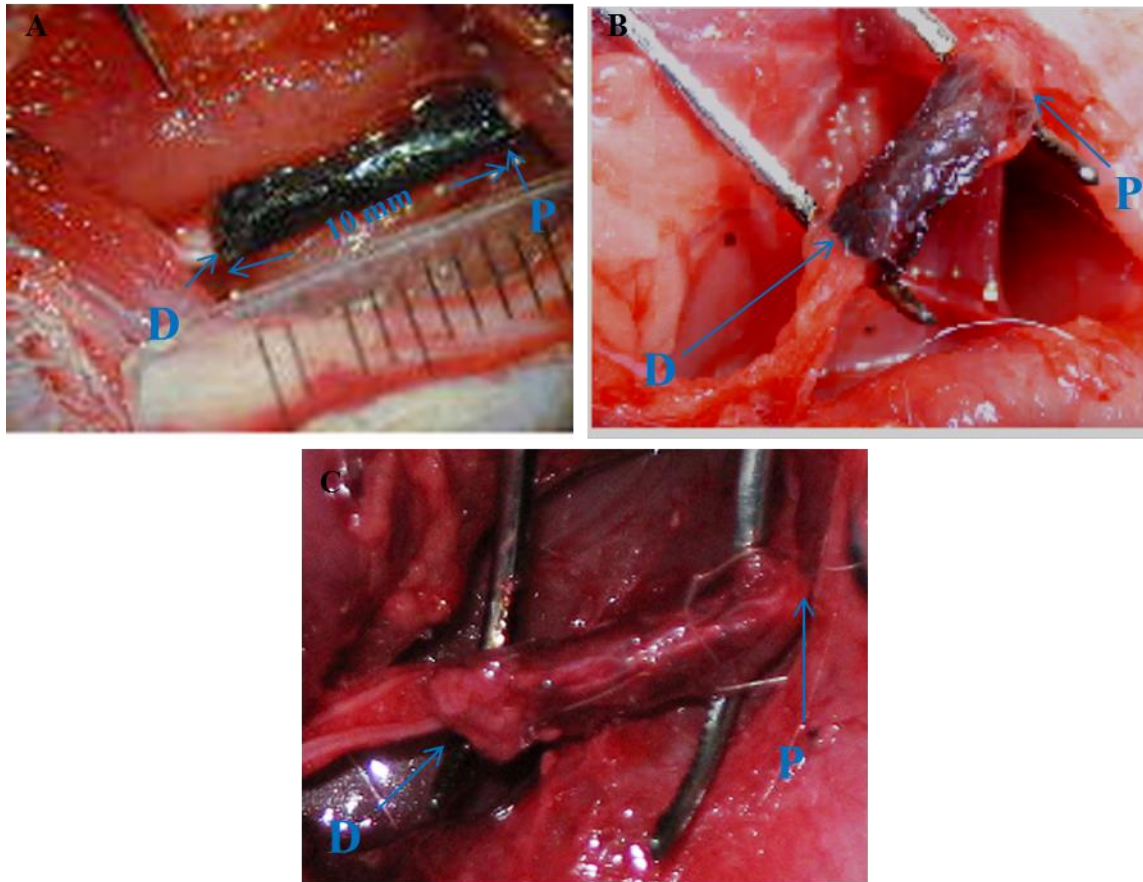
**Figure 3.7. Intraoperative photographs of the PPy/PDLLA nerve conduits. "P" signifies the proximal end and "D" signifies the distal end. A) Immediately after grafting. B) 3 months postoperatively. C) 6 months postoperatively.**

*Walking track analysis*

Walking track analysis was used to assess the functional recovery of all operated animals and quantified by calculating the sciatic function index (SFI), a measure of the sciatic nerve function where a value close to 0 indicates normal function and a value close to -100 implies total impairment. **Figure 3.8** (top) demonstrates the recovery of sciatic nerve function 3 and 6 months after the operation. 3 months after implantation, the SFI of the PPy/PDLLA group, PDLLA group, and the autograft group were -47.5±2.3, -58.6±1.9, and -43.6±2.5, respectively. There was a significant difference between the PDLLA group and PPy/PDLLA group. There was

also significant difference between the PDLLA group and autograft group (p<0.05), while there was no significant difference between PPy/PDLLA group and autograft group (p>0.05). After 6 months post-operation, the three groups, PPy/PDLLA, PDLLA, and autograft, reached an SFI of -23.8±1.5, -37.2±1.9and -22.5±1.8, respectively. There was a significant difference between the PDLLA group and PPy/PDLLA group (p<0.05), while there was no significant difference between PPy/PDLLA group and autograft group (p>0.05). **Figure 3.8** (bottom) illustrates the footprints from walking track analysis of all nerve conduits after 6 months post-implantation. Footprints in the PPy/PDLLA group showed a greater improvement in toe spreading, and the footprints themselves were shorter and wider than those in the PDLLA group. Impressively, the PPy/PDLLA group had similar results to the autograft group.
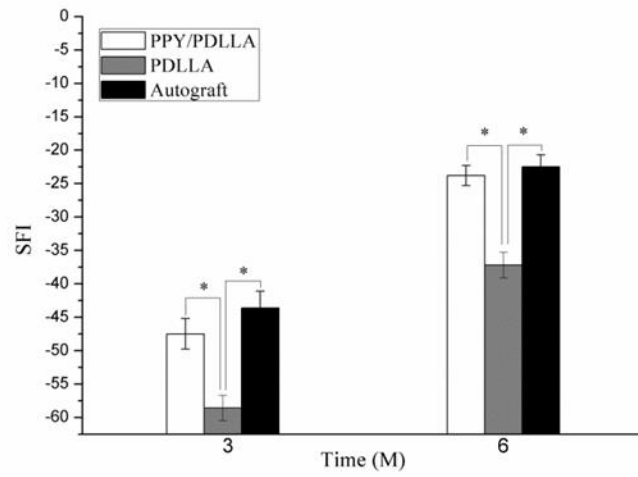
**Figure 3.8. Recovery of sciatic nerve function. Sciatic function index (SFI) as a function of implantation time (top). Footprint stamps in walking track analysis after 6 months of implantation (bottom). A) PPy/PDLLA. B) PDLLA. C) Autograft. D) Normal left leg**

*Electrophysiological evaluation*

Since the nerve conduction velocity (NCV) can offer important insight for studying the conducting function of a peripheral nerve, NCVs were recorded in the lower leg triceps at postoperative intervals 3 and 6 months. The NCVs of the PPy/PDLLA group were significantly faster than those of PDLLA group ($p<0.05$) and not significantly different from those of the autograft group ($p>0.05$) (**Figure 3.9**A). At 6 months after implantation the NCVs of the autograft were found to be $68.39\pm1.28$m/s, whereas those bridged with the PPy/PDLLA conduits were $66.59\pm7.97$m/s, and those bridged with the PDLLA conduits were $51.54\pm0.66$m/s.

*Triceps surae weight analysis*

As an index of muscle atrophy, the triceps surae muscle on the operated leg was compared to that of the healthy leg to calculate a muscle weight ratio. **Figure 3.9**B illustrates that the muscle weight ratio of the PPy/PDLLA and autograft groups was significantly higher than that of PDLLA group ($p<0.05$), while the triceps surae muscle weight ratio of autograft groups was not significantly different from that of PPy/PDLLA group ($p>0.05$). The improvement in muscle weight indicates that there was significant reinnervation of the target muscle.
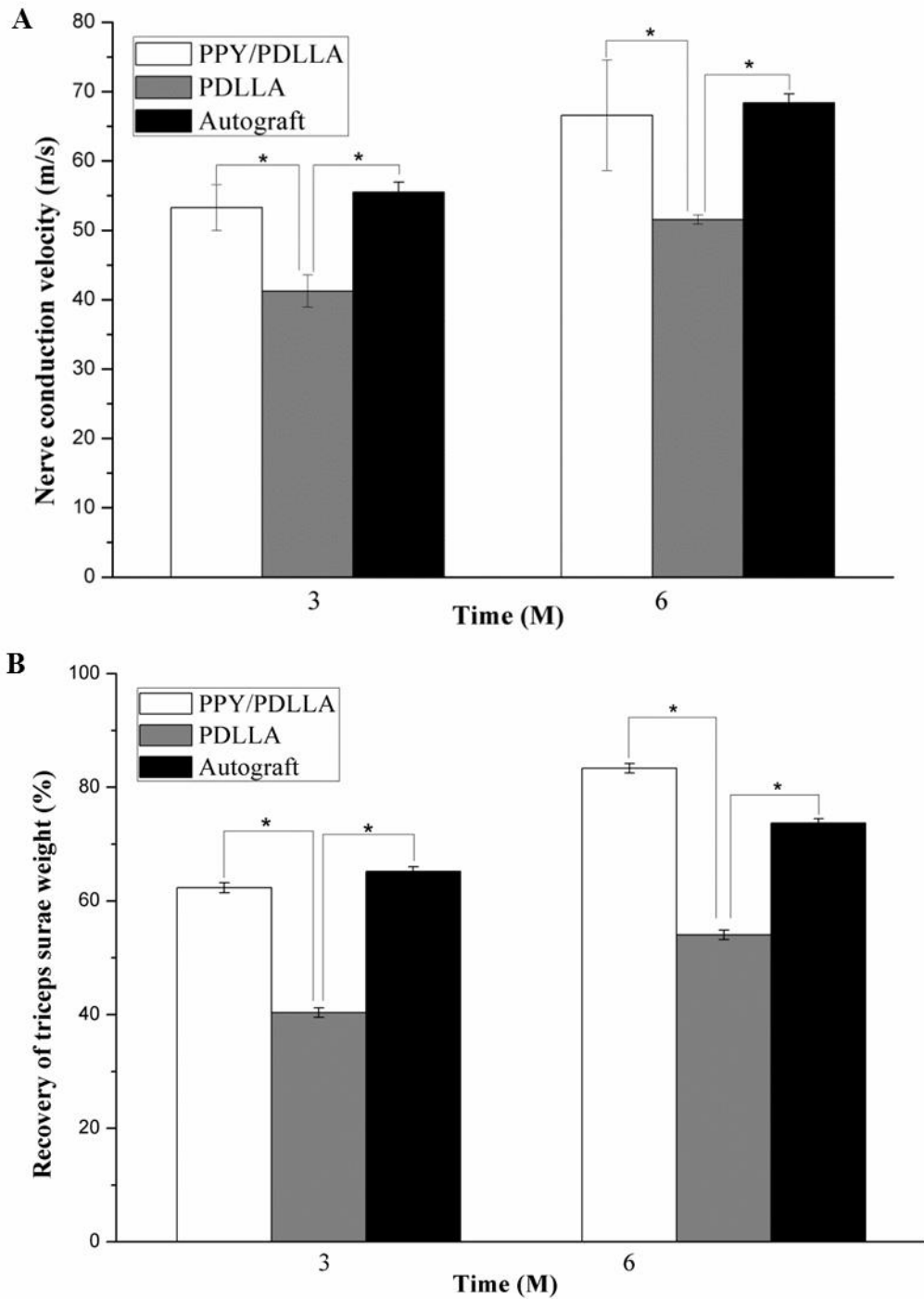
**Figure 3.9. Electrophysiological behavior of regenerated nerve. A) Nerve conduction velocities (NCVs) 3 and 6 months after implantation (n=6, *p<0.05). B) Triceps surae weight (%) 3 and 6 months post-operation (n=6, *p<0.05).**

*Nerve morphological assessment*

During the early nerve regeneration process, the structure of PPy/PDLLA conduits remained intact (**Figure 3.7**). After 3 months, the conduit showed signs of degradation and was covered with connective tissue. The degradation was more apparent after 6 months and the presence of PPy was visibly reduced. The 10mm gap removed by surgery had been bridged by the regenerated tissue 3 months after implantation.

The regenerated nerve samples were removed from the conduits and stained with methylene blue to evaluate the number and diameters of regenerated axons in all of the conduit groups. Numerous bundles of regenerated nerve fibers were clearly identified in the sections of the regenerated tissues (**Figure 3.10**). Transmission electron microscopy (TEM) of the mid-portion of the regenerated nerve tissues 3 months after implantation revealed that the formation of regenerated myelinated fibers occurred at similar levels in both the PPy/PDLLA and autograft groups. In addition, the structure of the myelinated fibers in the regenerated tissues of those two groups was more compact and more uniform than that of the PDLLA group (**Figure 3.10**).
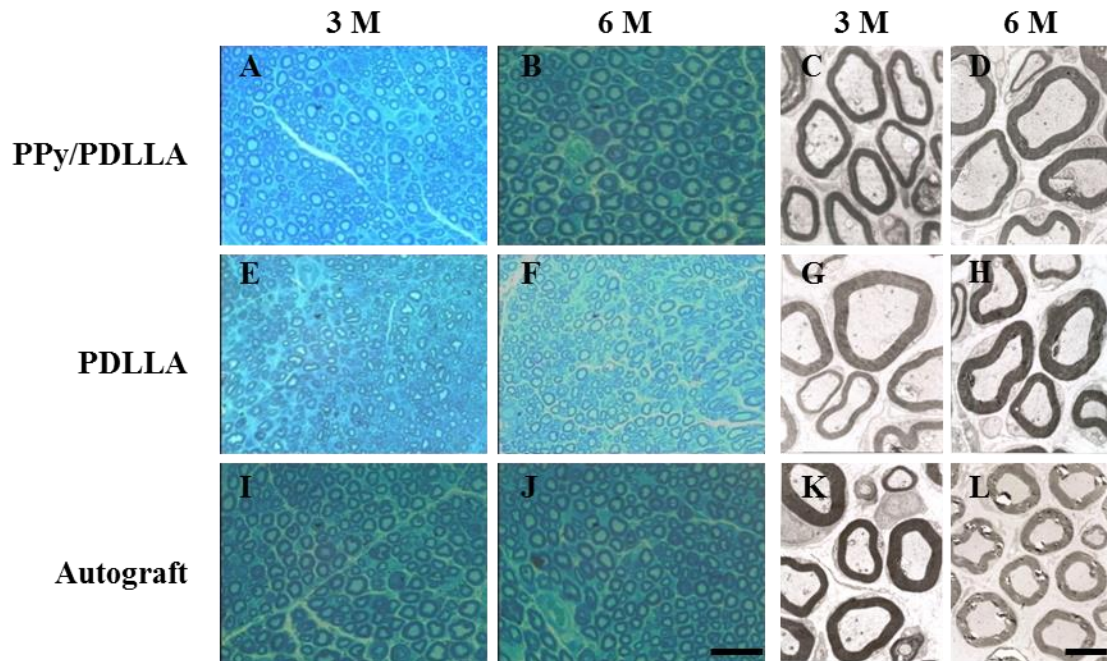
**Figure 3.10. Histology images of regenerated nerve. Sections were stained with methylene blue or fixed for transmission electron microscopy (TEM). Images represent cross sections of regenerated nerves taken from types of nerve conduits implanted in rats after 3 and 6 months. Histology scale bar 50µm. TEM scale bar 2µm.**

Statistical analysis was performed on the average axon diameter (**Figure 3.11**A), the myelinated fiber diameter (**Figure 3.11**B), the thickness of regenerated myelin sheath (**Figure 3.11**C), and the density of myelinated fibers of the regenerated nerve (**Figure 3.11**D). For all of the parameters measured, there was a significant difference between the PPy/PDLLA and the PDLLA groups (p<0.05). Not only was there a higher density of myelinated fibers in the PPy/PDLLA conduits, comparable to that in the autograft, but the myelin sheath was thicker. To evaluate the ingrowth of connective tissue to the wall of conduits, the regenerated nerves were stained with hematoxylin and eosin (HE). The histological sections demonstrated that the inner layers of PPy/PDLLA group were compact enough to prevent any connective tissue ingrowth, while the PDLLA group was filled with connective tissue (**Figure 3.12**). In addition, the PPy

content in the PPy/PDLLA group is visibly reduced from 3 to 6 months, mirroring the gross

observations from **Figure 3.7**.
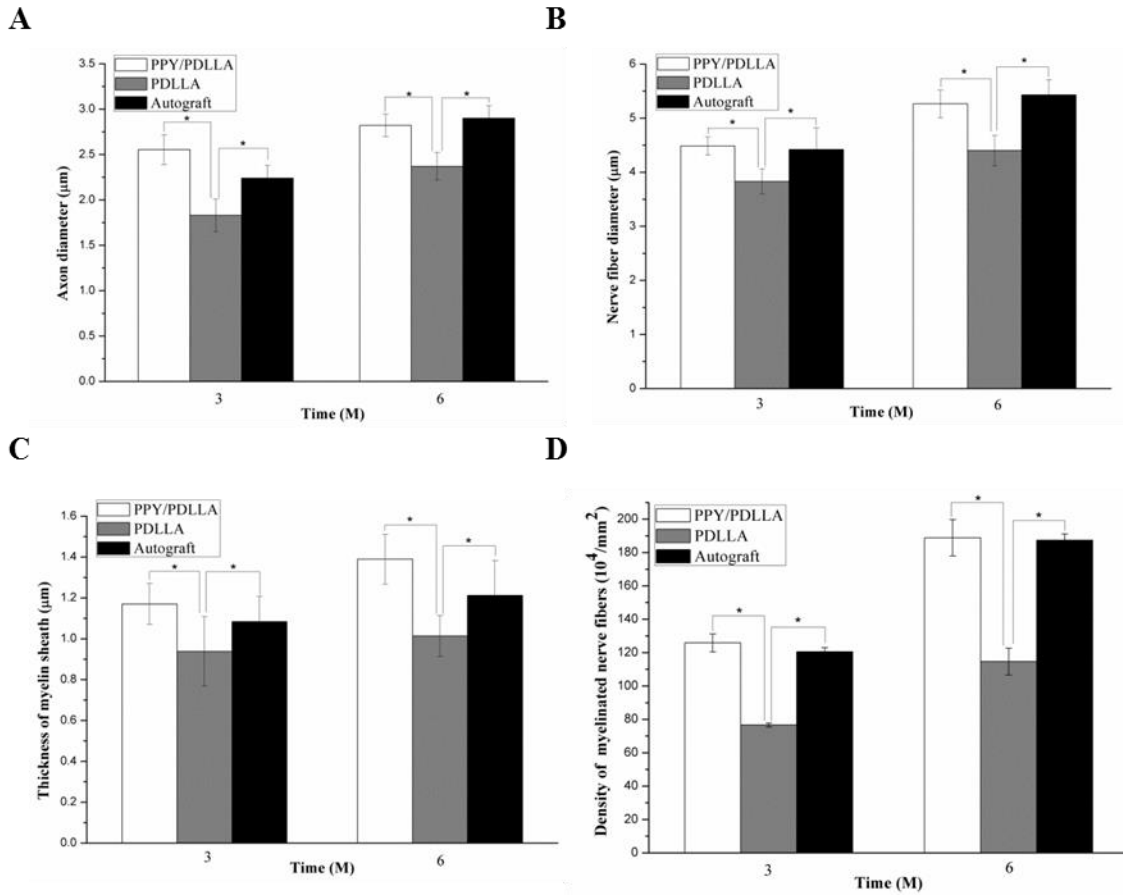


**Figure 3.11. Quantification of the histological assessment of the regenerated nerve fibers. A) Average axon diameter of regenerated myelinated nerve fibers. B) Average diameter of the regenerated nerve fiber. C) Average thickness of regenerated myelinated sheath. D) The average density of regenerated myelinated nerve fibers (n=6, \*p<0.05).**
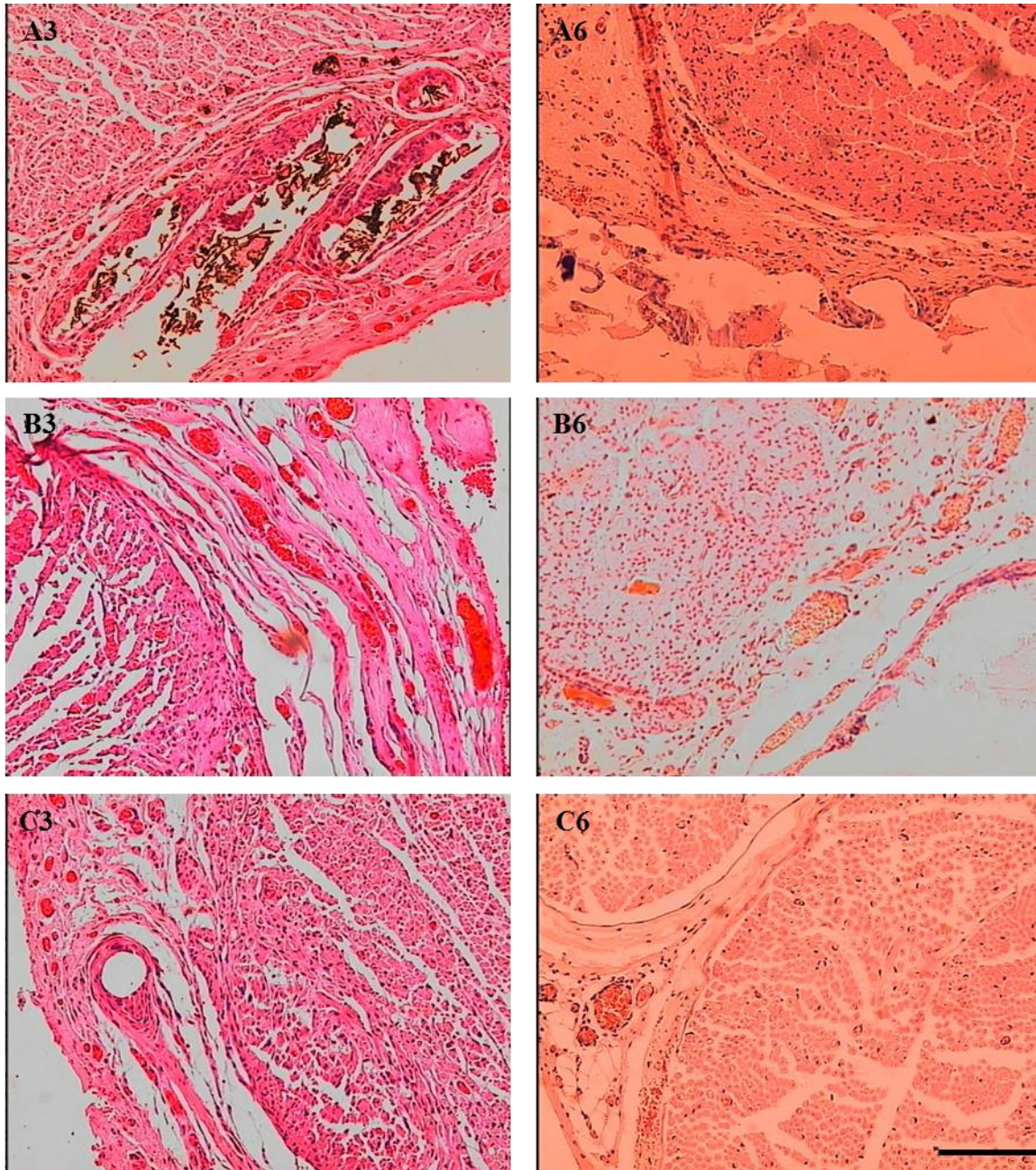
**Figure 3.12. Cross sections of regenerated nerve. Samples were taken 3 months and 6 months post-operation and stained with hematoxylin and eosin (HE). Scale bar 50µm. A) PPy/PDLLA. B) PDLLA. C) Autograft. A3, B3, C3) 3 months after implantation. A6, B6, C6) 6 months after implantation.**

## Discussion

Tissue engineering combines a scaffold with cells and growth factors to functionally repair tissue defects. Each tissue has its own unique requirements for each component. For nerve, the scaffold must guide the regenerating axons across the gap to connect with the distal end. Only then will signal transduction occur. Moreover, since nerve is an electrically active tissue, perhaps the scaffold should likewise be able to conduct an electrical signal. Most polymers used in tissue engineering are unable to do so, but the addition of a conducting polymer, PPy in our study, greatly increases the electrical properties of the scaffold. Additionally, the scaffold must be biocompatible to avoid any adverse response, and biodegradable to allow the newly regenerated nerve to fully develop and eliminate the need for a secondary surgery to remove the implant.

In our study, we attempted to address all of the above requirements using a PPy/PDLLA conduit. The *in vitro* experiments showed that increasing amounts of PPy resulted in more and longer neurites. Interestingly, this suggests that electrically stimulated differentiation of PC12 cells is mediated by the conductivity of the substrate. While the mechanism behind how electrical stimulation promotes neurite formation is not fully understood, these data may provide insight for further investigation. However, pure PPy is brittle and marginally biodegradable, so we used the minimum amount necessary for the *in vivo* study. Our *in vitro* experiments confirmed that 5% PPy/PDLLA was sufficient to induce more and longer neurites while maintaining the mechanical flexibility of PDLLA. This was likely caused by the distribution of the PPy on the surface of the material in micro-domains. Thus, the 5% PPy/PDLLA conduits were used in the *in vivo* experiments.

Impressively, the PPy/PDLLA group had similar results to the autograft group. There was an encouraging level of functional regeneration for a synthetic nerve conduit. After 6 months, there was no statistical difference in the SFI between the PPy/PDLLA group and the autograft group. NCVs were clearly detected in all nerve conduits groups after 3 months, indicating a rapid functional recovery for the injured nerves. Moreover, 6 months after conduit implantation the NCVs were faster than those after 3 months, showing no deterioration of the conducting function of the regenerated nerve tissues. Conduction velocities of healthy nerve can range from 60 to 70m/s [207], which compare favorably to the PPy/PDLLA and autograft groups. NCVs are dependent on a variety of factors including the diameter of the axons, myelin sheath thickness, and internode length [208], so they provide important insight into the ability of the nerve to conduct an action potential. Generally, NCVs of regenerated nerves are less than those of healthy nerves. To recover the electrophysiological properties of the nerve and achieve NCVs that are within the range of those of healthy nerve is an important step toward achieving functional regeneration. Histological analysis also showed significant similarities between the PPy/PDLLA conduit and the autograft. Taken together, these data suggest that the presence of PPy to make the PPy/PDLLA conduits electrically conductive had a significant positive effect on the axon regeneration and myelination compared to those in the PDLLA conduits.

Previous work has illustrated the beneficial effects a conducting polymer with electrical stimulation has on neurite outgrowth [192, 200]. This study translates that effect to an *in vivo* system to show the feasibility PPy/PDLLA conduits have for nerve tissue regeneration. By achieving similar results to the gold standard autograft, PPy/PDLLA conduits are a prime candidate for a nerve tissue engineering construct. While this is a great achievement, the ultimate

68

goal would be to create a synthetic nerve conduit that outperforms an autologous graft, not just matches it, and that is the next hurdle to overcome.

## Conclusion

Nerve tissue engineering offers an innovative and promising approach to treating nerve defects. Conductive polymers have great potential as biomaterials to fabricate synthetic nerve conduits. We fabricated PPy/PDLLA composite nerve conduits using emulsion polymerization and dip coating methods. PC12 cells were used to assess the cell compatibility *in vitro*, and the cells exhibited more and longer neurites than on PDLLA conduits after being stimulated with 100mV for 2hrs. The 5% PPy/PDLLA was used to fabricate nerve conduits to bridge a 10mm defect in the sciatic nerve of a rat. After 6 months, the rats with the PPy/PDLLA conduits showed functional recovery similar to that of the gold standard autologous nerve graft and significantly better than that of the PDLLA conduits.

While achieving recovery on the level of healthy nerve is the goal of tissue engineering, creating a graft that provides the same functional recovery level as an autologous graft is exciting because such a conduit eliminates the drawbacks associated with using an autologous graft, including limited donor source, donor site morbidity, multiple surgery sites, and possible size mismatch. In this study, we have demonstrated that the synthetic PPy/PDLLA conduit has great potential for nerve tissue regeneration.

# CHAPTER 4

## Electrical stimulation of mouse ESCs seeded on PPy/PLLA nanofibers

## Abstract

Embryonic stem cells (ESCs) are a promising choice for neural tissue engineering, a field without an easily harvested and expandable cell source. What makes ESCs desirable, their ability to proliferate indefinitely and their pluripotency, also makes their use challenging. Three parameters have been shown to affect the neuronal differentiation and neurite growth of various cell types: fiber size, electrical stimulation, and fiber orientation. In this study, the goal is to investigate how these parameters affect the neurite outgrowth of mouse D3 ESCs. An array of electrospun poly (l-lactic acid) (PLLA) nanofibers with varying amounts of polypyrrole (PPy) (0%, 5%, 10%, and 15%) were fabricated in both a random and aligned fashion. Fiber diameters were around 150nm, 550nm, 900nm, and 1800nm. D3 ESCs were seeded on the fibers and stimulated with 100mV for 2hrs. As fiber size increased, the percentage of neurite-bearing cells increased, with the 900nm and 1800nm nanofibers resulting in the highest values. Electrical stimulation further increased neurite outgrowth compared to unstimulated cells. Finally, there were a higher percentage of neurite-bearing cells on the aligned fibers compared to random fibers in the presence of electrical stimulation. These results lay the foundation for using substrate properties and electrical stimulation as additional layers of control in promoting the neuronal differentiation of ESCs for neural tissue engineering.

## Introduction

Nerve injuries in both the spinal cord and periphery remain significant clinical issues. They are commonly caused by trauma, but cancer or congenital defects also tribute to the 12,000 new spinal cord injuries each year [1] and 100,000 peripheral nerve repair procedures are performed in the United States and Europe [9]. Tissue engineering, a field that combines regenerative medicine, engineering, and materials science, provides a promising means to develop a new treatment method. By combining a scaffold with cells and growth factors, the hope is to create a biocompatible and biodegradable synthetic implant capable of regenerating injured tissue.

Previous work has established nanofibers as a prime scaffold architecture candidate [65]. Nanofibers mimic the natural extracellular matrix (ECM) and can induce behavior in a way similar to collagen [145], a major ECM component. Nanofibrous structures can modulate adhesion, proliferation, and differentiation [142, 209-211]. Electrospinning is arguably the most simple and flexible method of producing nanofibers with myriad materials, both synthetic and natural, being compatible with electrospinning [176-178, 180, 212-214]. In neural tissue engineering, electrospun fibers have been shown to interact favorably with various cell types. NSCs seeded on poly (l-lactic acid) (PLLA) nanofibers were able to adhere better compared to solid films, differentiate, and grow neurites [62, 210]. PC12 cells, commonly used to model neurite outgrowth, have been shown to exhibit great neurites on nanofibers [215, 216]. More differentiated cells, including dorsal root ganglion [217] and hippocampal neurons [218], were also shown to have significant neurite outgrowth and improved adhesion on nanofibers. Even mesenchymal stem cells (MSCs) were able to differentiate into neuronal on electrospun PLLA-co-polycaprolactone nanofibers [64].

71

With electrospun fibers as successful as they have been, a significant amount of research has been performed to improve their properties in different fashions. Since nerve is an anisotropic electrically active tissue, the common areas of interest are fabricating conductive fibers and creating aligned fibers. There are several options for conducting polymers, including polyaniline (PAni), polythiophene (PTh), and polypyrrole (PPy). PAni has been shown to be biocompatible [219], but its poor cell compatibility has limited its use in tissue engineering [220-223]. PTh, compared to PAni and PPY, is relatively new to the field of tissue engineering, and while it shows early promise [224-226], more work needs to be done to establish its potential for neural tissue engineering. PPy is well established, has a high electrical conductivity, flexible preparation method, easily modified surface, high environmental stability, high biocompatibility, and supports the attachment and proliferation of numerous cell types [190, 191, 227-229]. Incorporating conducting polymers allows for the use of electrical stimulation [50, 52, 192, 230]. PC12 seeded on electrospun poly(lactic-co-glycolic) (PLGA) and stimulated with 10mV had 40-50% longer neurites and 40-90% more neurites compared to unstimulated [200]. Nanofiber alignment was also shown to have a positive effect on cell behavior. Mouse cerebellum C17.2 stem cells grown on random and aligned PLLA nanofibers grew longer and oriented neurites on the aligned fibers [62]. Furthermore, more cells were neurofilament-positive on the aligned fibers. The ability to control the directionality of neurite outgrowth with fiber orientation makes aligned fibers very promising for neural tissue engineering.

While many strides have been made in scaffold design and fabrication, the cell source remains a significant issue. The most studied cells are NSCs or tissue derived adult neurons, both of which are extremely difficult to harvest and expand in a clinically relevant fashion. For instance, NSCs are commonly isolated from the subventricular zone of the lateral ventricle [109,

72

110], though there are other sources as well, and neurons can be isolated from the dorsal root ganglion or hippocampus[217, 218], among other sources. On the other hand, embryonic stem cells (ESCs) have the ability to differentiate into every cell time and can proliferate indefinitely. Their pluripotency makes them a great candidate for tissue engineering, but it also makes controlling their fate more difficult. The two most common methods of inducing neuronal differentiation is with retinoic acid (RA), a derivative of vitamin A, or lineage selection [131]. Little work has been done on using substrate architecture to control ESC differentiation.

In a previous study, we demonstrated the ability of electrically stimulated PPy/PLLA films synthesized using emulsion polymerization to induce neurite outgrowth of PC12 cells [231]. Nerve conduits made from this PPy/PLLA proved to be very successful at regenerating a sciatic nerve defect in a rat model. In this study, an array of nanofibers with different fiber sizes, electrical conductivities, and orientations was electrospun. ESCs were seeded on these fibers to determine their ability to induce neuronal differentiation with and without electrical stimulation.

## Materials and Methods

*Materials*

PLLA was purchased from Boehringer Ingelheim (Ingelheim, Germany). Pyrrole (Py) was purchased from Sigma-Aldrich (St. Louis, MO, USA). Py was vacuum distilled at about 130°C until it became a colorless liquid, and then stored at 4°C in the dark until use. All other chemicals were analytical grade reagents.

*Electrospun PPy/PLLA nanofibrous matrix fabrication*

PPy/PLLA was prepared as previously described (**Figure 3.1**) [231]. Briefly, PLLA was dissolved in CHCl$_3$ to obtain a 10% (w/v) solution. An aqueous solution of Py was added under rigorous stirring, followed drop-wise by 10% (w/v) aqueous FeCl$_3$ to trigger the oxidative emulsion polymerization. The weight ratio of Py to PLLA was 5%, 10%, or 15%. After 5hrs of polymerization, the PPy/PLLA composite was obtained.

For electrospinning, a polymer solution of PLLA, 5% PPy/PLLA, 10% PPy/PLLA, or 15% PPy/PLLA was prepared by dissolving either 6%, 8%, 15%, or 20% w/v of the polymer in hexafluoroisopropanol (HFIP). Fibers were electrospun using a horizontal electrospinning setup. A high-voltage power supply (Gamma High-voltage Research, Ormond Beach, FL, USA) provided a 15kV potential between the needed and the grounded collector. A syringe pump housed a 10ml syringe attached to a 22 gauge flat point needle and was placed 12cm away from the collector. Solution was dispensed at 1.5ml/hr. For the random fibers, the collector was a stationary copper plate covered by aluminum foil with glass coverslips. For the aligned fibers, the collector was a rotating drum covered by aluminum foil with glass coverslips.

*Surface resistivity*

The surface resistivity of the nanofibrous matrices was measured using a basic setup [232]. Two wire electrodes were placed either side of the sample with dimensions length (L) by width (W). Both directions of the aligned and random fibers were measured. Constant DC voltage (V) was applied and the current (I) was noted. Those parameters were used to calculate the surface resistivity ($\rho_s$) as follows:

$$\rho_s = \frac{W}{L} R_s = \frac{W}{L} \frac{V}{I}$$

It should be noted that while the unit of surface resistivity is the ohm ($\Omega$), it is usually denoted as ohm/square ($\Omega$/sq) to indicate that it can be applied to any uniform surface.

*Nanofiber characterization*

Matrices were gold coated (Desk-II, Denton Vacuum, Moorestown, NJ, USA) and observed using a Philips XL30 FEG scanning electron microscope. Images of fibers were analyzed with ImageJ (National Institutes of Health, Bethesda, MD, USA) to determine the average fiber diameters. At least 100 fibers for each matrix were measured. ImageJ was also used to determine the orientation of both random and aligned fibers. Measurements were normalized to 90° and at least 150 fibers were measured.

*Matrix preparation*

The electrospun matrices were placed in 6-well plates. The matrices were sterilized under UV light for 30min, wet briefly with ethanol, and then washed 3 times with phosphate-buffered saline (PBS). A polydimethylsiloxane (PDMS, Sylgard 184®, Dow Corning, Midland, MI, USA) donut was used to secure the matrices in the bottom of the wells. For the films to be electrically stimulated, rectangular sections of the PLLA and PPy/PLLA nanofibrous matrices were cut and placed in a device similar to previously described (**Figure 3.2**) [200]. Briefly, the film was placed on a thin section of PDMS covering a glass slide. Two wires were placed on either side of the film and covered with a PDMS well to seal the wires from the inner chamber (1cm × 1cm × 1cm dimension). The device was clipped together on two sides and sterilized under UV light for 2hrs. All films were coated with 20µg/ml poly-l-ornithine overnight at 4°C, washed twice with sterile water, coated with 10µg/ml laminin overnight at 4°C, and then washed with PBS. Finally,

the films were incubated in neural media (80% F-12/20% Neurobasal medium with N2 and B27 supplements, 10mM sodium pyruvate and 1μM retinoic acid) for 1hr in a 37°C incubator.

*D3 culture and seeding*

D3 mouse embryonic stem cells [151] were cultured on 0.1% gelatin-coated tissue culture flasks in complete ESC media (DMEM supplemented with 10% FBS, $10^{-4}$M β-mercaptoethanol, 0.224μg/ml L-glutamine, 1.33μg/ml HEPES, and 1,000 units/ ml human recombinant LIF). Cells were passaged every 2 days and stored in a humid 37°C incubator with 5% $CO_2$. 30,000 cells were seeded on each matrix in neural medium and it was changed daily for a total of 7 days. For electrical stimulation, cells were allowed to adhere for 24hrs and then 100mV was applied for 2hrs. Similar to control cells, neural medium was changed daily for a total of 7 days.

*Immunofluorescence and image analysis*

Samples were washed 3 times in PBS, fixed in 4% paraformaldehyde, washed an additional 3 times in PBS, and permeabilized with 0.2% Triton X-100. After 2 more PBS washes, samples were blocked with 1% bovine serum albumin (BSA) in PBS for 1hr. Samples were then incubated in primary antibodies for βIII-tubulin (TUJ1, Covance, Princeton, NJ, USA) at 1:500, followed by an appropriate secondary antibody. 4',6-diamidino-2-phenylindole (DAPI, Vectashield®, Vector Laboratories, Burlingame, CA, USA) was used to stain the nucleus. Images were acquired using a Nikon Eclipse C1 confocal microscope (Nikon, Tokyo, Japan). Cell counts were made using ImageJ using at least 400 cells from 4 replicate samples. Median neurite lengths were also measured with ImageJ using a population of at least 400 cells.

*Statistical analysis*

For all experiments, values are reported as a mean ± standard deviation (SD). Experiments were repeated at least 2 times to validate results. Two-way analysis of variance was used to determine the statistical significance of differences between data sets. For the neurite analysis, median lengths were calculated since the distribution was not normal. Statistical differences between medians were determined with a Mann-Whitney U test. A value of $p<0.05$ was considered to be statistically significant.

## Results

*PPy/PLLA nanofiber fabrication*

PLLA, 5% PPy/PLLA, 10% PPy/PLLA, and 15% PPy/PLLA were used to fabricate random and aligned nanofibers. Solutions containing 6%, 8%, 15%, and 20% of each polymer were used. **Table 4.1** summarizes the resultant fiber sizes fabricated. Random and aligned fibers had comparable sizes with the 6%, 8%, and 15% solutions at approximately 150nm, 550nm, and 900nm respectively. There was a slight difference between the aligned and random fibers using 20% polymer solution at approximately 1600nm and 1900nm respectively, though the difference was not statistically significant. A possible explanation for this is the rotating drum collector exerts a slight force on the jetted fibers, causing a degree of stretching that only manifests on the larger fibers due to the high viscosity solution. However, this needs further investigation. In addition, varying content of PPy did not affect fiber size. From here on out, the fibers will be denoted by their approximate size and electrospinning fabrication method: 150ES, 550ES, 900ES, and 1800ES. **Figure 4.1** and **Figure 4.2** show scanning electron micrographs of the

77

random and aligned fibers respectively. The presence of PPy in the polymer did not manifest any

changes in fiber morphology as all fibers had a smooth surface.

**Table 4.1. Summary of random and aligned electrospun composite fiber sizes.**

| PPy Content | Electrospinning Solution (w/v) | Fiber Size (nm) | |
|---|---|---|---|
| | | **Random** | **Aligned** |
| PLLA | 6% | 129±27 | 156±66 |
| 5% | 6% | 120±33 | 147±47 |
| 10% | 6% | 136±37 | 157±35 |
| 15% | 6% | 149±52 | 137±40 |
| PLLA | 8% | 529±141 | 564±133 |
| 5% | 8% | 572±104 | 597±125 |
| 10% | 8% | 590±141 | 513±122 |
| 15% | 8% | 515±110 | 534±110 |
| PLLA | 15% | 901±214 | 1029±192 |
| 5% | 15% | 945±190 | 977±208 |
| 10% | 15% | 904±202 | 889±155 |
| 15% | 15% | 891±216 | 864±141 |
| PLLA | 20% | 1889±216 | 1538±227 |
| 5% | 20% | 1827±183 | 1569±180 |
| 10% | 20% | 1840±209 | 1633±195 |
| 15% | 20% | 1872±235 | 1627±180 |
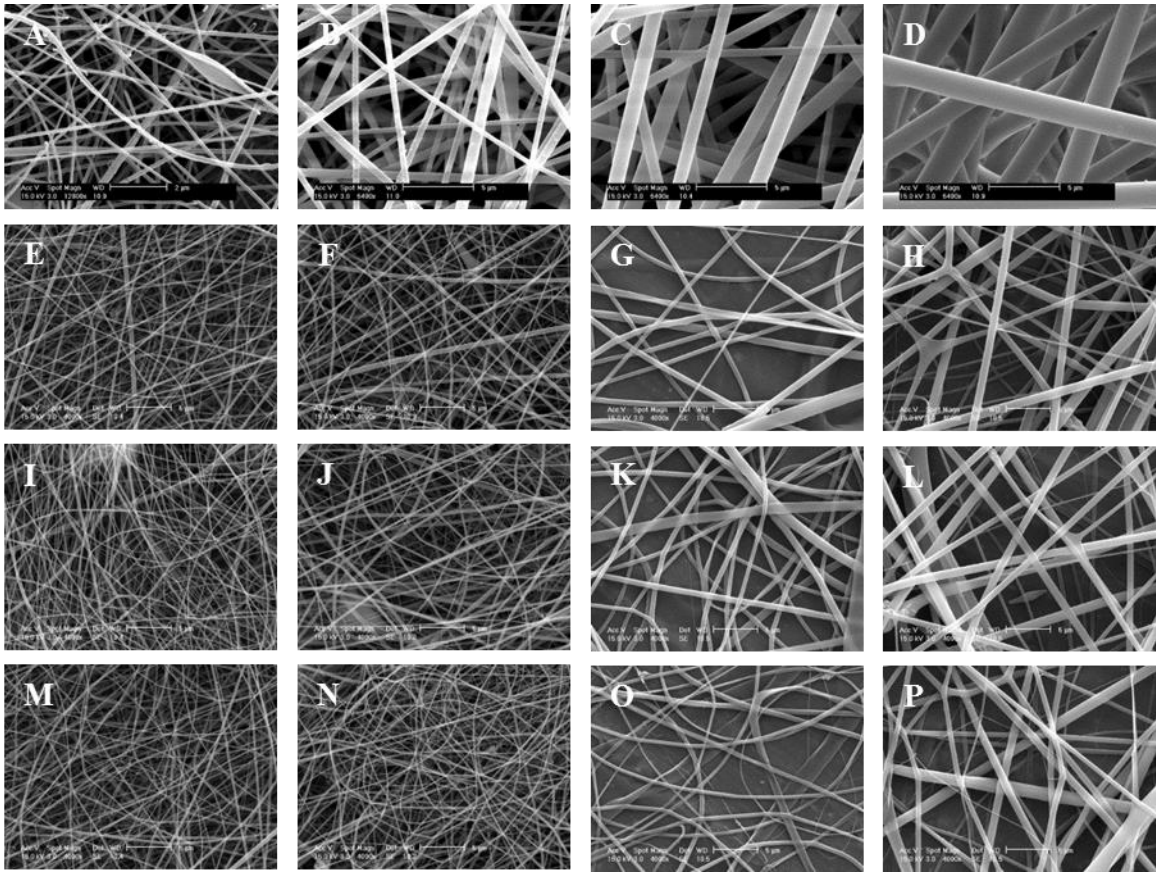
**Figure 4.1. Scanning electron micrographs of random electrospun composite nanofibers. An array of nanofibers was fabricated from PLLA (A-D), 5% PPy/PLLA (E-H), 10% PPy/PLLA (I-L), and 15% PPy/PLLA (M-P). Sizes ranged around 150nm (A, E, I, M), 550nm (B, F, J, N), 900nm (C, G, K, O), and 1800nm (D, H, L, P).**
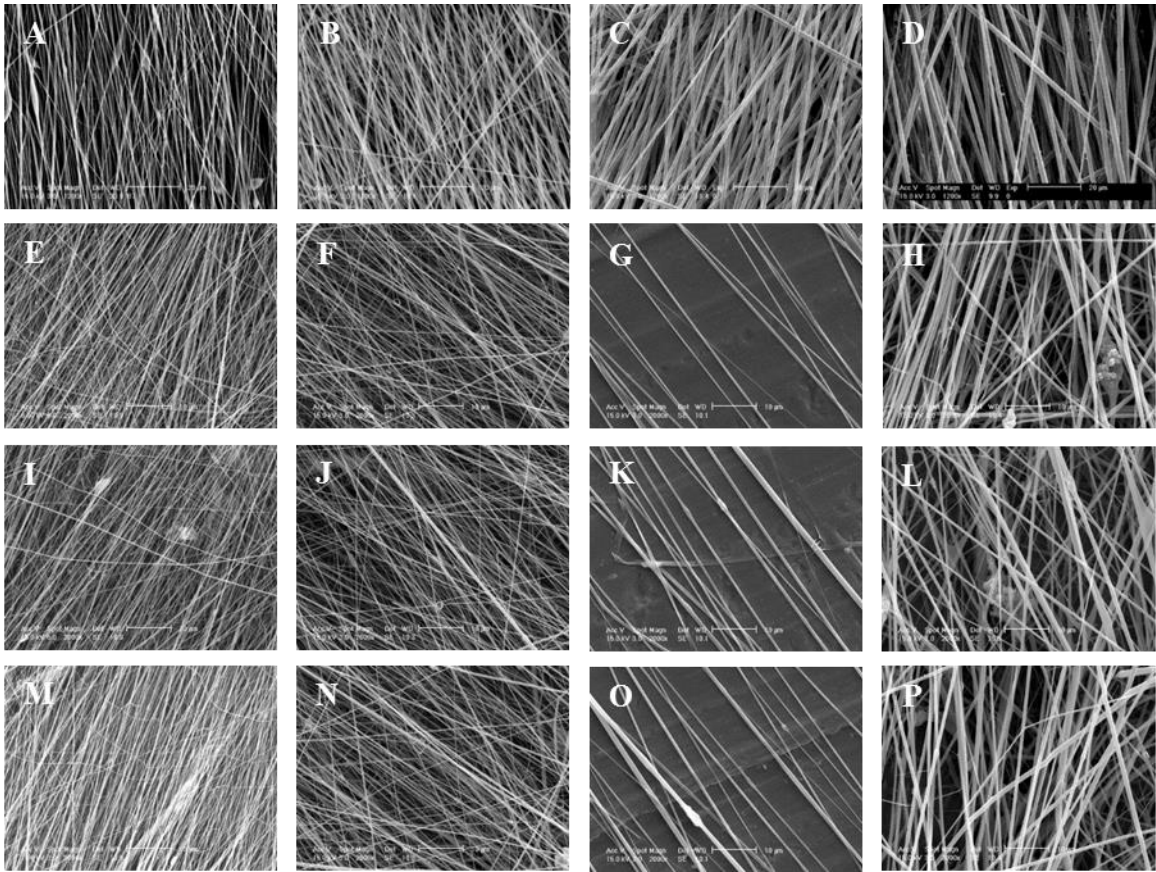
**Figure 4.2. Scanning electron micrographs of aligned electrospun composite nanofibers. An array of nanofibers was fabricated from PLLA (A-D), 5% PPy/PLLA (E-H), 10% PPy/PLLA (I-L), and 15% PPy/PLLA (M-P). Sizes ranged around 150nm (A, E, I, M), 550nm (B, F, J, N), 900nm (C, G, K, O), and 1800nm (D, H, L, P).**

The degree of orientation was visualized in **Figure 4.3**. Random fibers showed no directional bias. Aligned fibers, however, were tightly oriented by the rotating drum collector with standard deviations of 11, 17, 15, and 9 degrees for the 150ES, 550ES, 900ES, and 1800ES nanofibers respectively. Alignment also resulted in fibers that were more tightly packed. While there were large gaps and pores between the random fibers, more noticeable as fiber size increased, aligned fibers created a more uniform surface.
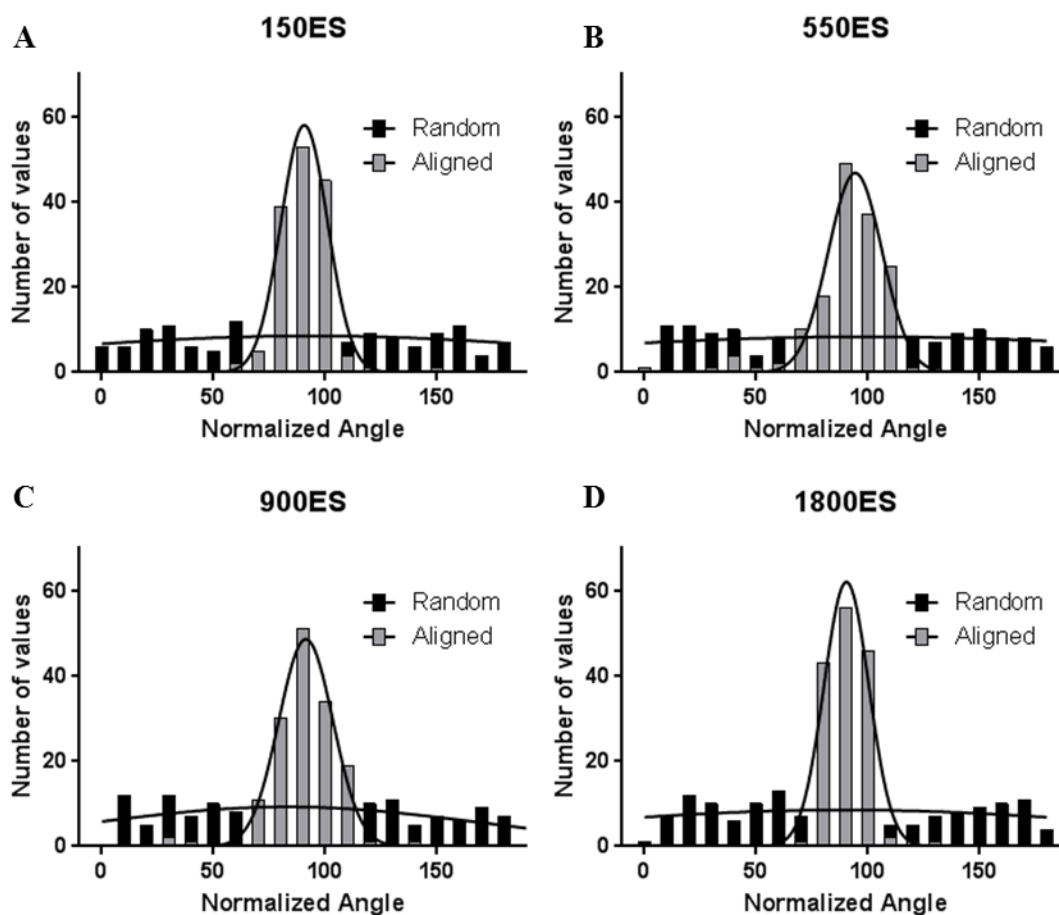


**Figure 4.3. Degree of orientation of electrospun composite nanofibers. Electrospinning with a stationary collector produced evenly distributed random nanofibers. Using a rotating drum oriented the fibers to a high degree, with standard deviations of 11, 17, 15, and 9 degrees for 150ES (A), 550ES (B), 900ES (C), and 1800ES (D) nanofibers respectively. The orientation of at least 150 fibers was measured.**

For the purpose of applying electrical stimulation, the surface resistivity of each nanofibrous matrix was measured. Surface resistivity is a material property useful for describing the ability of a thin film of uniform thickness to conduct a current. The pseudo-2D nanofibrous matrix fit the definition of a thin film for this measurement. It should be noted that while the unit of surface resistance is the ohm, to avoid confusion with bulk resistance, the unit is commonly denoted as an ohm/square, which is uniquely used for surface resistivity. A reading could not be attained on the PLLA fibers, indicating a very high surface resistivity. The length-wise and width-wise directions of the random fibers were measured to confirm the lack of directional bias, and the values obtained were indistinguishable (data not shown). The highest surface resistivity values were obtained measuring perpendicular to the aligned fibers (**Figure 4.4**). Measuring parallel to the aligned fibers greatly reduced the surface resistivity, which showed that the aligned nanofibers exhibited anisotropic electrical properties that mirrored their anisotropic orientation. In addition, surface resistivity decreased as PPy content increased.
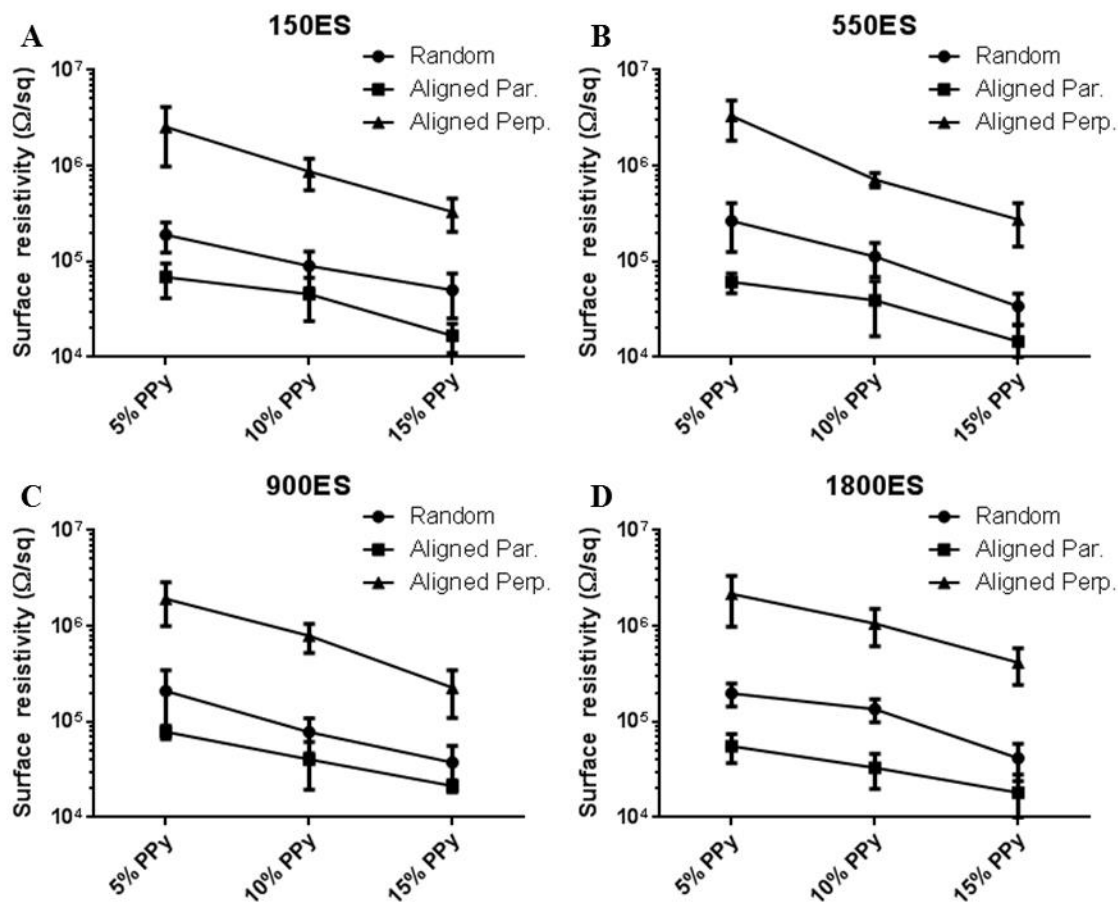
**Figure 4.4. Surface resistivity of aligned and random electrospun composite nanofibers. Measurements for random fibers were similar along both directions. Surface resistivity did not change with fiber size: 150ES (A), 550ES (B), 900ES (C), and 1800ES (D) nanofibers. Resistivity was highest perpendicular to the aligned fibers, which was approximately an order of magnitude higher than the resistivity across the random fibers. Surface resistivity along the aligned fibers was the lowest of the groups. In general, surface resistivity steadily decreased as PPy content increased. Measurements could not be attained on the PLLA nanofibers.**

*Effect of electrical stimulation on ESC neurite growth.*

Mouse D3 ESCs were seeded on the composite nanofibers, allowed to adhere for 24h, and then stimulated with 100mV for 2hrs. The cells were cultured for an additional 6 days for a total of 7 days before being fixed for immunofluorescence and labeled for βIII-tubulin, a cytoskeletal protein that forms microtubules and marker of neuronal differentiation. In the absence of electrical stimulation, there was very little βIII-tubulin expression and a negligible amount of neurites on the 150ES random fibers (**Figure 4.5**A, E, I, M). The amount of PPy go to along with the PLLA did not have an effect on cell morphology. There were more neurites formed on the 550ES random fibers (**Figure 4.5**B, F, J, N) and they grew in all directions, showing that there was no directional bias. Similar to the 150ES fibers, the PPy content had no effect on cell morphology. For the two largest fiber sizes, 900ES (**Figure 4.5**C, G, K, O) and 1800ES (**Figure 4.5**D, H, L, P), there was a large increase in βIII-tubulin expression and neurite growth. The neurite growth was random, mirroring the random orientation of the nanofibrous matrices.
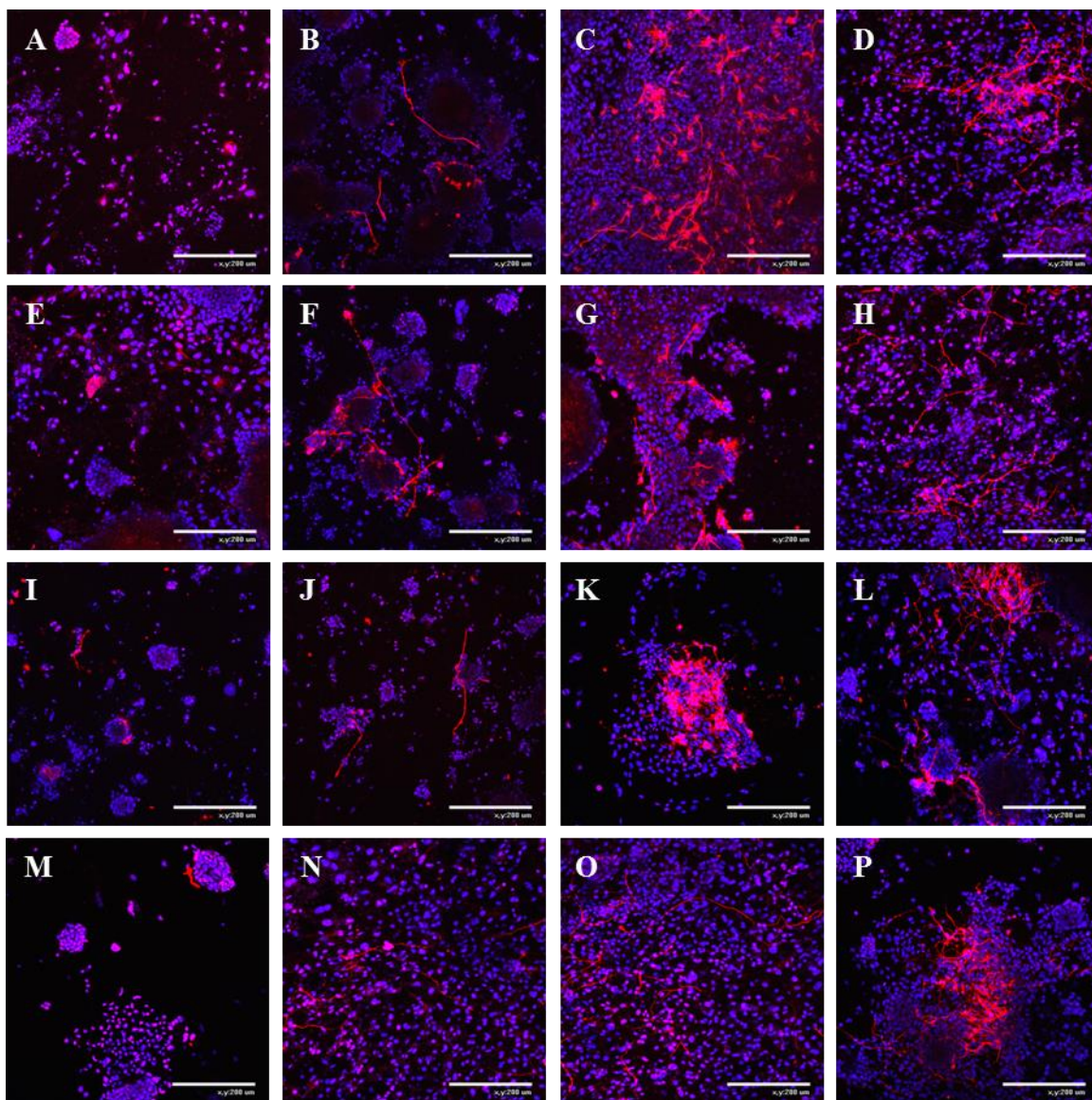
**Figure 4.5. ESC neurite growth on random composite nanofibers without electrical stimulation. ESC were cultured for a total of 7 days, and then labeled with DAPI for nuclei (blue) and βIII-tubulin (red). The nanofibrous matrix array included PLLA (A-D), 5% PPy/PLLA (E-H), 10% PPy/PLLA (I-L), and 15% PPy/PLLA (M-P) with fiber diameters of 150nm (A, E, I, M), 550nm (B, F, J, N), 900nm (C, G, K, O), and 1800nm (D, H, L, P). Neurite outgrowth increased as fiber size increased while PPy content had no effect.**

When the ESCs were stimulated with 100mV for 2hrs, a difference within the fiber size groups between differing PPy content arose. The smallest nanofibers, 150ES (**Figure 4.6**A, E, I, M), still inhibited neurite growth and little βIII-tubulin was observed. Similarly, though there was a small amount of neurite growth on the 550ES nanofibers (**Figure 4.6**B, F, J, N), the amount of PPy did not seem to have an effect in spite of the electrical stimulation. The largest fibers, 900ES (**Figure 4.6**C, G, K, O) and 1800ES (**Figure 4.6**D, H, L, P), similar to the control group, promoted the most and longest neurites. However, as PPy content increased, there seemed to be even more and longer neurites. This is especially noticeable comparing 15% PPy (**Figure 4.6**O, P) and 10% PPy (**Figure 4.6**K, L) to PLLA (**Figure 4.6**C, D). The orientation of the neurite growth remained random with neurites growing in all directions despite being stimulated by an oriented electric potential. This indicated that nanofibers retained control over the directional outgrowth of neurites, though electrical stimulation had an effect on the quantity and length of neurite growth. It should be noted that even though ESCs have the tendency to aggregate, very few aggregates were observed on any of the matrices. For the most part, cells were in a monolayer on the surface of the fibers, ensuring that any differences in behavior were due to the nanofibrous matrix and not interactions among aggregates.
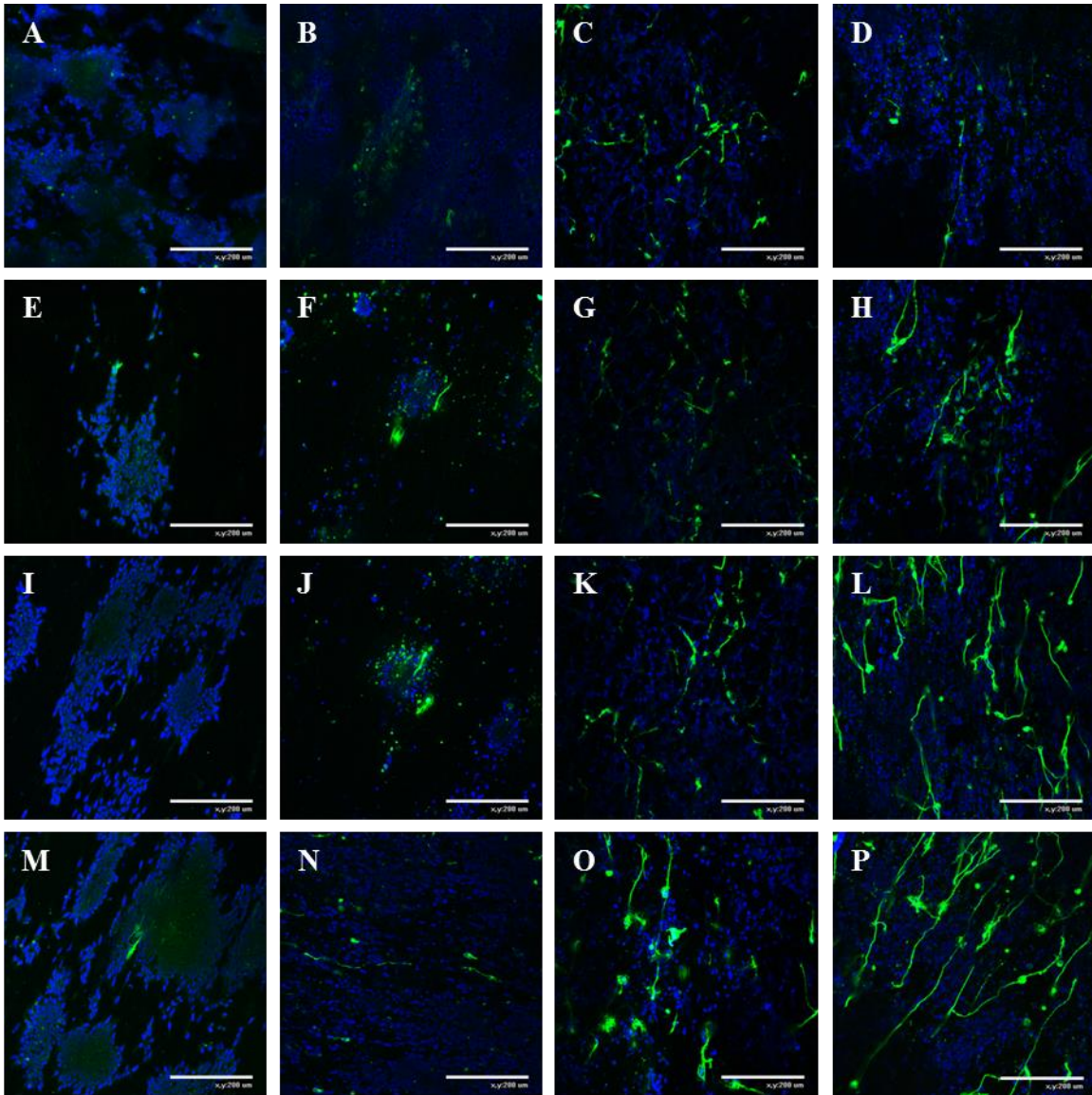
**Figure 4.6. ESC neurite growth on random composite nanofibers with electrical stimulation. ESC were stimulated with 100mV for 2h, cultured for a total of 7 days, and then labeled with DAPI for nuclei (blue) and βIII-tubulin (green). The nanofibrous matrix array included PLLA (A-D), 5% PPy/PLLA (E-H), 10% PPy/PLLA (I-L), and 15% PPy/PLLA (M-P) with fiber diameters of 150nm (A, E, I, M), 550nm (B, F, J, N), 900nm (C, G, K, O), and 1800nm (D, H, L, P). Neurite outgrowth increased as both fiber size and PPy content increased.**

The immunofluorescence images provided insight into how fiber size combined with electrical stimulation affected the neurite growth of D3ESCs. To better understand the observed differences, the median neurite length and percentage of neurite-bearing cells was quantified. On the 150ES nanofibers, 0.5-0.8% of cells bore neurites with no stimulation and that only grew to as many as 2.8% and 4.0% on the stimulated 10% PPy and 15%PPy, respectively (**Figure 4.7**A). Those figures increased to 5.3-6.8% on unstimulated 550ES nanofibers with 10.0% on stimulated 10% PPy and 11.8% on stimulated 15% PPy (**Figure 4.7**B). 900ES and 1800ES nanofibers had the highest baseline percentage of neurite-bearing cells at 11.0-13.5% and 9.5-12.0%, respectively (**Figure 4.7**C, D). When electrical stimulation was applied, the difference was significant on 900ES 15% PPy with 16.0%, 1800ES 10% PPy with 15.3%, and 1800ES 15% PPy with 17.8%.
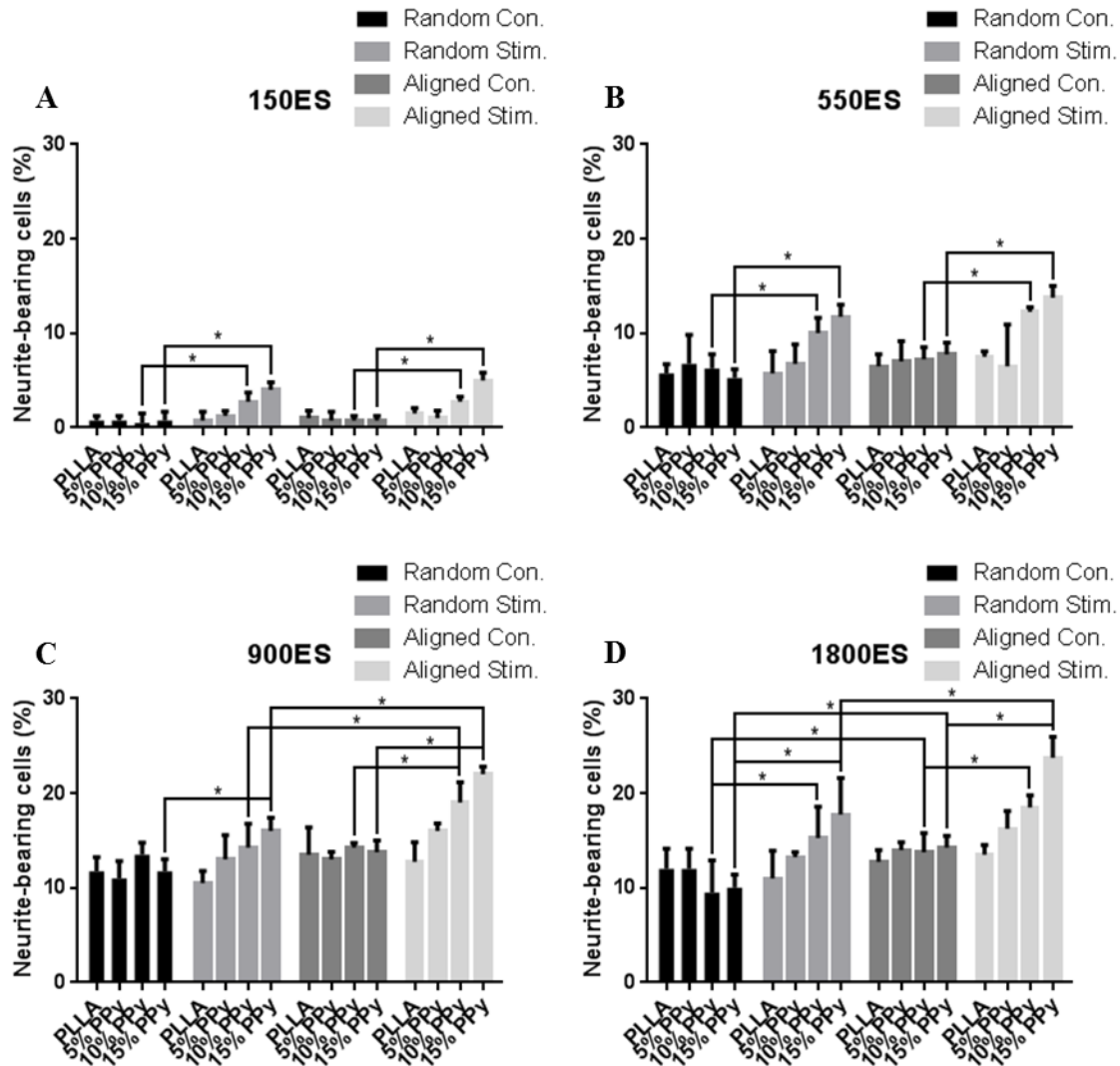
**Figure 4.7. Percentage of neurite-bearing cells on random and aligned electrospun composite nanofibers with and without electrical stimulation. Very few cells expressed neurites on the 150ES nanofibers (A), even though 100mV stimulation for 2h increased the number on the 10% PPy and 15% PPy nanofibers. A similar trend was evident on the 550ES nanofibers (B) with more cells producing neurites across the board. The percentage of neurite-bearing cells increased further from 550ES nanofibers to 900ES (C) and 1800ES (D) nanofibers. Furthermore, there was an increase in neurite-bearing cells on the aligned fibers compared to random fibers when the ESCs were stimulated on the 10% PPy (C) and 15% PPy nanofibers (C, D). At least 400 cells were counted from 4 samples. (\* p<0.05)**

For the median neurite length, a minimum of 10 neurites from 400 observed cells was required. On the 150ES nanofibers, only cells seeded on the electrically stimulated 10% PPy and 15% PPy eclipsed that requirement, producing median neurite lengths of 24 and 28µm, respectively (**Figure 4.8**A). On the 550ES nanofibers, in the absence of stimulation median neurite lengths ranged from 32-42µm. With stimulation, the range increased to 33-56µm, though it was not statistically significant (**Figure 4.8**B). The longest neurites were observed on 900ES (**Figure 4.8**C) and 1800ES (**Figure 4.8**D) nanofibers, with unstimulated median neurite lengths of 71-85µm and 67-82µm, respectively. With stimulation, the length grew significantly on 15% PPy to 112µm for 900ES nanofibers and 127µm for 1800ES nanofibers.
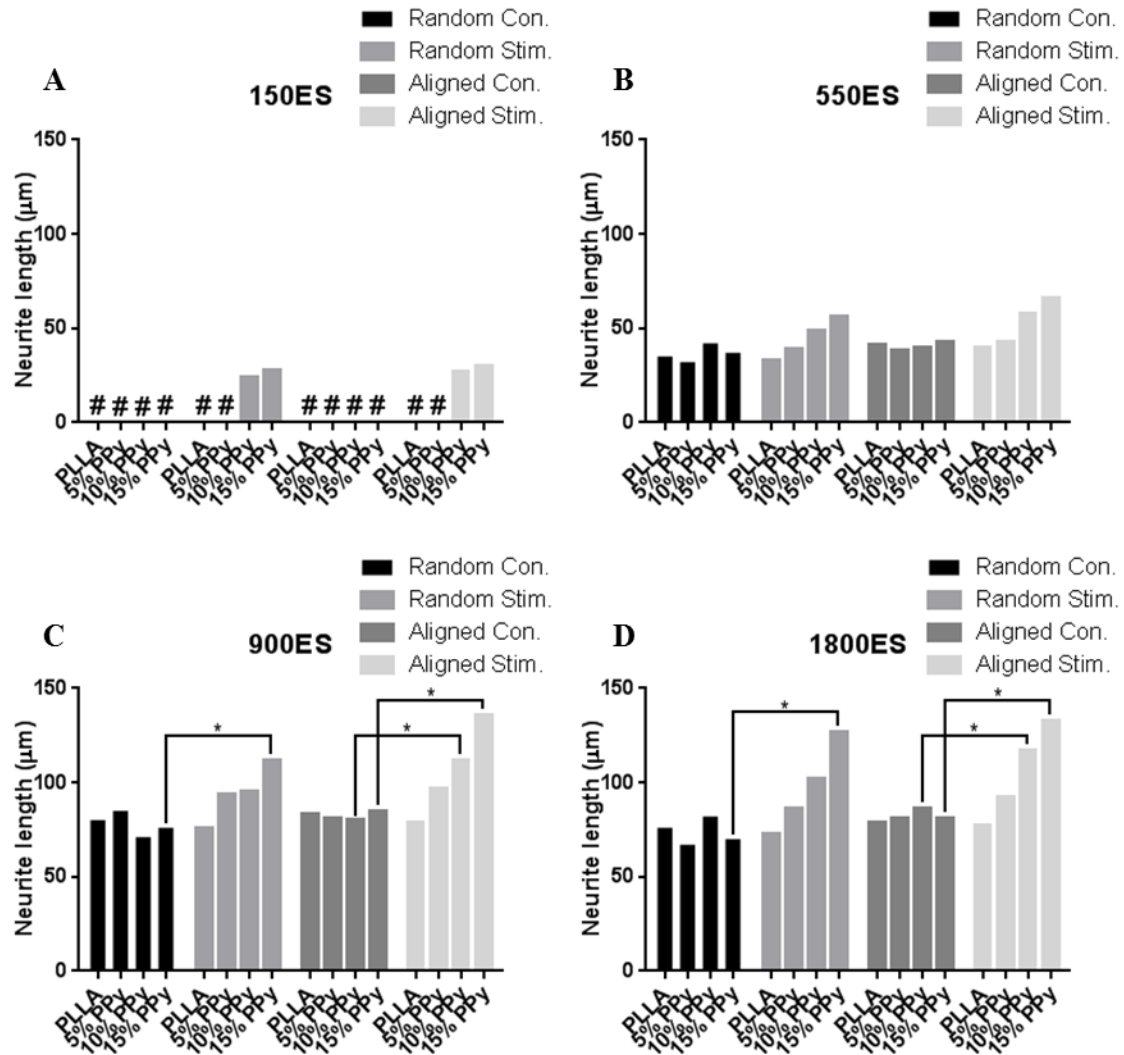
**Figure 4.8. Median neurite length on random and aligned electrospun composite nanofibers with and without electrical stimulation. A (#) denotes less than 10 neurites were observed on at least 400 cells counted from 4 samples. Too few neurites were observed on the majority of the 150ES samples (A). On the 550ES nanofibers (B) there was a slight trend of longer neurites after 100mV stimulation for 2h as PPy content increased, though it was not statistically significant. This was also evident on the 900ES (C) and 1800ES (D) nanofibers. Electrical stimulation resulted in longer neurites on both random and aligned 15% PPy nanofibers (C, D), and aligned 10% PPy nanofibers (C, D). (\* p<0.05)**

*Effect of fiber alignment on ESC neurite growth*

Electrical stimulation was able to increase the percentage of neurite bearing cells and median neurite length on the two largest fiber sizes with the increasing PPy content. Aligning the fibers decreased the surface resistivity of the matrices, so the combination of aligned fibers with electrical stimulation was employed. Without electrical stimulation, similar to the random fibers, there was minimal βIII-tubulin and neurite formation on the 150ES nanofibers (**Figure 4.9**A, E, I, M). More neurites were observed on the 550ES nanofibers (**Figure 4.9**B, F, J, N), and the most and longest neurites were observed on the largest two fiber sizes, 900ES (**Figure 4.9**C, G, K, O) and 1800ES (**Figure 4.9**D, H, L, P). Also similar to the random fibers, without electrical stimulation the amount of PPy had little effect on neurite formation. However, aligned fibers were able to align the neurite outgrowth to a high degree, which is a desirable characteristic for neural tissue engineering.
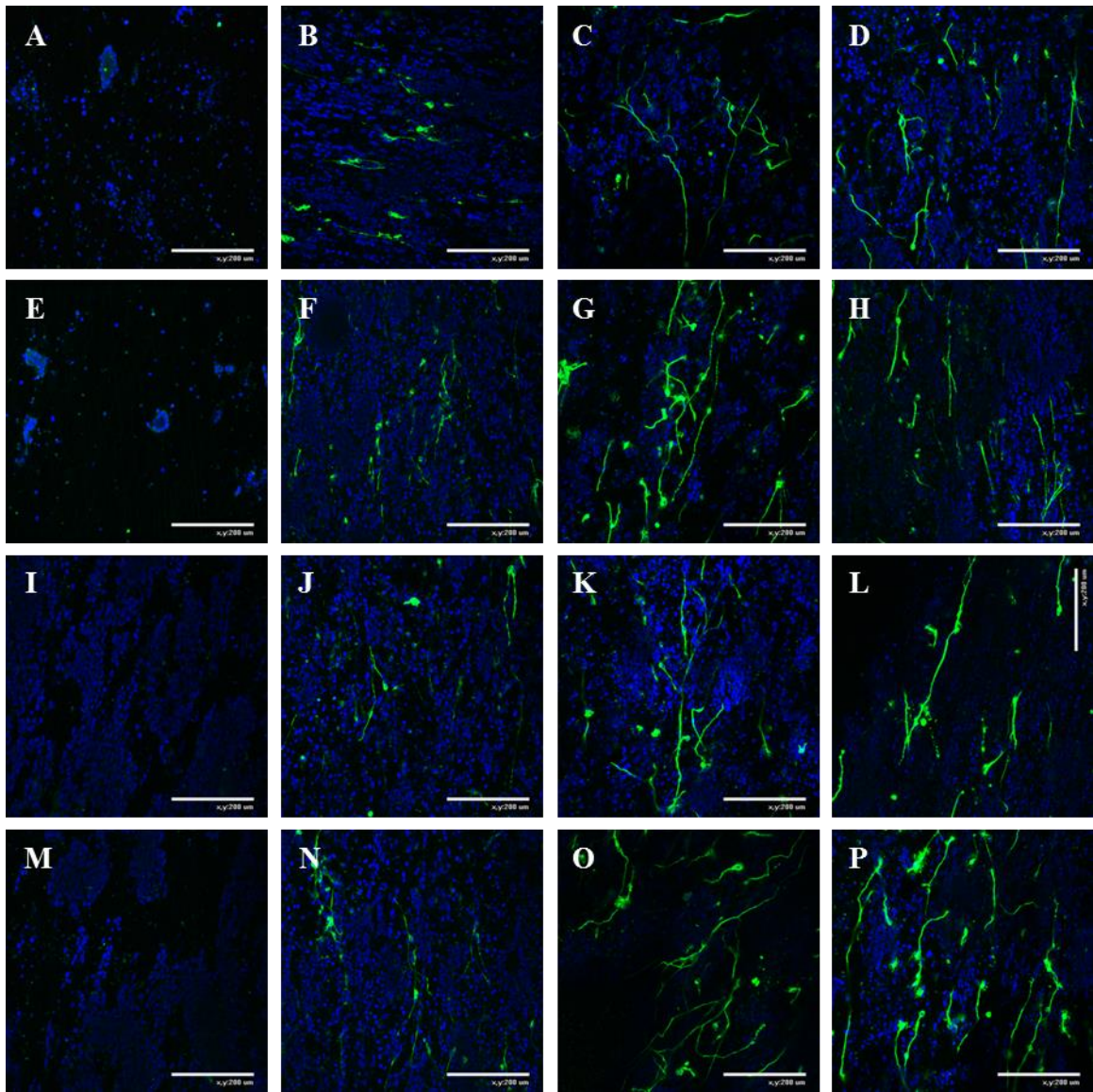
**Figure 4.9. ESC neurite growth on aligned composite nanofibers without electrical stimulation. ESC were cultured for a total of 7 days, and then labeled with DAPI for nuclei (blue) and βIII-tubulin (green). The nanofibrous matrix array included PLLA (A-D), 5% PPy/PLLA (E-H), 10% PPy/PLLA (I-L), and 15% PPy/PLLA (M-P) with fiber diameters of 150nm (A, E, I, M), 550nm (B, F, J, N), 900nm (C, G, K, O), and 1800nm (D, H, L, P). Neurite outgrowth increased as fiber size increased while PPy content had no effect. Scale bar 200μm.**

With the addition of 100mV electrical stimulation for 2hrs, the content of PPy started to have an effect on neurite growth. Minimal or few short neurites were observed on the 150ES (**Figure 4.10**A, E, I, M) and 550ES (**Figure 4.10**B, F, J, N). On the 900ES (**Figure 4.10**C, G, K, O) and 1800ES (**Figure 4.10**D, H, L, P) fiber sizes, the 10% PPy (**Figure 4.10**K, L) and 15% PPy (**Figure 4.10**O, P) fibers seemed to have more and longer neurites. These neurites were also highly aligned with the orientation of the nanofibers.
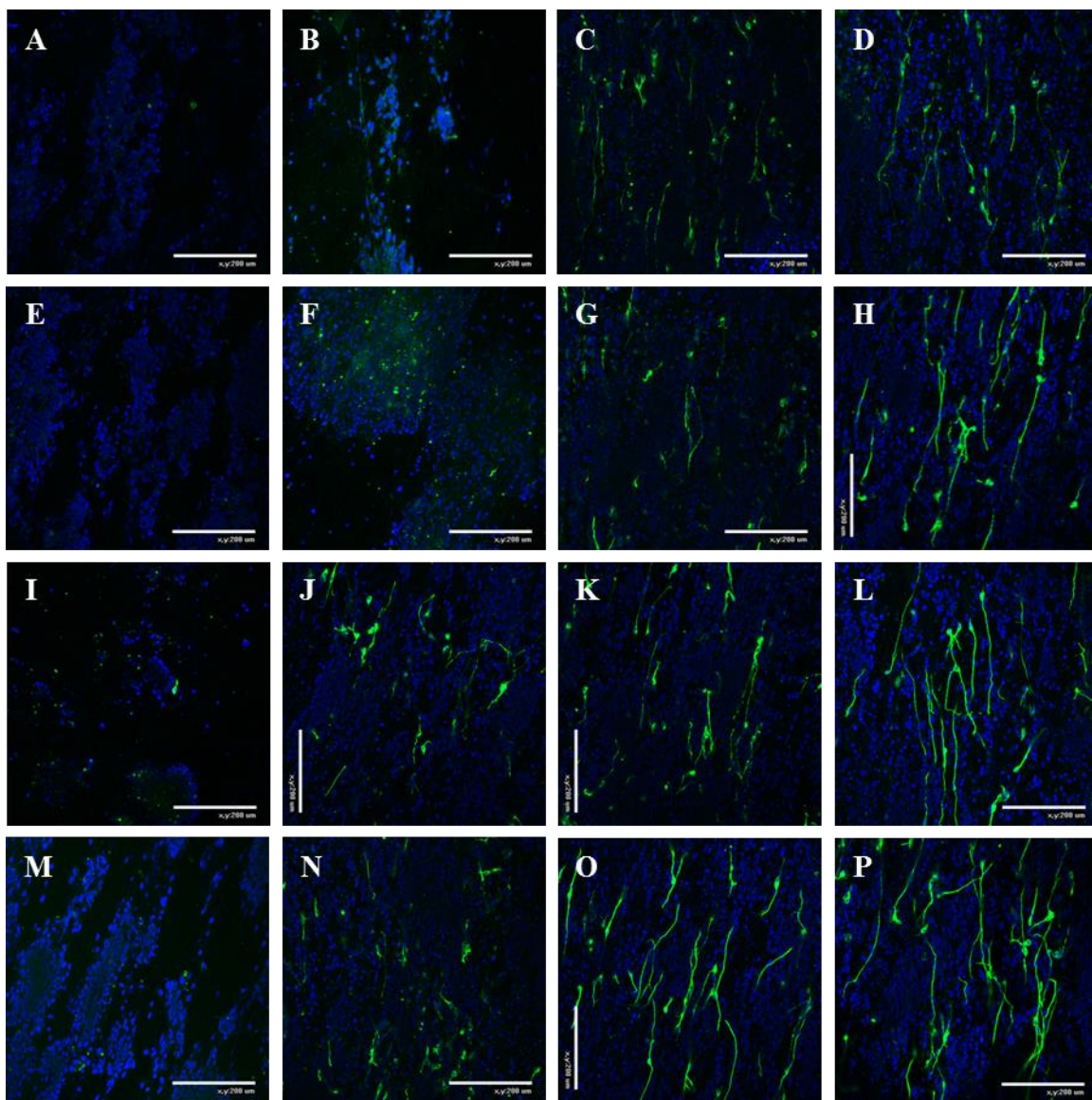
**Figure 4.10. ESC neurite growth on aligned composite nanofibers with electrical stimulation. ESC were stimulated with 100mV for 2h, cultured for a total of 7 days, and then labeled with DAPI for nuclei (blue) and βIII-tubulin (green). The nanofibrous matrix array included PLLA (A-D), 5% PPy/PLLA (E-H), 10% PPy/PLLA (I-L), and 15% PPy/PLLA (M-P) with fiber diameters of 150nm (A, E, I, M), 550nm (B, F, J, N), 900nm (C, G, K, O), and 1800nm (D, H, L, P). Neurite outgrowth increased as both fiber size and PPy content increased. Scale bar 200μm.**

The percentage of neurite bearing cells and median neurite length was quantified to better elucidate the differences between the nanofibrous matrices. Only 0.8-1.0% of cells were neurite-bearing on the unstimulated aligned 150ES nanofibers (**Figure 4.7**A). With electrical stimulation, that jumped to 2.8% and 5.0% on the 150ES 10% PPy and 150ES 15% PPy nanofibers, respectively. 6.5-7.8% of cells bore neurites on unstimulated aligned 550ES fibers, increasing to 12.3% and 13.8% on 10% PPy and 15% PPy 550ES nanofibers, respectively (**Figure 4.7**B). Aligned 900ES nanofibers yielded 13.0-14.3% neurite-bearing cells in the absence of electrical stimulation. With electrical stimulation, the increase was significant on 10% PPy and 15% PPy, with 19.0% and 22.0%, respectively (**Figure 4.7**C). Finally, without stimulation the percentage of neurite-bearing cells was 12.8-14.3% on 1800ES fibers. With stimulation, there was a significant increase to 18.5% on 10% PPy and 23.8% on 15% PPy (**Figure 4.7**D).

Comparing random and aligned fibers, there was a significant difference on the two large sizes, 900ES and 1800ES, which displayed the highest percentages of neurite-bearing cells along with the longest median neurite lengths. With stimulation, there were more neurite-bearing cells on the 10% PPy and 15% PPy fibers. Without stimulation, there was only a significant difference between the 10% PPy and 15% PPy fibers at the largest 1800ES fiber size, though it should be noted that the p value for both was only 0.04 (**Figure 4.7**C, D). There were no significant differences in median neurite lengths between random and aligned nanofibers (**Figure 4.8**). These results indicated that alignment alone was not enough to promote neurite outgrowth for mouse D3 ESCs. In combination with electrical stimulation and large fiber sizes, alignment increased the percentage of neurite-bearing cells, but had little effect on neurite length.

**Discussion**

The relationship between fiber size, orientation, and electrical stimulation and ESC behavior has not been fully explored. Work has been done using various NSCs and neurons. These cells can be great models for neurite growth when new strategies for neural tissue are being explored. After all, inducing neurite growth for many of them is relatively simple. However, for practical applications in the clinic and for tissue engineering as a whole, their use becomes less attractive since they are difficult to harvest and grow to clinically relevant numbers. Embryonic stem cells, on the other hand, can proliferate indefinitely and have the ability to differentiate into any cell type in the body. In this study, properties of electrospun nanofibrous substrates were investigated to determine their capacity to induce neurite outgrowth of mouse D3 ESCs.

For fiber size, small nanofibers around 150nm effectively inhibited neurite growth. As fiber size increased, more ESCs produced longer neurites. The 900ES and 1800ES nanofibers promoted neurite growth in a similar fashion, indicating that somewhere between 550nm and 900nm there was a threshold met where the cells could fully produce neurites. This size threshold corresponds with the size of focal adhesions [165]. Between 900ES and 1800ES fibers, the 900ES fibers are likely more applicable for neural tissue engineering. With a similar cell response, the smaller 900ES fibers would allow for more fibers in a given area, increasing the amount of guidance a scaffold could perform.

Conducting polymer PPy was added to the PLLA in varying amounts to reduce the surface resistivity, opening up the potential to use electrical stimulation. Electrical stimulation with 100mV for 2hrs increased the percentage of neurite-bearing cells on the large fibers with

the highest PPy contents. This effect was further increased when the fibers were aligned. Electrical stimulation also increased the median neurite length on those same fibers, however, aligning the fibers did not have an additional effect on increasing neurite length. This is in contrast to other studies performed with PC12 cells [200] and NSCs [178] which showed that aligned fibers did result in an increase in neurite length. As mentioned, these cells are used as models for neurite growth and thus, their behavior is the ideal case. With ESCs, it is possible that there are conditions or time points that could result in aligned fibers having a significant effect on neurite growth. Further investigation is required to confirm these results. Interestingly, despite there being a difference in surface resistivity, electrical stimulation promoted neurite growth on both aligned and random nanofibers. The direction of the neurite growth was predominantly affected by the nanofibers and not the direction of the electrical field. Neurites that formed on the random fibers grew in random direction instead of with the applied electric potential. Previous work showed that even when the electrical potential was applied perpendicular to aligned nanofibers, the neurite outgrowth of dorsal root ganglia neurons increased [233]. This is an important factor in combining electrical stimulation with aligned conducting nanofibers.

The mechanism by which electrical stimulation promotes neurite growth is not well understood. There are several hypotheses that have been proposed including a difference in surface protein adsorption [230], a decrease in membrane potentials causing depolarization [234], and electrically-mediated rearrangement of membrane-bound proteins [235], yet more work needs to be done to fully elucidate the effect electrical stimulation has on cell behavior. A better understanding of the underlying mechanism will open up additional avenues for controlling cell behavior using electrical stimulation. This work continued the effort of understanding the interactions between ESCs, biomaterials, and electrical stimulation and offers

guidance to scaffold design for neural tissue engineering. Previously, we showed the fiber size-dependent promotion of neurite growth and neuronal differentiation of mouse D3 ESCs can be attributed to integrin α6β1 through extracellular signal-regulated kinase (ERK) activation. There is also some additional evidence that focal adhesions could play a role [236], potentially implicating focal adhesion kinase (FAK). Future work should delve into the mechanism and apply these composite PPy/PLLA nanofibers *in vivo*.

Other characteristics need to be taken into account when translating to an *in vivo* application. Though PPy is biocompatible and the electrical properties its inclusion imparts on the composite polymer result in improved *in vitro* results, PPy is not biodegradable. The benefits of PPy must be balanced with the drawbacks in order to optimize the use of composite nanofibers *in vivo*, including *in vivo* electrical stimulation. Work has been done on the use of electrical stimulation *in vivo* to improve nerve repair [237-239], both short term and long term. However, these studies do not use a long defect bridged with a nerve conduit. This study shows the potential electrical stimulation could have for neural tissue engineering with electrically conductive nanofibers.

**Conclusion**

Understanding the interaction between cells and biomaterials is a critical aspect of tissue engineering. For neural tissue engineering, a major aspect of this cell-biomaterial interaction involves neurite outgrowth promotion. In addition to nanofibrous biomaterials, electrical stimulation can also induce neurite outgrowth. Here, an array of random and aligned nanofibers with fiber diameters ranging from around 150nm up to around 1800nm was fabricated. Varying

amount of PPy was added to improve their electrical properties for *in vitro* electrical stimulation. Mouse D3 ESCs were seeded on these fibers to determine the effect topographical features in combination with electrical stimulation had on the neurite outgrowth of pluripotent stem cells, an extremely promising cell source for tissue engineering as a whole. As fiber size increased, neurite growth increased, with 900nm and 1800nm fibers promoting neurite growth the most. With the addition of electrical stimulation, applying 100mV for 2hrs increased the percentage of neurite-bearing cells and median neurite length on the large nanofibers with the highest content of PPy. Aligning these nanofibers increased the percentage of neurite-bearing cells and oriented the neurites along the direction of the fibers.

These results show that fiber size, electrical stimulation, and fiber alignment can control ESC behavior. In addition to making their use in neural tissue engineering more promising, applications of this work could stretch to other aspects of tissue engineering. ESCs and other pluripotent stem cells offer numerous benefits, including indefinite proliferation and versatile differentiation, yet controlling their fate remains a significant challenge. In this study, additional layers of control have been demonstrated to further the drive toward clinical applications.

# CHAPTER 5

## Summary

This project began by noticing a difference in the way embryonic stem cells (ESCs) behaved on thermally-induced phase separated (TIPS) and electrospun nanofibers. As this difference was explored, a fiber size-mediated effect on the neuronal differentiation of ESCs was discovered. Small nanofibers on the order of 150nm inhibited neuronal differentiation while nanofibers above approximately 900nm promoted neuronal differentiation. The mechanism behind this was investigated and it was found that integrin $\alpha6\beta1$, a major laminin binding integrin, was responsible and it acted through the mitogen-activated protein kinase (MAPK) pathway by activating extracellular signal-regulated kinase (ERK).

In parallel with studying the mechanism, a composite polymer using polypyrrole (PPy) and poly (l-lactic acid) (PLLA) was synthesized. Films fabricated with this polymer were seeded with rat pheochromocytoma 12 (PC12) cells and stimulated with 100mV for 2hrs. Electrical stimulation increased the percentage of neurite-bearing cells and the median neurite length, showing that PPy/PLLA had potential for nerve tissue engineering. A nerve conduit was then fabricated and used to regenerate a critical-sized sciatic nerve defect in a rat. The PPy/PLLA greatly exceeded the performance of PLLA conduits and performed on par with the current gold standard, a nerve autograft.

Combining the first two studies, PPy/PLLA was used to electrospin an array of nanofibers with varying fiber diameter, PPy content, and orientation. The purpose of this was to expound on the ability of nanofibers to control the neurite outgrowth of ESCs by incorporating additional cues, including topography and electrical stimulation. It was discovered that electrical stimulation promoted neurite outgrowth as PPy content increased and that aligned fibers increased the number of neurite-bearing cells.

Taken as a whole, these results significantly advance the fields of neural tissue engineering and neural development. Elucidating the mechanism by which ESCs interact with nanofibers could provide insight into the role the extracellular matrix (ECM) plays during neurodevelopment. In addition, it could provide guidance to scaffold design by revealing a target pathway to induce neuronal differentiation and neurite growth. Combined with the success showed by incorporating electrical stimulation and fiber alignment, there is significant promise in using this work as a platform for the clinical translation of ESCs for neural tissue engineering, and potentially tissue engineering as a whole.

# CHAPTER 6

## Future Work

One of the main accomplishments of this work was elucidating the mechanism of embryonic stem cell (ESC)-nanofiber interactions. While discovering the role of integrin α6β1 and extracellular signal-regulated kinase (ERK) was a great start, they are just two players in a complex system of pathways. Finding the links between α6β1 and ERK and then to other downstream transcription factors would fully reveal the cascade responsible for fiber size-mediated neuronal differentiation. Potential targets include focal adhesion kinase (FAK), phosphoinositide 3-kinase (PI3K)/protein kinase B (PKB/Akt), Ras/Raf, and signal transducer and activator of transcription 3 (STAT3) [240]. In addition, Wnt signaling has also been shown to be required for neuronal differentiation so the effects of nanofibers on Wnt activity should be investigated [241]. Later on, the effect of nanofibers on the differentiation of ESCs into other lineages could be explored for additional applications in development and tissue engineering.

Furthermore, this knowledge should be applied to scaffold design. The overarching goal of this project was to better understand the neuronal differentiation of ESCs to be applied to neural tissue engineering. The logical next step then towards the clinic is to use aligned PPy/PLLA nanofibers, around 900nm in diameter, within a nerve guidance conduit to repair a critically-sized sciatic nerve defect in a rat, the most common model for peripheral nerve

regeneration. The insight into the mechanism provides candidates to target with extracellular binding moieties or drug delivery. Binding integrin α6β1 or activating ERK could possibly enhance the fiber size-mediated effect on neuronal differentiation, though care would have to be taken to test for potential side effects. A higher goal would be to address a spinal cord injury (SCI). SCIs are a more difficult clinical challenge and less work has been done to address them.

In addition, more work could be with electrical stimulation on three fronts. First, this work only used one mode of stimulation, a single dose of 100mV direct current for 2hrs. One parameter that could be studied is the wave form of stimulation. Perhaps something similar to an action potential could be optimal. The magnitude should also be investigated since 100mV is a relatively high *in vitro* potential and there is some evidence that lower voltages yield better neurite growth [200]. Finally, the timing of electrical stimulation needs to be optimized. Stimulation over time could improve on the single early dose used in this study, though perhaps only early stimulation is important. More work needs to be done to better understand when and how much electrical stimulation is best for the neurite growth of ESCs. Second, in translating *in vivo*, electrical stimulation has not been investigated in conjunction with an electrically active nerve conduit. Like *in vitro*, the parameters of stimulation should be optimized in vivo. With a different environment, it is likely that a different mode of electrical stimulation will be optimal. Third, and finally, the mechanism behind the effect electrical stimulation has on neurite growth should be elucidated. There are several hypotheses that have been proposed, involving protein adsorption, membrane depolarization, and ion channel organization. Each has merit and is worthy of further investigation.

Finally, all the work in this thesis has been done with animal cells, either mouse D3 ESCs or rat pheochromocytoma 12 (PC12) cells. To translate to a clinical application, human cells

104

need to be studied. Working with human ESCs comes with moral, political, and ethical concerns, making their use less than ideal. As a promising alternative, induced pluripotent stem cells (iPSCs) could be used [119-121]. Derived from adult somatic cells, commonly fibroblasts, and reprogrammed with genes, either Oct3/4, Sox2, c-Myc, and KLF4 [122, 123], or Oct3/4, Sox2, Nanog, and Lin28 [124], they have the same pluripotent capabilities of ESCs without the extracurricular drawbacks. It is possible that the results of this work could not translate perfectly to a new cell line from a different species, so these studies performed should be repeated to ensure their veracity with human iPSCs. However, it is expected that the results should hold, possibly with only minor variation. Establishing the potential of human iPSCs for neural tissue engineering by increasing the control over their neuronal differentiation with scaffold architecture and determining the mechanism of action would be an enormous leap toward clinical applications in humans.

Although this work improves the foundation for neural tissue engineering, the timeline of clinical applications using ESCs or iPSCs may still be decades away. In the meantime, the significant questions will continue to be addressed as the field steps toward fully regeneration damaged tissues.

# BIBLIOGRAPHY

[1] National spinal cord injury statistical center: Facts and figures at a glance. Birmingham, AL: University of Alabama at Birmingham; March 2013.

[2] Cao Y, Chen Y, DeVivo M. Lifetime direct costs after spinal cord injury. Top Spinal Cord Inj. 2011;16:10-6.

[3] Chen Y, Tang Y, Vogel LC, DeVivo MJ. Causes of spinal cord injury. Top Spinal Cord Inj. 2013;19:1-8.

[4] Bauchet L, Lonjon N, Perrin FE, Gilbert C, Privat A, Fattal C. Strategies for spinal cord repair after injury: A review of the literature and information. Ann Phys Rehabil Med. 2009;52:330-51.

[5] Donnelly DJ, Popovich PG. Inflammation and its role in neuroprotection, axonal regeneration and functional recovery after spinal cord injury. Exp Neurol. 2008;209:378-88.

[6] Volpato FZ, Führmann T, Migliaresi C, Hutmacher DW, Dalton PD. Using extracellular matrix for regenerative medicine in the spinal cord. Biomaterials. 2013;34:4945-55.

[7] Kwon BK, Okon E, Hillyer J, Mann C, Baptiste D, Weaver LC, et al. A systematic review of non-invasive pharmacologic neuroprotective treatments for acute spinal cord injury. J Neurotraum. 2011;28:1545-88.

[8] Teasell RW, Mehta S, Aubut J-AL, Foulon B, Wolfe DL, Hsieh JTC, et al. A systematic review of pharmacological treatments of pain following spinal cord injury. Arch Phys Med Rehab. 2010;91:816-31.

[9] Schlosshauer B, Dreesmann L, Schaller HE, Sinis N. Synthetic nerve guide implants in humans: A comprehensive survey. Neurosurgery. 2006;59:740-8.

[10] Evans GR. Peripheral nerve injury: A review and approach to tissue engineered constructs. Anat Rec. 2001;263:396-404.

[11] Burnett MG, Zager EL. Pathophysiology of peripheral nerve injury: A brief review. Neurosurg Focus. 2004;16:E1.

[12] Scherman P, Kanje M, Dahlin LB. Bridging short nerve defects by direct repair under tension, nerve grafts or longitudinal sutures. Restor Neurol Neurosci. 2004;22:65-72.

[13] Strasberg SR, Mackinnon SE, Genden EM, Bain JR, Purcell CM, Hunter DA, et al. Long-segment nerve allograft regeneration in the sheep model: Experimental study and review of the literature. J Reconstr Microsurg. 1996;12:529-37.

[14] Zacchigna S, Giacca M. Chapter 20: Gene therapy perspectives for nerve repair. Int Rev Neurobiol. 2009;87:381-92.

[15] Dahlin L, Johansson F, Lindwall C, Kanje M. Chapter 28: Future perspective in peripheral nerve reconstruction. Int Rev Neurobiol. 2009;87:507-30.

[16] Hallgren A, Björkman A, Chemnitz A, Dahlin LB. Subjective outcome related to donor site morbidity after sural nerve graft harvesting: a survey in 41 patients. BMC Surg. 2013;13:39-.

[17] Meek MF, Coert JH. Clinical use of nerve conduits in peripheral-nerve repair: Review of the literature. J Reconstr Microsurg. 2002;18:97-109.

[18] Büngner OV. Ueber die degenerations und regenerationsvorgange am nerven nach verletzungen. Beitr Pathol Anat. 1891;10:321.

[19] Foramitti C. Zur technik der nervennaht. Arch Klin Chir. 1904;73:643-8.

[20] Nageotte J. Le processus de la cicatrisation des nerfs. CR Soc Biol. 1915;78:249.

[21] Wrede L. Ueberbrückung eines nervendefektes mittels seidennaht and lebenden venenstückes. Deut Med Wochenschr. 1909;35:1125.

[22] Tang JB, Gu YQ, Song YS. Repair of digital nerve defect with autogenous vein graft during flexor tendon surgery in zone-2. J Hand Surg-Brit Eur. 1993;18B:449-53.

[23] Tang JB. Vein conduits with interposition of nerve-tissue for peripheral-nerve defects. J Reconstr Microsurg. 1995;11:21-6.

[24] Malizos KN, Dailiana ZH, Anastasiou EA, Sarmas I, Soucacos PN. Neuromas and gaps of sensory nerves of the hand: Management using vein conduits. Am J Orthop. 1997;26:481-5.

[25] Pogrel MA, Maghen A. The use of autogenous vein grafts for inferior alveolar and lingual nerve reconstruction. J Oral Maxil Surg. 2001;59:985-8.

[26] Lundborg G, Dahlin L, Danielsen N, Zhao Q. Trophism, tropism, and specificity in nerve regeneration. J Reconstr Microsurg. 1994;10:345-54.

[27] Satou T, Nishida S, Hiruma S, Tanji K, Takahashi M, Fujita S, et al. A morphological-study on the effects of collagen gel matrix on regeneration of severed rat sciatic-nerve in silicone tubes. Acta Pathol Japon. 1986;36:199-208.

[28] Glasby MA, Gschmeissner SE, Huang CLH, Desouza BA. Degenerated muscle grafts used for peripheral-nerve repair in primates. J Hand Surg-Brit Eur. 1986;11B:347-51.

[29] Norris RW, Glasby MA, Gattuso JM, Bowden REM. Peripheral-nerve repair in humans using muscle autografts - A new technique. J Bone Joint Surg Br. 1988;70:530-3.

[30] Pereira JH, Bowden REM, Gattuso JM, Norris RW. Comparison of results of repair of digital nerves by denatured muscle grafts and end-to-end sutures. J Hand Surg-Brit Eur. 1991;16B:519-23.

[31] Pereira JH, Palande DD, Subramanian A, Narayanakumar TS, Curtis J, Turk JL. Denatured autologous muscle graft in leprosy. Lancet. 1991;338:1239-40.

[32] Lokanathan Y, Ng MH, Hasan S, Ali A, Mahmod M, Htwe O, et al. Olfactory ensheathing cells seeded muscle-stuffed vein as nerve conduit for peripheral nerve repair: A nerve conduction study. J Biosci Bioeng. 2014;118:231-4.

[33] Mackinnon SE, Dellon AL, Hudson AR, Hunter DA. Chronic nerve compression - An experimental-model in the rat. Ann Plas Surg. 1984;13:112-20.

[34] Dellon AL. Tube, or not tube... J Hand Surg. 1994;19B:271-2.

[35] Merle M, Dellon AL, Campbell JN, Chang PS. Complications from silicon-polymer intubulation of nerves. Microsurg. 1989;10:130-3.

[36] Lundborg G, Dahlin LB, Danielsen N. Ulnar nerve repair by the silicone chamber technique - Case-report. Scand J Plast Recons. 1991;25:79-82.

[37] Pogrel MA, McDonald AR, Kaban LB. Gore-Tex tubing as a conduit for repair of lingual and inferior alveolar nerve continuity defects: A preliminary report. J Oral Maxil Surg. 1998;56:319-21.

[38] Garrity RW. The use of plastic and rubber tubing in the management of irreparable nerve injuries. Surg forum. 1956;6:517-20.

[39] Mackinnon SE, Dellon AL. Clinical nerve reconstruction with a bioabsorbable polyglycolic acid tube. Plast Reconstr Surg. 1990;85:419-24.

[40] Weber RA, Breidenbach WC, Brown RE, Jabaley ME, Mass DP. A randomized prospective study of polyglycolic acid conduits for digital nerve reconstruction in humans. Plast Reconstr Surg. 2000;106:1036-45.

[41] Qiu T, Yin YX, Li BB, Xie LJ, Yan QJ, Dai HL, et al. PDLLA/PRGD/beta-TCP conduits build the neurotrophin-rich microenvironment suppressing the oxidative stress and promoting the sciatic nerve regeneration. J Biomed Mater Res A. 2014;102:3734-43.

[42] Matsumine H, Sasaki R, Yamato M, Okano T, Sakurai H. A polylactic acid non-woven nerve conduit for facial nerve regeneration in rats. J Tissue Eng Regen M. 2014;8:454-62.

[43] Widmer MS, Gupta PK, Lu LC, Meszlenyi RK, Evans GRD, Brandt K, et al. Manufacture of porous biodegradable polymer conduits by an extrusion process for guided tissue regeneration. Biomaterials. 1998;19:1945-55.

[44] Evans GRD, Brandt K, Katz S, Chauvin P, Otto L, Bogle M, et al. Bioactive poly(L-lactic acid) conduits seeded with Schwann cells for peripheral nerve regeneration. Biomaterials. 2002;23:841-8.

[45] Evans GRD, Brandt K, Widmer MS, Lu L, Meszlenyi RK, Gupta PK, et al. In vivo evaluation of poly(L-lactic acid) porous conduits for peripheral nerve regeneration. Biomaterials. 1999;20:1109-15.

[46] Li A, Hokugo A, Yalom A, Berns EJ, Stephanopoulos N, McClendon MT, et al. A bioengineered peripheral nerve construct using aligned peptide amphiphile nanofibers. Biomaterials. 2014;35:8780-90.

[47] Sulong AF, Hassan NH, Hwei NM, Lokanathan Y, Naicker AS, Abdullah S, et al. Collagen-coated polylactic-glycolic acid (PLGA) seeded with neural-differentiated human mesenchymal stem cells as a potential nerve conduit. Adv Clin Exp Med. 2014;23:353-62.

[48] Hadlock T, Sundback C, Hunter D, Cheney M, Vacanti JP. A polymer foam conduit seeded with Schwann cells promotes guided peripheral nerve regeneration. Tissue Eng. 2000;6:119-27.

[49] de Luca AC, Terenghi G, Downes S. Chemical surface modification of poly-epsilon-caprolactone improves Schwann cell proliferation for peripheral nerve repair. J Tissue Eng Regen M. 2014;8:153-63.

[50] Nguyen HT, Sapp S, Wei C, Chow JK, Nguyen A, Coursen J, et al. Electric field stimulation through a biodegradable polypyrrole-co-polycaprolactone substrate enhances neural cell growth. J Biomed Mater Res A. 2014;102:2554-64.

[51] Schnell E, Klinkhammer K, Balzer S, Brook G, Klee D, Dalton P, et al. Guidance of glial cell migration and axonal growth on electrospun nanofibers of poly-epsilon-caprolactone and a collagen/poly-epsilon-caprolactone blend. Biomaterials. 2007;28:3012-25.

[52] Forciniti L, Ybarra J, Zaman MH, Schmidt CE. Schwann cell response on polypyrrole substrates upon electrical stimulation. Acta Biomater. 2014;10:2423-33.

[53] Yu WW, Jiang XQ, Cai M, Zhao W, Ye DX, Zhou Y, et al. A novel electrospun nerve conduit enhanced by carbon nanotubes for peripheral nerve regeneration. Nanotechnology. 2014;25.

[54] Dinis TM, Vidal G, Jose RR, Vigneron P, Bresson D, Fitzpatrick V, et al. Complementary effects of two growth factors in multifunctionalized silk nanofibers for nerve reconstruction. Plos One. 2014;9.

[55] Gu Y, Zhu JB, Xue CB, Li ZMY, Ding F, Yang YM, et al. Chitosan/silk fibroin-based, Schwann cell-derived extracellular matrix-modified scaffolds for bridging rat sciatic nerve gaps. Biomaterials. 2014;35:2253-63.

[56] Cui Y, Lu C, Meng DQ, Xiao ZF, Hou XL, Ding WY, et al. Collagen scaffolds modified with CNTF and bFGF promote facial nerve regeneration in minipigs. Biomaterials. 2014;35:7819-27.

[57] di Summa PG, Kingham PJ, Campisi CC, Raffoul W, Kalbermatten DF. Collagen (NeuraGen (R)) nerve conduits and stem cells for peripheral nerve gap repair. Neurosci Lett. 2014;572:26-31.

[58] Ma F, Xiao Z, Meng D, Hou X, Zhu J, Dai J, et al. Use of natural neural scaffolds consisting of engineered vascular endothelial growth factor immobilized on ordered collagen fibers filled in a collagen tube for peripheral nerve regeneration in rats. Int J Mol Sci. 2014;15:18593-609.

[59] Li GC, Zhao XY, Zhao WX, Zhang LZ, Wang CP, Jiang MR, et al. Porous chitosan scaffolds with surface micropatterning and inner porosity and their effects on Schwann cells. Biomaterials. 2014;35:8503-13.

[60] Zhao J, Zheng XF, Fu CY, Qu W, Wei GQ, Zhang WG. FK506-loaded chitosan conduit promotes the regeneration of injured sciatic nerves in the rat through the upregulation of brain-derived neurotrophic factor and TrkB. J Neurol Sci. 2014;344:20-6.

[61] Biazar E, Keshel SH. Gelatin-modified nanofibrous PHBV tube as artificial nerve graft for rat sciatic nerve regeneration. Int J Polymer Mater Polymer Biomater. 2014;63:330-6.

[62] He LM, Liao SS, Quan DP, Ma K, Chan C, Ramakrishna S, et al. Synergistic effects of electrospun PLLA fiber dimension and pattern on neonatal mouse cerebellum C17.2 stem cells. Acta Biomater. 2010;6:2960-9.

[63] Horne MK, Nisbet DR, Forsythe JS, Parish CL. Three dimensional nanofibrous scaffolds incorporating immobilized BDNF promote proliferation and differentiation of cortical neural stem cells. Stem Cells and Dev. 2010;19:843-52.

[64] Prabhakaran MP, Venugopal JR, Ramakrishna S. Mesenchymal stem cell differentiation to neuronal cells on electrospun nanofibrous substrates for nerve tissue engineering. Biomaterials. 2009;30:4996-5003.

[65] Cao HQ, Liu T, Chew SY. The application of nanofibrous scaffolds in neural tissue engineering. Adv Drug Deliver Rev. 2009;61:1055-64.

[66] Sun CH, Jin XB, Holzwarth JM, Liu XH, Hu J, Gupte MJ, et al. Development of channeled nanofibrous scaffolds for oriented tissue engineering. Macromol Biosci. 2012;12:761-9.

[67] Samadikuchaksaraei A. An overview of tissue engineering approaches for management of spinal cord injuries. J Neuroeng Rehabil. 2007;4.

[68] Yoshii S, Oka M, Shima M, Akagi M, Taniguchi A. Bridging a spinal cord defect using collagen filament. Spine. 2003;28:2346-51.

[69] Yoshii S, Oka M, Shima M, Taniguchi A, Taki Y, Akagi M. Restoration of function after spinal cord transection using a collagen bridge. J Biomed Mater Res A. 2004;70A:569-75.

[70] Tsai EC, Dalton PD, Shoichet MS, Tator CH. Matrix inclusion within synthetic hydrogel guidance channels improves specific supraspinal and local axonal regeneration after complete spinal cord transection. Biomaterials. 2006;27:519-33.

[71] Liu S, Said G, Tadie M. Regrowth of the rostral spinal axons into the caudal ventral roots through a collagen tube implanted into hemisected adult rat spinal cord. Neurosurgery. 2001;49:143-50.

[72] Novikova LN, Mosahebi A, Wiberg M, Terenghi G, Kellerth JO, Novikov LN. Alginate hydrogel and matrigel as potential cell carriers for neurotransplantation. J Biomed Mater Res A. 2006;77A:242-52.

[73] Prang P, Muller R, Eljaouhari A, Heckmann K, Kunz W, Weber T, et al. The promotion of oriented axonal regrowth in the injured spinal cord by alginate-based anisotropic capillary hydrogels. Biomaterials. 2006;27:3560-9.

[74] Taylor SJ, McDonald JW, Sakiyama-Elbert SE. Controlled release of neurotrophin-3 from fibrin gels for spinal cord injury. J Control Release. 2004;98:281-94.

[75] Xiao M, Klueber KM, Lu CL, Guo ZF, Marshall CT, Wang HM, et al. Human adult olfactory neural progenitors rescue axotomized rodent rubrospinal neurons and promote functional recovery. Exp Neurol. 2005;194:12-30.

[76] King VR, Henseler M, Brown RA, Priestley JV. Mats made from fibronectin support oriented growth of axons in the damaged spinal cord of the adult rat. Exp Neurol. 2003;182:383-98.

[77] King VR, Phillips JB, Brown RA, Priestley JV. The effects of treatment with antibodies to transforming growth factor beta 1 and beta 2 following spinal cord damage in the adult rat. Neuroscience. 2004;126:173-83.

[78] Stokols S, Tuszynski MH. Freeze-dried agarose scaffolds with uniaxial channels stimulate and guide linear axonal growth following spinal cord injury. Biomaterials. 2006;27:443-51.

[79] Woerly S. Restorative surgery of the central nervous system by means of tissue engineering using NeuroGel implants. Neurosurg Rev. 2000;23:59-77.

[80] Tsai EC, Dalton PD, Shoichet MS, Tator CH. Synthetic hydrogel guidance channels facilitate regeneration of adult rat brainstem motor axons after complete spinal cord transection. J Neurotraum. 2004;21:789-804.

[81] Bakshi A, Fisher O, Dagci T, Himes BT, Fischer I, Lowman A. Mechanically engineered hydrogel scaffolds for axonal growth and angiogenesis after transplantation in spinal cord injury. J Neurosurg-Spine. 2004;1:322-9.

[82] Dalton PD, Flynn L, Shoichet MS. Manufacture of poly(2-hydroxyethyl methacrylate-co-methyl methacrylate) hydrogel tubes for use as nerve guidance channels. Biomaterials. 2002;23:3843-51.

[83] Woerly S, Doan V, Sosa N, de Vellis J, Espinosa A. Reconstruction of the transected cat spinal cord following NeuroGel (TM) implantation: Axonal tracing, immunohistochemical and ultrastructural studies. Int J Dev Neurosci. 2001;19:63-83.

[84] Woerly S, Doan V, Evans-Martin F, Paramore CG, Peduzzi JD. Spinal cord reconstruction using NeuroGel (TM) implants and functional recovery after chronic injury. J Neurosci Res. 2001;66:1187-97.

[85] Gautier SE, Oudega M, Fragoso M, Chapon P, Plant GW, Bunge MB, et al. Poly(alpha-hydroxyacids) for application in the spinal cord: Resorbability and biocompatibility with adult rat Schwann cells and spinal cord. J Biomed Mater Res. 1998;42:642-54.

[86] Maquet V, Martin D, Scholtes F, Franzen R, Schoenen J, Moonen G, et al. Poly(D,L-lactide) foams modified by poly(ethylene oxide)-block-poly(D,L-lactide) copolymers and a-FGF: In vitro and in vivo evaluation for spinal cord regeneration. Biomaterials. 2001;22:1137-46.

[87] Blacher S, Maquet V, Schils F, Martin D, Schoenen J, Moonen G, et al. Image analysis of the axonal ingrowth into poly(D,L-lactide) porous scaffolds in relation to the 3-D porous structure. Biomaterials. 2003;24:1033-40.

[88] Patist CM, Mulder MB, Gautier SE, Maquet V, Jerome R, Oudega M. Freeze-dried poly(D,L-lactic acid) macroporous guidance scaffolds impregnated with brain-derived neurotrophic factor in the transected adult rat thoracic spinal cord. Biomaterials. 2004;25:1569-82.

[89] Sedaghati T, Jell G, Seifalian A. Investigation of Schwann cell behaviour on RGD-functionalised bioabsorbable nanocomposite for peripheral nerve regeneration. New Biotechnol. 2014;31:203-13.

[90] Jasmin L, Janni G, Moallem TM, Lappi DA, Ohara PT. Schwann cells are removed from the spinal cord after effecting recovery from paraplegia. J Neurosci. 2000;20:9215-23.

[91] Guest JD, Hiester ED, Bunge RP. Demyelination and Schwann cell responses adjacent to injury epicenter cavities following chronic human spinal cord injury. Exp Neurol. 2005;192:384-93.

[92] Chernousov MA, Rothblum K, Tyler WA, Stahl RC, Carey DJ. Schwann cells synthesize type V collagen that contains a novel alpha 4 chain - Molecular cloning, biochemical characterization, and high affinity heparin binding of alpha 4(V) collagen. J Biol Chem. 2000;275:28208-15.

[93] Chernousov MA, Carey DJ. Schwann cell extracellular matrix molecules and their receptors. Histol Histopathol. 2000;15:593-601.

[94] Grothe C, Meisinger C, Claus P. In vivo expression and localization of the fibroblast growth factor system in the intact and lesioned rat peripheral nerve and spinal ganglia. J Comp Neurol. 2001;434:342-57.

[95] Mirsky R, Jessen KR, Brennan A, Parkinson D, Dong ZP, Meier C, et al. Schwann cells as regulators of nerve development. J Physiology-Paris. 2002;96:17-24.

[96] Keyvan-Fouladi N, Raisman G, Li Y. Delayed repair of corticospinal tract lesions as an assay for the effectiveness of transplantation of Schwann cells. Glia. 2005;51:306-11.

[97] Mackay-Sim A, Feron F, Cochrane J, Bassingthwaighte L, Bayliss C, Davies W, et al. Autologous olfactory ensheathing cell transplantation in human paraplegia: A 3-year clinical trial. Brain. 2008;131:2376-86.

[98] Tabakow P, Jarmundowicz W, Czapiga B, Fortuna W, Miedzybrodzki R, Czyz M, et al. Transplantation of autologous olfactory ensheathing cells in complete human spinal cord injury. Cell Transplant. 2013;22:1591-612.

[99] Rapalino O, Lazarov-Spiegler O, Agranov E, Velan GJ, Yoles E, Fraidakis M, et al. Implantation of stimulated homologous macrophages results in partial recovery of paraplegic rats. Nat Med. 1998;4:814-21.

[100] Bomstein Y, Marder JB, Vitner K, Smirnov I, Lisaey G, Butovsky O, et al. Features of skin-coincubated macrophages that promote recovery from spinal cord injury. J Neuroimmunol. 2003;142:10-6.

[101] Moalem G, Leibowitz-Amit R, Yoles E, Mor F, Cohen IR, Schwartz M. Autoimmune T cells protect neurons from secondary degeneration after central nervous system axotomy. Nat Med. 1999;5:49-55.

[102] Mikami Y, Okano H, Sakaguchi M, Nakamura M, Shimazaki T, Okano HJ, et al. Implantation of dendritic cells in injured adult spinal cord results in activation of endogenous neural stem/progenitor cells leading to de novo neurogenesis and functional recovery. J Neurosci Res. 2004;76:453-65.

[103] Hauben E, Gothilf A, Cohen A, Butovsky O, Nevo U, Smirnov I, et al. Vaccination with dendritic cells pulsed with peptides of myelin basic protein promotes functional recovery from spinal cord injury. J Neurosci. 2003;23:8808-19.

[104] Iwanami A, Kaneko S, Nakamura M, Kanemura Y, Mori H, Kobayashi S, et al. Transplantation of human neural stem cells for spinal cord injury in primates. J Neurosci Res. 2005;80:182-90.

[105] Hung CH, Lin YL, Young TH. The effect of chitosan and PVDF substrates on the behavior of embryonic rat cerebral cortical stem cells. Biomaterials. 2006;27:4461-9.

[106] Kanemura Y, Mori H, Kobayashi S, Islam O, Kodama E, Yamamoto A, et al. Evaluation of in vitro proliferative activity of human fetal neural stem/progenitor cells using indirect measurements of viable cells based on cellular metabolic activity. J Neurosci Res. 2002;69:869-79.

[107] Lu F, Wong CS. A clonogenic survival assay of neural stem cells in rat spinal cord after exposure to ionizing radiation. Radiat Res. 2005;163:63-71.

[108] Akiyama Y, Honmou O, Kato T, Uede T, Hashi K, Kocsis JD. Transplantation of clonal neural precursor cells derived from adult human brain establishes functional peripheral myelin in the rat spinal cord. Exp Neurol. 2001;167:27-39.

[109] Mishra SK, Braun N, Shukla V, Fullgrabe M, Schomerus C, Korf HW, et al. Extracellular nucleotide signaling in adult neural stem cells: Synergism with growth factor-mediated cellular proliferation. Development. 2006;133:675-84.

[110] Doetsch F, Caille I, Lim DA, Garcia-Verdugo JM, Alvarez-Buylla A. Subventricular zone astrocytes are neural stem cells in the adult mammalian brain. Cell. 1999;97:703-16.

[111] Priller J, Persons DA, Klett FF, Kempermann G, Kreutzberg GW, Dirnagl U. Neogenesis of cerebellar Purkinje neurons from gene-marked bone marrow cells in vivo. J Cell Biol. 2001;155:733-8.

[112] Mezey E, Chandross KJ, Harta G, Maki RA, McKercher SR. Turning blood into brain: Cells bearing neuronal antigens generated in vivo from bone marrow. Science. 2000;290:1779-82.

[113] Brazelton TR, Rossi FMV, Keshet GI, Blau HM. From marrow to brain: Expression of neuronal phenotypes in adult mice. Science. 2000;290:1775-9.

[114] Weimann JM, Charlton CA, Brazelton TR, Hackman RC, Blau HM. Contribution of transplanted bone marrow cells to Purkinje neurons in human adult brains. P Natl Acad Sci USA. 2003;100:2088-93.

[115] Mezey E, Key S, Vogelsang G, Szalayova I, Lange GD, Crain B. Transplanted bone marrow generates new neurons in human brains. P Natl Acad Sci USA. 2003;100:1364-9.

[116] Siemionow M, Kwiecien G, Madajka M, Uygur S, Bobkiewicz A, Caplan A. Functional results of peripheral nerve repair with human epineural sheath conduit supported with human mesenchymal stem cells. Transplantation. 2014;98:303-.

[117] Conley BJ, Young JC, Trounson AO, Mollard R. Derivation, propagation and differentiation of human embryonic stem cells. Int J Biochem Cell B. 2004;36:555-67.

[118] Kimura H, Yoshikawa M, Matsuda R, Toriumi H, Nishimura F, Hirabayashi H, et al. Transplantation of embryonic stem cell-derived neural stem cells for spinal cord injury in adult mice. Neurol Res. 2005;27:812-9.

[119] Ikeda M, Uemura T, Takamatsu K, Okada M, Kazuki K, Tabata Y, et al. Acceleration of peripheral nerve regeneration using nerve conduits in combination with induced pluripotent stem cell technology and a basic fibroblast growth factor drug delivery system. J Biomed Mater Res A. 2014;102:1370-8.

[120] Uemura T, Takamatsu K, Ikeda M, Okada M, Kazuki K, Ikada Y, et al. Transplantation of induced pluripotent stem cell-derived neurospheres for peripheral nerve repair. Biochem Bioph Res Co. 2012;419:130-5.

[121] Wang A, Tang Z, Park I-H, Zhu Y, Patel S, Daley GQ, et al. Induced pluripotent stem cells for neural tissue engineering. Biomaterials. 2011;32:5023-32.

[122] Takahashi K, Tanabe K, Ohnuki M, Narita M, Ichisaka T, Tomoda K, et al. Induction of pluripotent stem cells from adult human fibroblasts by defined factors. Cell. 2007;131:861-72.

[123] Park I-H, Zhao R, West JA, Yabuuchi A, Huo H, Ince TA, et al. Reprogramming of human somatic cells to pluripotency with defined factors. Nature. 2008;451:141-U1.

[124] Yu J, Vodyanik MA, Smuga-Otto K, Antosiewicz-Bourget J, Frane JL, Tian S, et al. Induced pluripotent stem cell lines derived from human somatic cells. Science. 2007;318:1917-20.

[125] Faroni A, Smith RJP, Reid AJ. Adipose derived stem cells and nerve regeneration. Neural Regen Res. 2014;9:1341-6.

[126] Kolar MK, Kingham PJ. Regenerative effects of adipose-tissue-derived stem cells for treatment of peripheral nerve injuries. Biochem Soc T. 2014;42:697-701.

[127] Liu BS, Yang YC, Shen CC. Regenerative effect of adipose tissue-derived stem cells transplantation using nerve conduit therapy on sciatic nerve injury in rats. J Tissue Eng Regen M. 2014;8:337-50.

[128] Jezierski A, Gruslin A, Tremblay R, Ly D, Smith C, Turksen K, et al. Probing stemness and neural commitment in human amniotic fluid cells. Stem Cell Rev Rep. 2010;6:199-214.

[129] Strubing C, Ahnerthilger G, Shan J, Wiedenmann B, Hescheler J, Wobus AM. Differentiation of pluripotent embryonic stem-cells into the neuronal lineage in-vitro gives rise to mature inhibitory and excitatory neurons. Mech Develop. 1995;53:275-87.

[130] Schmidt MM, Guan K, Wobus AM. Lithium influences differentiation and tissue-specific gene expression of mouse embryonic stem (ES) cells in vitro. Int J Dev Biol. 2001;45:421-9.

[131] Guan KM, Chang H, Rolletschek A, Wobus AM. Embryonic stem cell-derived neurogenesis - Retinoic acid induction and lineage selection of neuronal cells. Cell Tissue Res. 2001;305:171-6.

[132] Wobus AM, Rohwedel J, Maltsev V, Hescheler J. In-vitro differentiation of embryonic stem-cells into cardiomyocytes or skeletal-muscle cells is specifically modulated by retinoic acid. Roux Arch Dev Biol. 1994;204:36-45.

[133] Bain G, Kitchens D, Yao M, Huettner JE, Gottlieb DI. Embryonic stem-cells express neuronal properties in-vitro. Dev Biol. 1995;168:342-57.

[134] Fraichard A, Chassande O, Bilbaut G, Dehay C, Savatier P, Samarut J. In-vitro differentiation of embryonic stem-cells into glial-cells and functional-neurons. J Cell Sci. 1995;108:3181-8.

[135] Okabe S, ForsbergNilsson K, Spiro AC, Segal M, McKay RDG. Development of neuronal precursor cells and functional postmitotic neurons from embryonic stem cells in vitro. Mech Develop. 1996;59:89-102.

[136] Lee SH, Lumelsky N, Studer L, Auerbach JM, McKay RD. Efficient generation of midbrain and hindbrain neurons from mouse embryonic stem cells. Nat Biotechnol. 2000;18:675-9.

[137] Thomson JA, Itskovitz-Eldor J, Shapiro SS, Waknitz MA, Swiergiel JJ, Marshall VS, et al. Embryonic stem cell lines derived from human blastocysts. Science. 1998;282:1145-7.

[138] Reyes JH, O'Shea KS, Wys NL, Velkey JM, Prieskorn DM, Wesolowski K, et al. Glutamatergic neuronal differentiation of mouse embryonic stem cells after transient expression of neurogenin 1 and treatment with BDNF and GDNF: In vitro and in vivo studies. J Neurosci. 2008;28:12622-31.

[139] Colombo E, Giannelli SG, Galli R, Tagliafico E, Foroni C, Tenedini E, et al. Embryonic stem-derived versus somatic neural stem cells: A comparative analysis of their developmental potential and molecular phenotype. Stem Cells. 2006;24:825-34.

[140] Christopherson GT, Song H, Mao HQ. The influence of fiber diameter of electrospun substrates on neural stem cell differentiation and proliferation. Biomaterials. 2009;30:556-64.

[141] Xie J, Willerth SM, Li X, Macewan MR, Rader A, Sakiyama-Elbert SE, et al. The differentiation of embryonic stem cells seeded on electrospun nanofibers into neural lineages. Biomaterials. 2009;30:354-62.

[142] Nur-E-Kamal A, Ahmed I, Kamal J, Schindler M, Meiners S. Three-dimensional nanofibrillar surfaces promote self-renewal in mouse embryonic stem cells. Stem Cells. 2006;24:426-33.

[143] Smith LA, Liu X, Hu J, Wang P, Ma PX. Enhancing osteogenic differentiation of mouse embryonic stem cells by nanofibers. Tissue Eng Pt A. 2009;15:1855-64.

[144] Woo KM, Chen VJ, Ma PX. Nano-fibrous scaffolding architecture selectively enhances protein adsorption contributing to cell attachment. J Biomed Mater Res A. 2003;67A:531-7.

[145] Woo KM, Jun J-H, Chen VJ, Seo J, Baek J-H, Ryoo H-M, et al. Nano-fibrous scaffolding promotes osteoblast differentiation and biomineralization. Biomaterials. 2007;28:335-43.

[146] Leevers SJ, Paterson HF, Marshall CJ. Requirement for Ras in Raf activation is overcome by targeting Raf to the plasma-membrane. Nature. 1994;369:411-4.

[147] Li ZG, Theus MH, Wei L. Role of ERK 1/2 signaling in neuronal differentiation of cultured embryonic stem cells. Dev Growth Differ. 2006;48:513-23.

[148] Jain N, Zhang T, Fong SL, Lim CP, Cao XM. Repression of Stat3 activity by activation of mitogen-activated protein kinase (MAPK). Oncogene. 1998;17:3157-67.

[149] Qui MS, Green SH. PC12 cell neuronal differentiation is associated with prolonged p21ras activity and consequent prolonged ERK activity. Neuron. 1992;9:705-17.

[150] Leppa S, Saffrich R, Ansorge W, Bohmann D. Differential regulation of c-Jun by ERK and JNK during PC12 cell differentiation. Embo Journal. 1998;17:4404-13.

[151] Doetschman TC, Eistetter H, Katz M, Schmidt W, Kemler R. The in vitro development of blastocyst-derived embryonic stem-cell lines - Formation of visceral yolk-sac, blood islands and myocardium. J Embryol Exp Morph. 1985;87:27-&.

[152] Nykvist P, Tu H, Ivaska J, Käpylä J, Pihlajaniemi T, Heino J. Distinct recognition of collagen subtypes by α1β1 and α2β1 integrins: α1β1 mediates cell adhesion to type XIII collagen. J Biol Chem. 2000;275:8255-61.

[153] Kern A, Eble J, Golbik R, Kuhn K. Interaction of type IV collagen with the isolated integrins alpha 1 beta 1 and alpha 2 beta 1. Eur J Biochem. 1993;215:151-9.

[154] Kikkawa Y, Sanzen N, Fujiwara H, Sonnenberg A, Sekiguchi K. Integrin binding specificity of laminin-10/11 : laminin-10/11 are recognized by alpha 3 beta 1, alpha 6 beta 1 and alpha 6 beta 4 integrins. J Cell Sci. 2000;113:869-76.

[155] Nishiuchi R, Takagi J, Hayashi M, Ido H, Yagi Y, Sanzen N, et al. Ligand-binding specificities of laminin-binding integrins: A comprehensive survey of laminin-integrin interactions using recombinant alpha 3 beta 1, alpha 6 beta 1, alpha 7 beta 1 and alpha 6 beta 4 integrins. Matrix Biol. 2006;25:189-97.

[156] Moursi AM, Globus RK, Damsky CH. Interactions between integrin receptors and fibronectin are required for calvarial osteoblast differentiation in vitro. J Cell Sci. 1997;110:2187-96.

[157] Tiger CF, Fougerousse F, Grundstrom G, Velling T, Gullberg D. alpha 11 beta 1 integrin is a receptor for interstitial collagens involved in cell migration and collagen reorganization on mesenchymal nonmuscle cells. Dev Biol. 2001;237:116-29.

[158] Zhang WM, Kapyla J, Puranen JS, Knight CG, Tiger CF, Pentikainen OT, et al. alpha(11)beta(1) integrin recognizes the GFOGER sequence in interstitial collagens. J Biol Chem. 2003;278:7270-7.

[159] Doetsch F. A niche for adult neural stem cells. Curr Opin Genet Dev. 2003;13:543-50.

[160] Lensch MW, Daheron L, Schlaeger TM. Pluripotent stem cells and their niches. Stem Cell Rev. 2006;2:185-201.

[161] Goetz AK, Scheffler B, Chen HX, Wang SS, Suslov O, Xiang H, et al. Temporally restricted substrate interactions direct fate and specification of neural precursors derived from embryonic stem cells. P Natl Acad Sci USA. 2006;103:11063-8.

[162] Flanagan LA, Rebaza LM, Derzic S, Schwartz PH, Monuki ES. Regulation of human neural precursor cells by laminin and integrins. J Neurosci Res. 2006;83:845-56.

[163] Kearns SM, Laywell ED, Kukekov VK, Steindler DA. Extracellular matrix effects on neurosphere cell motility. Exp Neurol. 2003;182:240-4.

[164] Smith LA, Beck J, Ma PX. Fabrication and tissue formation with nano-fibrous scaffolds. In: Kumar C, editor. Nanotechnologies for Tissue, Cell and Organ Engineering. Weinheim, Germany: Wiley-VCH; 2007.

[165] Kim D-H, Wirtz D. Focal adhesion size uniquely predicts cell migration. Faseb J. 2013;27:1351-61.

[166] Torimura T, Ueno T, Kin M, Ogata R, Inuzuka S, Sugawara H, et al. Integrin alpha6beta1 plays a significant role in the attachment of hepatoma cells to laminin. J Hepatol. 1999;31:734-40.

[167] Carloni V, Romanelli RG, Mercurio AM, Pinzani M, Laffi G, Cotrozzi G, et al. Knockout of alpha6 beta1-integrin expression reverses the transformed phenotype of hepatocarcinoma cells. Gastroenterology. 1998;115:433-42.

[168] Maitra N, Flink IL, Bahl JJ, Morkin E. Expression of alpha and beta integrins during terminal differentiation of cardiomyocytes. Cardiovasc Res. 2000;47:715-25.

[169] Tate MC, Garcia AJ, Keselowsky BG, Schumm MA, Archer DR, LaPlaca MC. Specific beta1 integrins mediate adhesion, migration, and differentiation of neural progenitors derived from the embryonic striatum. Mol Cell Neurosci. 2004;27:22-31.

[170] Nurcombe V. Laminin in neural development. Pharmacol Ther. 1992;56:247-64.

[171] Liesi P. Extracellular-matrix and neuronal movement. Experientia. 1990;46:900-7.

[172] Aouadi M, Bost F, Caron L, Laurent K, Le Marchand Brustel Y, Binetruy B. p38 mitogen-activated protein kinase activity commits embryonic stem cells to either neurogenesis or cardiomyogenesis. Stem Cells. 2006;24:1399-406.

[173] Reffas S, Schlegel W. Compartment-specific regulation of extracellular signal-regulated kinase (ERK) and c-Jun N-terminal kinase (JNK) mitogen-activated protein kinases (MAPKs) by ERK-dependent and non-ERK-dependent inductions of MAPK phosphatase (MKP)-3 and MKP-1 in differentiating P19 cells. Biochem J. 2000;352:701-8.

[174] Campos LS, Leone DP, Relvas JB, Brakebusch C, Fassler R, Suter U, et al. beta 1 integrins activate a MAPK signalling pathway in neural stem cells that contributes to their maintenance. Development. 2004;131:3433-44.

[175] Klesse LJ, Meyers KA, Marshall CJ, Parada LF. Nerve growth factor induces survival and differentiation through two distinct signaling cascades in PC12 cells. Oncogene. 1999;18:2055-68.

[176] Holzwarth JM, Ma PX. Biomimetic nanofibrous scaffolds for bone tissue engineering. Biomaterials. 2011;32:9622-9.

[177] Holzwarth JM, Ma PX. 3D nanofibrous scaffolds for tissue engineering. J Mater Chem. 2011;21:10243-51.

[178] Yang F, Murugan R, Wang S, Ramakrishna S. Electrospinning of nano/micro scale poly(L-lactic acid) aligned fibers and their potential in neural tissue engineering. Biomaterials. 2005;26:2603-10.

[179] Xu CY, Inai R, Kotaki M, Ramakrishna S. Aligned biodegradable nanotibrous structure: A potential scaffold for blood vessel engineering. Biomaterials. 2004;25:877-86.

[180] Sill TJ, von Recum HA. Electro spinning: Applications in drug delivery and tissue engineering. Biomaterials. 2008;29:1989-2006.

[181] Ignatiadis IA, Yiannakopoulos CK, Barbitsioti AD, Avram AM, Patralexis HG, Tsolakis CK, et al. Diverse types of epineural conduits for bridging short nerve defects: An experimental study in the rabbit. Microsurg. 2007;27:98-104.

[182] Wang X, Hu W, Cao Y, Yao J, Wu J, Gu X. Dog sciatic nerve regeneration across a 30-mm defect bridged by a chitosan/PGA artificial nerve graft. Brain. 2005;128:1897-910.

[183] Nakayama K, Takakuda K, Koyama Y, Itoh S, Wang W, Mukai T, et al. Enhancement of peripheral nerve regeneration using bioabsorbable polymer tubes packed with fibrin gel. Artif Organs. 2007;31:500-8.

[184] Neubauer D, Graham JB, Muir D. Nerve grafts with various sensory and motor fiber compositions are equally effective for the repair of a mixed nerve defect. Exp Neurol. 2010;223:203-6.

[185] Roganovic Z, Ilic S, Savic M. Radial nerve repair using an autologous denatured muscle graft: Comparison with outcomes of nerve graft repair. Acta Neurochir. 2007;149:1033-8.

[186] Fansa H, Keilhoff G, Wolf G, Schneider W. Tissue engineering of peripheral nerves: A comparison of venous and acellular muscle grafts with cultured Schwann cells. Plast Reconstr Surg. 2001;107:485-96.

[187] Wilson DH, Jagadeesh P. Experimental regeneration in peripheral nerves and the spinal cord in laboratory animals exposed to a pulsed electromagnetic field. Paraplegia. 1976;14:12-20.

[188] Gurunathan K, Murugan AV, Marimuthu R, Mulik UP, Amalnerkar DP. Electrochemically synthesised conducting polymeric materials for applications towards technology in electronics, optoelectronics and energy storage devices. Mater Chem Phys. 1999;61:173-91.

[189] Jager EW, Smela E, Inganas O. Microfabricating conjugated polymer actuators. Science. 2000;290:1540-5.

[190] Guimard NK, Gomez N, Schmidt CE. Conducting polymers in biomedical engineering. Prog Polym Sci. 2007;32:876-921.

[191] Ateh DD, Navsaria HA, Vadgama P. Polypyrrole-based conducting polymers and interactions with biological tissues. J R Soc Interface. 2006;3:741-52.

[192] Schmidt CE, Shastri VR, Vacanti JP, Langer R. Stimulation of neurite outgrowth using an electrically conducting polymer. P Natl Acad Sci USA. 1997;94:8948-53.

[193] Gomez N, Schmidt CE. Nerve growth factor-immobilized polypyrrole: Bioactive electrically conducting polymer for enhanced neurite extension. J Biomed Mater Res A. 2007;81:135-49.

[194] Sanghvi AB, Miller KP, Belcher AM, Schmidt CE. Biomaterials functionalization using a novel peptide that selectively binds to a conducting polymer. Nat Mater. 2005;4:496-502.

[195] Song HK, Toste B, Ahmann K, Hoffman-Kim D, Palmore GT. Micropatterns of positive guidance cues anchored to polypyrrole doped with polyglutamic acid: A new platform for characterizing neurite extension in complex environments. Biomaterials. 2006;27:473-84.

[196] Gomez N, Lee JY, Nickels JD, Schmidt CE. Micropatterned polypyrrole: A combination of electrical and topographical characteristics for the stimulation of cells. Adv Funct Mater. 2007;17:1645-53.

[197] Li GN, Hoffman-Kim D. Tissue-engineered platforms of axon guidance. Tissue Eng Part B Rev. 2008;14:33-51.

[198] Amado S, Simoes MJ, Armada da Silva PA, Luis AL, Shirosaki Y, Lopes MA, et al. Use of hybrid chitosan membranes and N1E-115 cells for promoting nerve regeneration in an axonotmesis rat model. Biomaterials. 2008;29:4409-19.

[199] Tan X, Lu L, Wang Z. An experimental study of repairing facial nerve defect in rabbit with silk fibroin-chitosan conduit. Int J Oral Maxillofac Surg. 2009;38:500.

[200] Lee JY, Bashur CA, Goldstein AS, Schmidt CE. Polypyrrole-coated electrospun PLGA nanofibers for neural tissue applications. Biomaterials. 2009;30:4325-35.

[201] Leach JB, Brown XQ, Jacot JG, Dimilla PA, Wong JY. Neurite outgrowth and branching of PC12 cells on very soft substrates sharply decreases below a threshold of substrate rigidity. J Neural Eng. 2007;4:26-34.

[202] Xu H, Yan Y, Li S. PDLLA/chondroitin sulfate/chitosan/NGF conduits for peripheral nerve regeneration. Biomaterials. 2011;32:4506-16.

[203] Ozmen S, Ayhan S, Latifoglu O, Siemionow M. Stamp and paper method: A superior technique for the walking track analysis. Plast Reconstr Surg. 2002;109:1760-1.

[204] Dijkstra JR, Meek MF, Robinson PH, Gramsbergen A. Methods to evaluate functional nerve recovery in adult rats: Walking track analysis, video analysis and the withdrawal reflex. J Neurosci Methods. 2000;96:89-96.

[205] Hare GM, Evans PJ, Mackinnon SE, Best TJ, Bain JR, Szalai JP, et al. Walking track analysis: A long-term assessment of peripheral nerve recovery. Plast Reconstr Surg. 1992;89:251-8.

[206] Bain JR, Mackinnon SE, Hunter DA. Functional evaluation of complete sciatic, peroneal, and posterior tibial nerve lesions in the rat. Plast Reconstr Surg. 1989;83:129-38.

[207] Ao Q, Fung C-K, Tsui AY-P, Cai S, Zuo H-C, Chan Y-S, et al. The regeneration of transected sciatic nerves of adult rats using chitosan nerve conduits seeded with bone marrow stromal cell-derived Schwann cells. Biomaterials. 2011;32:787-96.

[208] Matsumoto K, Ohnishi K, Kiyotani T, Sekine T, Ueda H, Nakamura T, et al. Peripheral nerve regeneration across an 80-mm gap bridged by a polyglycolic acid (PGA)-collagen tube filled with laminin-coated collagen fibers: A histological and electrophysiological evaluation of regenerated nerves. Brain Res. 2000;868:315-28.

[209] Gerardo-Nava J, Fuehrmann T, Klinkhammer K, Seiler N, Mey J, Klee D, et al. Human neural cell interactions with orientated electrospun nanofibers in vitro. Nanomedicine. 2009;4:11-30.

[210] Yang F, Xu CY, Kotaki M, Wang S, Ramakrishna S. Characterization of neural stem cells on electrospun poly(L-lactic acid) nanofibrous scaffold. J Biomat Sci-Polym E. 2004;15:1483-97.

[211] Silva GA, Czeisler C, Niece KL, Beniash E, Harrington DA, Kessler JA, et al. Selective differentiation of neural progenitor cells by high-epitope density nanofibers. Science. 2004;303:1352-5.

[212] Li WJ, Laurencin CT, Caterson EJ, Tuan RS, Ko FK. Electrospun nanofibrous structure: A novel scaffold for tissue engineering. J Biomed Mater Res. 2002;60:613-21.

[213] Matthews JA, Wnek GE, Simpson DG, Bowlin GL. Electrospinning of collagen nanofibers. Biomacromolecules. 2002;3:232-8.

[214] Pham QP, Sharma U, Mikos AG. Electrospinning of polymeric nanofibers for tissue engineering applications: A review. Tissue Eng. 2006;12:1197-211.

[215] Koh HS, Yong T, Chan CK, Ramakrishna S. Enhancement of neurite outgrowth using nano-structured scaffolds coupled with laminin. Biomaterials. 2008;29:3574-82.

[216] Chew SY, Wen J, Yim EKF, Leong KW. Sustained release of proteins from electrospun biodegradable fibers. Biomacromolecules. 2005;6:2017-24.

[217] Patel S, Kurpinski K, Quigley R, Gao H, Hsiao BS, Poo M-M, et al. Bioactive nanofibers: Synergistic effects of nanotopography and chemical signaling on cell guidance. Nano Lett. 2007;7:2122-8.

[218] Ahmed I, Liu HY, Mamiya PC, Ponery AS, Babu AN, Weik T, et al. Three-dimensional nanofibrillar surfaces covalently modified with tenascin-C-derived peptides enhance neuronal growth in vitro. J Biomed Mater Res A. 2006;76A:851-60.

[219] Mattioli-Belmonte M, Giavaresi G, Biagini G, Virgili L, Giacomini M, Fini M, et al. Tailoring biomaterial compatibility: In vivo tissue response versus in vitro cell behavior. Int J Arif Organs. 2003;26:1077-85.

[220] Soliman S, Pagliari S, Rinaldi A, Forte G, Fiaccavento R, Pagliari F, et al. Multiscale three-dimensional scaffolds for soft tissue engineering via multimodal electrospinning. Acta Biomater. 2010;6:1227-37.

[221] Kamalesh S, Tan PC, Wang JJ, Lee T, Kang ET, Wang CH. Biocompatibility of electroactive polymers in tissues. J Biomed Mater Res. 2000;52:467-78.

[222] Wang CH, Dong YQ, Sengothi K, Tan KL, Kang ET. In-vivo tissue response to polyaniline. Synthetic Met. 1999;102:1313-4.

[223] Macdiarmid AG, Epstein AJ. Polyanilines - A novel class of conducting polymers. Faraday Discuss. 1989;88:317-+.

[224] McCullough LA, Matyjaszewski K. Conjugated conducting polymers as components in block copolymer systems. Mol Cryst Liq Cryst. 2010;521:1-55.

[225] Sahmetlioglu E, Yuruk H, Toppare L, Cianga I, Yagci Y. Synthesis and characterization of conducting copolymers of poly(vinyl alcohol) with thiophene side-groups and pyrrole. Polym Int. 2004;53:2138-44.

[226] McCullough RD. The chemistry of conducting polythiophenes. Adv Mater. 1998;10:93-+.

[227] Gelmi A, Higgins MJ, Wallace GG. Physical surface and electromechanical properties of doped polypyrrole biomaterials. Biomaterials. 2010;31:1974-83.

[228] Jin L, Feng Z-Q, Zhu M-L, Wang T, Leach MK, Jiang Q. A novel fluffy conductive polypyrrole nano-layer coated PLLA fibrous scaffold for nerve tissue engineering. J Biomed Nanotechnol. 2012;8:779-85.

114

[229] Liu X, Chen J, Gilmore KJ, Higgins MJ, Liu Y, Wallace GG. Guidance of neurite outgrowth on aligned electrospun polypyrrole/poly(styrene-beta-isobutylene-beta-styrene) fiber platforms. J Biomed Mater Res A. 2010;94A:1004-11.

[230] Kotwal A, Schmidt CE. Electrical stimulation alters protein adsorption and nerve cell interactions with electrically conducting biomaterials. Biomaterials. 2001;22:1055-64.

[231] Xu H, Holzwarth JM, Yan Y, Xu P, Zheng H, Yin Y, et al. Conductive PPY/PDLLA conduit for peripheral nerve regeneration. Biomaterials. 2014;35:225-35.

[232] Jiang XP, Tessier D, Dao LH, Zhang Z. Biostability of electrically conductive polyester fabrics: An in vitro study. J Biomed Mater Res. 2002;62:507-13.

[233] Koppes AN, Zaccor NW, Rivet CJ, Williams LA, Piselli JM, Gilbert RJ, et al. Neurite outgrowth on electrospun PLLA fibers is enhanced by exogenous electrical stimulation. J Neural Eng. 2014;11.

[234] Patel NB, Poo MM. Perturbation of the direction of neurite growth by pulsed and focal electric-fields. J Neurosci. 1984;4:2939-47.

[235] Patel N, Poo MM. Orientation of neurite growth by extracellular electric-fields. J Neurosci. 1982;2:483-96.

[236] Suter DM, Miller KE. The emerging role of forces in axonal elongation. Prog Neurobiol. 2011;94:91-101.

[237] Alrashdan MS, Park JC, Sung MA, Yoo SB, Jahng JW, Lee TH, et al. Thirty minutes of low intensity electrical stimulation promotes nerve regeneration after sciatic nerve crush injury in a rat model. Acta Neurol Belg. 2010;110:168-79.

[238] Al-Majed AA, Brushart TM, Gordon T. Electrical stimulation accelerates and increases expression of BDNF and trkB rnRNA in regenerating rat femoral motoneurons. Eur J Neurosci. 2000;12:4381-90.

[239] Al-Majed AA, Neumann CM, Brushart TM, Gordon T. Brief electrical stimulation promotes the speed and accuracy of motor axonal regeneration. J Neurosci. 2000;20:2602-8.

[240] Paling NRD, Wheadon H, Bone HK, Welham MJ. Regulation of embryonic stem cell self-renewal by phosphoinositide 3-kinase-dependent signaling. J Biol Chem. 2004;279:48063-70.

[241] Slawny NA, O'Shea KS. Dynamic changes in Wnt signaling are required for neuronal differentiation of mouse embryonic stem cells. Mol Cell Neurosci. 2011;48:205-16.